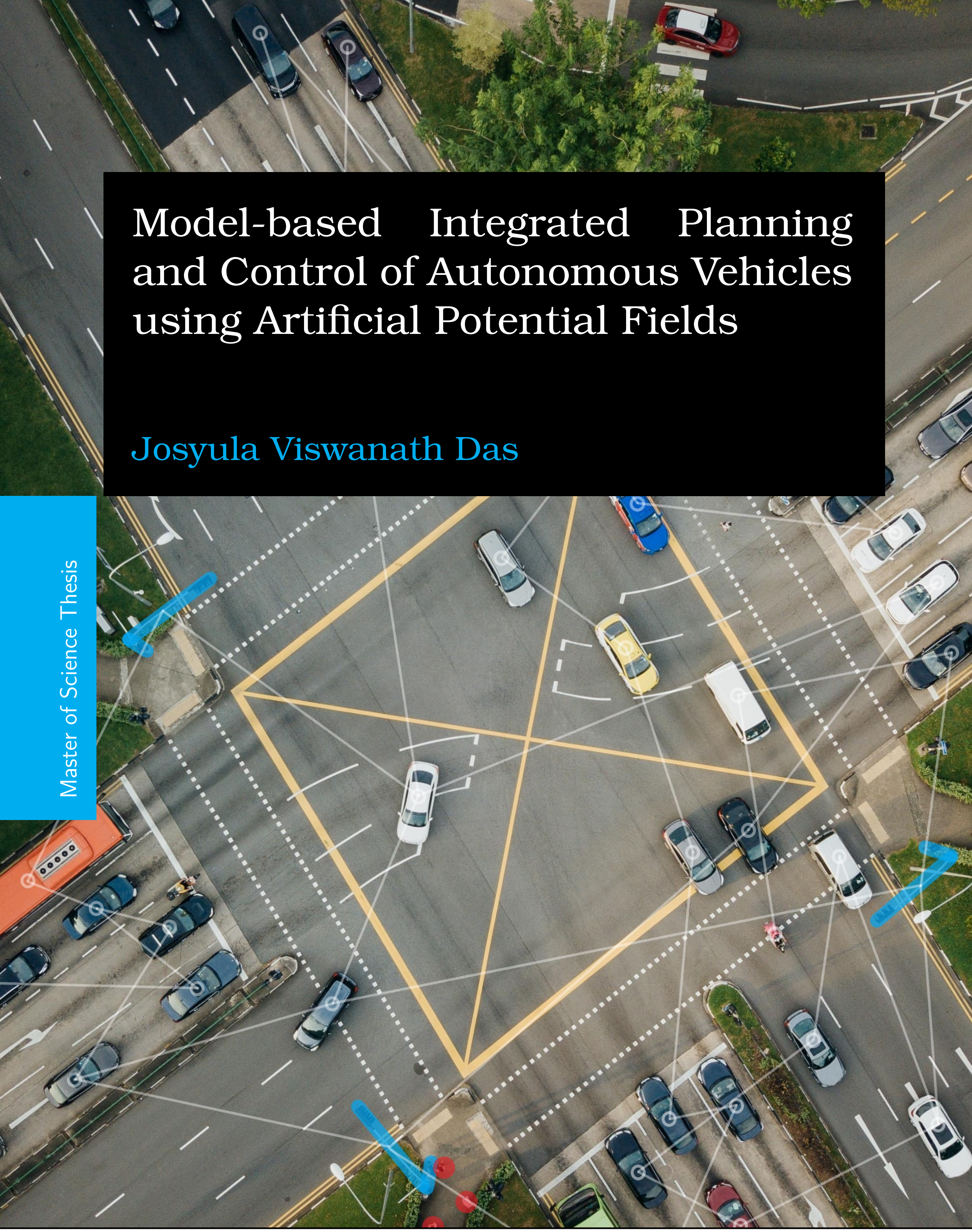

Model-based Integrated Planning and Control of Autonomous Vehicles using Artificial Potential Fields

Josyula Viswanath Das

Master of Science Thesis

Delft Center for Systems and Control

Model-based Integrated Planning and Control of Autonomous Vehicles using Artificial Potential Fields

Master of Science Thesis

For the degree of Master of Science in Systems and Control at Delft University of Technology

Josyula Viswanath Das

February 22, 2023

Faculty of Mechanical, Maritime and Materials Engineering (3mE) · Delft University of Technology

Abstract

Navigation systems in an Autonomous Vehicles (AV) can be divided into two parts: a path planning block which takes in the environmental data and rules to design a collision-free obstacle and a vehicle control and tracking block which generates actuator inputs for the AV to follow the reference path generated by the path planning block. Each task is fulfilled by a different algorithm with its own performance indices. These algorithms are not usually designed to get the best overall vehicle performance but the best performance of their respective blocks. A planned path that the vehicle cannot follow can therefore be generated and can lead to high tracking error and in some cases collision with obstacles. This can be solved by integrating path planning and vehicle control blocks with the dynamics of the AV.

The goal of this graduation project is therefore to develop an integrated planning and vehicle control algorithm for an Autonomous Vehicles (AV). This is done by integrating a novel-Artificial Potential Fields (APF) with Model Predictive Control (MPC) to solve both path planning and vehicle control using a single optimization problem. The addition of the AV and the Obstacle Vehicle (OV) dynamics to the optimization problem as prediction models along with recursive computation can determine accurate inputs to be given to the AV.

Unlike traditional APF-based path planning where the minimum potential path is generated as the result of a gradient descent method applied on the available map data and obstacle information, the APF is added as a cost to the objective function of the MPC based optimization problem to find the minimum potential path. By using a receding horizon approach for solving the final optimization problem, the potential field can be updated at each time step to avoid moving obstacles. The dynamics of the vehicle added to the optimization problem include both lateral and longitudinal dynamics and are linearized at each time step at the current state of the AV.

This however generates a path which does not travel in the centre of the lane and makes risky manoeuvres. Therefore, an Mixed-Integer Model Predictive Control (MIMPC) algorithm with logical constraints is used to generate an optimal lane to travel in. This optimal lane is used to generate a road potential which can guide the vehicle to the centre of the optimal lane. The MIMPC and the APF-MPC algorithms are run successively to generate a collision-free path.

The logical constraints, also called MLD constraints are converted into a set of linear inequalities with the introduction of logical variables. These logical variables are used to represent individual logical constraints based on the states of the system and on a combination of logical and state constraints. A novel-APF inspired by the Yukawa Potential [1] is designed to represent each obstacle. A convex representation of this non-convex obstacle potential is formulated to simplify the optimization problem. The convex representation of the obstacle APF is obtained by approximating it using a region-based APF where the region is defined by the position of the AV around the obstacle. This is further simplified by approximation using a quadratic Taylor-series expansion.

The simulation was performed on MATLAB on a two-lane road with multiple obstacles. The thesis report ends with a discussion on future work to be taken to further enhance the performance of the controller and to make it road-ready.

Table of Contents

List of Figures

List of Tables

Preface

The idea for this graduation dissertation comes from my interest in studying and developing an ideal transportation system. The ideal transportation system integrates and controls multiple sub-systems with high level of accuracy to obtain the optimal result at all fronts by taking into account the uncontrollable and uncertain aspects. The lack of synchronisation between these individual sub-systems can therefore create a cascading effect which can lead the breakdown of the entire system.

Road Vehicles are one such important sub-system which form an important building block for the ideal transportation network as it deals with most inland transportation of products and people. The advent of autonomous counterparts to traditional road vehicles has helped develop algorithms to integrate them seamlessly into the transportation system while increasing efficiency.

An autonomous road vehicle is in itself divided into multiple functional blocks, each of which perform a certain important aspect to move the vehicle to its goal. These functional blocks are usually run by individual algorithms working independently. However, these blocks have to run in synchronisation with each other to obtain the best performance. The idea of this graduation dissertation was therefore to develop an algorithm to integrate the functional blocks of the autonomous road vehicle to improve performance.

Acknowledgements

I am immensely thankful to a large number of people who have helped, pushed and motivated me to work hard and bring my thesis to completion. I would start with thanking my daily supervisor, Emilio Benenati for his kind words, support and guidance without which I would have felt very lost. I would also like Sergio Grammatico for checking my work and giving feedback and helping me refine the topic for my thesis.

To all my friends who have spoken to me, calmed me down during time of self-doubt, I want to thank you for being there and listening to be thinking out loud about my work. To Ruud and Jasper from RoyalHaskoning DHV, I would like to thank for being understanding and letting me focus on my thesis and giving me a break from my job when required.

A special shout-out to Ayushi Kandoi, my better half and world for being beside me and being my pillar of strength that I could lean on and for standing by my side to the end.

Lastly, I want to thank my incredible parents who have supported me both financially and emotionally and who have made me everything I am today and for talking about other things in life to divert my mind from work and study.

Delft, University of Technology
February 22, 2023

Josyula Viswanath Das

Chapter 1

Introduction

The design of the Autonomous Vehicles (AV) technology has been in a state of constant improvement since the first half of the 20^{th} century when the idea of cars driving themselves on "smart" roads gained widespread public exposure at the General Motors Futurama exhibit in the New York World's Fair in 1939. Though multiple tests for the development of AV were performed in the next half century, the next landmark event in AV history appeared in the form of the EUREKA Prometheus Project funded by European Commission [16] in the 1980s which lead to the development of "VaMoRs", the first fully autonomous vehicle to drive on a road at high speed with the help of computer vision to identify obstacles and road signs. Further interest was created with the introduction of autonomous driving competitions like the Defense Advanced Research Projects Agency (DARPA) Urban Challenge and the DARPA Grand Cooperation Driving Challenge in the early 2000s [17, 18]. These challenges and the increasing interest in both academic and industrial circles in the development of AV lead to the Society of Automotive Engineers (SAE) to introduce the J3016 "Levels of Driving Automation" standard in 2014, which defines six distinct levels of driver automation [19] as shown in Figure 1-1.

With significant technological advancements as well as with the increase in speed and volume of transport, AV have evolved to solve a number of problems. Those problems are : (1) an increasing number of road accidents, (2) an increase in traffic volume leading to long congestion and waiting time, and (3) better energy efficiency to reduce global climate impact. The introduction of AV to mainstream transport can reduce these problems. AV are expected to have a significant impact on the overall transport system as they remove the chance of mistakes by the human element, can optimize their decisions over driving goals and can communicate with other vehicles and infrastructure to reduce traffic congestion. Figure 1-2 which shows the strong influence of human factors on road-based accidents in Germany. The removal of the human factor from driving can therefore reduce the number of accidents. With the widespread implementation of AV and its relative infrastructure to reach large scale by 2030 [20] and its economic impact of about 0.2 to 1.9 trillion per year [21], it is necessary to develop algorithms which can achieve safe and efficient methods to avoid obstacles.

The use of AV reduces the risk of collision due to human error, but adds to the complexity of

	Name and Description	Execution of Steering and Acceleration/ Deceleration	Monitoring of Driving Environment	Fallback Performance of Dynamic Driving	Driving Modes	
SAE Level 0	**NO AUTOMATION** The human driver performs all aspects of driving	Human Driver	Human Driver	Human Driver	Provide Warnings	Driving environment monitered by the human driver
SAE Level 1	**DRIVER ASSISTANCE** Either steering or braking and acceleration assist is incorporated with the vehicle and the human performs the other driving tasks by himself.	Human Driver + Automated System	Human Driver	Human Driver	Steering **or** brake/ accleration Control	
SAE Level 2	**PARTIAL AUTOMATION** A steering and braking and acceleration assist is incorporated into the vehicle using environmental data and the human performs the other driving tasks by himself.	Automated System	Human Driver	Human Driver	Steering **and** brake/ accleration Control	
SAE Level 3	**CONDITIONAL AUTOMATION** An automated driving system performs all the driving tasks using environmental data assuming that human driver can take over when requested	Automated System	Automated System	Human Driver	Some driving modes	Driving environment monitered by the automated system
SAE Level 4	**HIGH AUTOMATION** An automated driving system performs all the driving tasks using environmental data even when the human driver cannot or does not take over when requested	Automated System	Automated System	Automated System	Some driving modes	
SAE Level 5	**FULL AUTOMATION** An automated driving system performs all the driving tasks using environmental data in all road and environmental conditions just like a human driver	Automated System	Automated System	Automated System	All driving modes	

Figure 1-1: Levels of Driving Automation [2],[3]

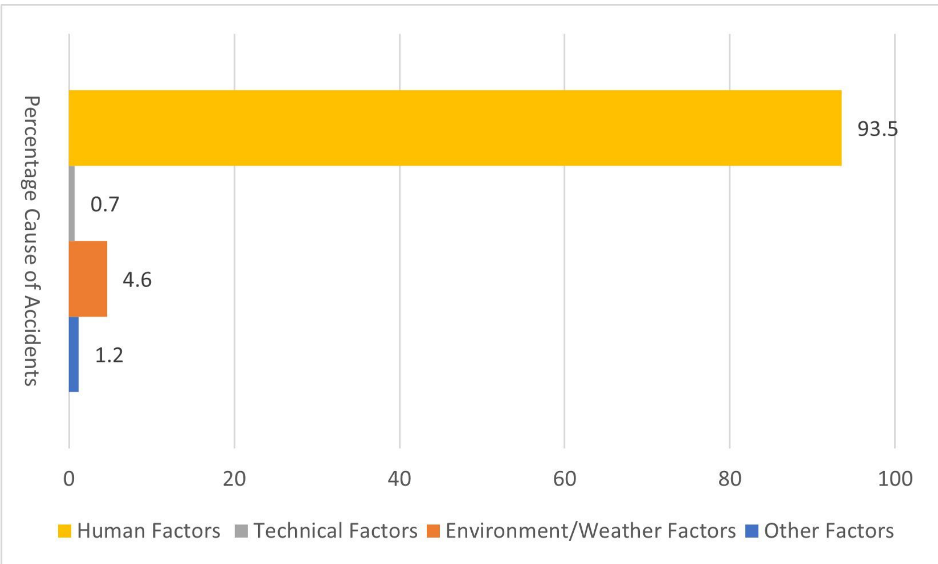

Figure 1-2: Percentage of Accidents caused by various factors [4]

the system, both in software and hardware. The functional architecture of an Autonomous Vehicles (AV) can be divided into perception, path planning, vehicle control and system supervision based on a high level of abstraction [5].

1-1 Functional Architecture

Figure 1-3 shows the functional blocks as well as their inputs and outputs. The inputs to the AV consist of sensor data as well as static maps, world rules, user input etc., and the outputs are the actuator inputs which decide the movement of the AV. The role of each of the functional blocks is discussed further.

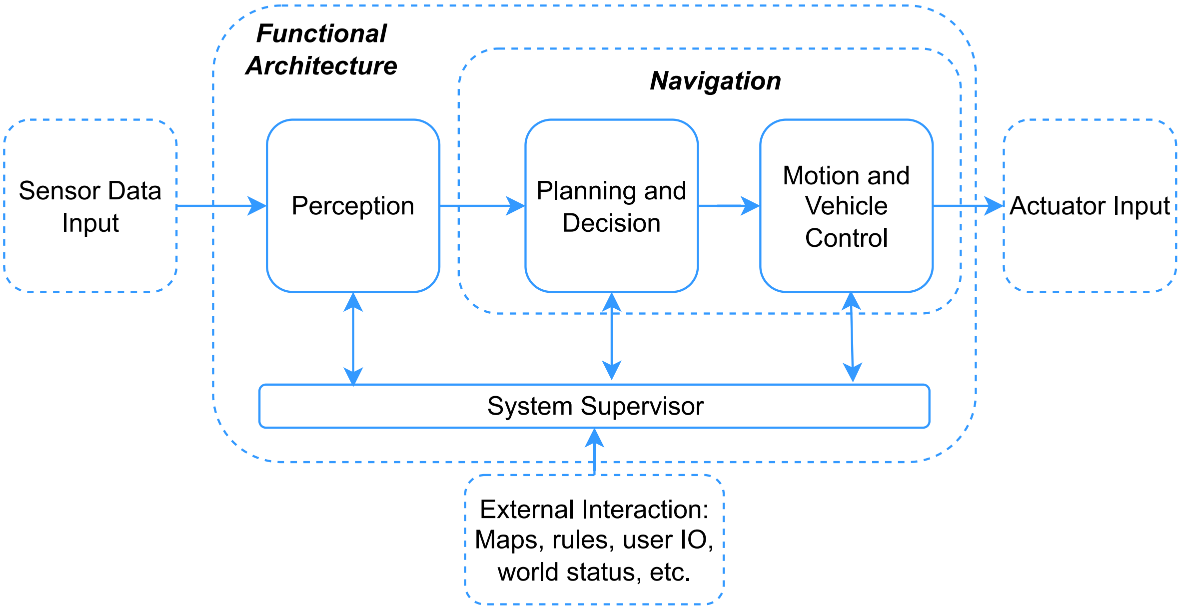

Figure 1-3: Functional Architecture of an Autonomous Vehicles (AV) [5]

The *perception* block collects environmental data obtained by the sensors and uses this data to perform localization. A basic description of different sensor types and the common sensors used in AV are described in Figure 1-4. Readers interested in understanding more about the different sensors are encouraged to see [3]. This sensor data coming from the heterogeneous array of sensors is fused together with the aim of making a unified map of the surroundings in which the AV can perform its function with high efficiency while maintaining a high degree of safety.

The *path planning* block is central in the architecture of any AV as its goal is to generate a safe and comfortable path while avoiding the different obstacles present in the environment. The idea of path planning was first presented in [22] and consequently a large number of algorithms to achieve path planning have been researched and developed for vehicle navigation over the last few decades. Path planning algorithms can be classified as global or local path planning algorithms. Global path planning algorithms uses static map data to plan a high-level path determining which roads, highways, tunnels, etc, to take to reach the destination to the goal. Local path planning algorithms use the global path generated as a stencil to follow while taking into account collision avoidance with other dynamic obstacles on the road.

	Description	Proprioceptive* or Exteroceptive*	Passive* or Active*
Camera	It provide the ADS with high resolution images and videos with both color and texture information. Relatively inexpensive and can be used for visual tasks such as lane and sign detection. Highly dependent on environmental conditions.	Exteroceptive	Passive
RADAR	It measures distance, angle and velocity of the OV in the area of interest. Can work well in multiple weather conditions. Drawbacks: a limited field of vision and need to be calibrated to detect OV.	Exteroceptive	Active
LiDAR	Emits laser and measures the time of flight to find the distance to OV. Similar to RADAR, but has higher accuracy and runs at higher frequency. Has drawbacks in terms of sensitivity to weather conditions, generating a large amount of sensor data as well as having a short range.	Exteroceptive	Active
GPS	Satellite based navigation system which is used to find the absolute location of the HV. It can provide accurate position and timing information.	Proprioceptive	Passive
IMU	Measures the HV's acceleration, heading angle, and relative position with the help of a combination of accelerometers, gyroscopes, and sometimes magnetometers.	Proprioceptive	Passive

*__Active sensors__ emit energy (electromagnetic signals) into the environment
*__Passive sensors__ perceive electromagnetic signals already in the environment to detect obstacles
*__Proprioceptive sensors__ are sensors which measure values which are internal to the system
*__Exteroceptive sensors__ are sensors which acquire data about its surroundings

Figure 1-4: Basic description of the most used sensors used in most sensor fusion algorithm [3],[6],[7],[8],[9]

The *motion and vehicle control* block is used to track the output from the *path planning block* with maximum accuracy. It is the interface between the *path planning* block and the actual dynamics of the vehicle, and generates the control signals to the actuators to run the AV in the designed manner. It is therefore important for the block to incorporate the dynamics of the vehicle to avoid collisions. The authors in [23] provide a deep insight to the different algorithms used for path tracking.

The *system supervisor* block is used as a control centre to help communication between the different blocks, to store required data, world rules, driving rules, user input, and other external interactions. It is also responsible to handle functional safety mechanisms like fault detection to activate safety critical systems when required.

1-2 Motivation and Challenges

The *path planning* block and the *motion and vehicle control* block are functional blocks to allow for safe and collision-free travel and together form the navigation block. Most AV use A* [24], Dijkstra [25], Rapidly-exploring Random Trees (RRT) [26] or APF [27] for path planning due to their simplicity of implementation as well as their requirement of low computation power [28]. However, many of these path planning algorithms take only the kinematics of the AV into account while designing the path. This is done to simplify the path planning algorithm and therefore reduce computation time. However, this makes the designed path sub-optimal. For example, RRT is a sampling based path-planning algorithm that finds the path with the least distance while avoiding collisions and was introduced by LaValle et al. However, RRT does not take into account the kinematics of the AV and neither is it optimal. RRT* [29] extends RRT such that it is asymptotically optimal as the number of samples goes to infinity.

There can therefore be a mismatch between the path planned by the *path planning* block and the path which can be tracked by the *motion and vehicle control* block and in turn the AV. This is true if the dynamics of the HV as well as the OV are not captured well by the path planning algorithm and can lead to large deviations from the planned path and collisions with obstacles. One method to solve this problem and to generate a safe and collision-free path is by integrating the *path planning block* and the *vehicle motion and control block*.

The motivation of this thesis is therefore to design an integrated path planning and vehicle control algorithm that can avoid obstacles while meeting control requirements.

1-3 Relevant Work

MPC has been widely used as both a local path planning as well as a path-tracking controller in both academia and industry due to its ability to handle multiple-input multiple-output, non-linear systems along wiuth system and environmental constraints. MPC consists of a prediction model of the system and an optimization algorithm. The prediction model of the system helps predict and evaluate the future trajectory generated by the input sequences. The optimization problem runs to optimize over the input sequences recursively to incorporate the future predictions of the system trajectories to make sure that the system is collision-free given a feasible initial state and long enough prediction horizon [30] [31]. The first value of the optimal input sequence is then applied to the system and MPC is run again with the new initial state. This is known as a receding horizon approach. There are multiple different ways to integrate the *path planning block* and the *vehicle motion and control block* using MPC.

Paths from a global path planner can be re-planned by an MPC optimization problem to overcome the lack of inclusion of dynamics of the vehicle in the path planning algorithm. The authors in [32] use the A* algorithm as the global path planner and then use MPC as a local path planner to avoid obstacles. The MPC algorithm takes into account the system and obstacle dynamics as well as constraints of both the system and the surroundings.

MPC can be used together with parametric curves to represent the travelled path to integrate path planning and vehicle control where the parametric curves are a function of the MPC decision variable. The authors in [33] design the reference trajectory as a function of the optimal decision variable generated by the MPC optimal control problem to capture both path planning and trajectory tracking in a single MPC problem. To avoid dynamic obstacles, the AV first checks if it can avoid collision by braking using a safe distance measure which is dependent on the distance between the vehicles, the relative velocity, and maximum deceleration. If braking cannot avoid a collision, a lane change manoeuvre is adopted. The authors in [34] developed a b-spline-based MPC algorithm to integrate path planning and tracking algorithm for autonomous underwater vehicles. Boundary and continuity constraints on the recursively planned and parameterized b-spline path along with an error-based prediction model between the actual system and a reference system are used to define the MPC optimal control problem.

A large number of algorithms have been developed for MPC to work with Artificial Potential Fields (APF) to unify local planning and control with obstacle avoidance in AV. An APF designates an attractive or repulsive nature to the goal and obstacles respectively by means of a potential. Figure 1-5a shows an example of repulsive potential whereas Figure 1-5b depicts an example of attractive potential. A gradient descent method is generally applied to the

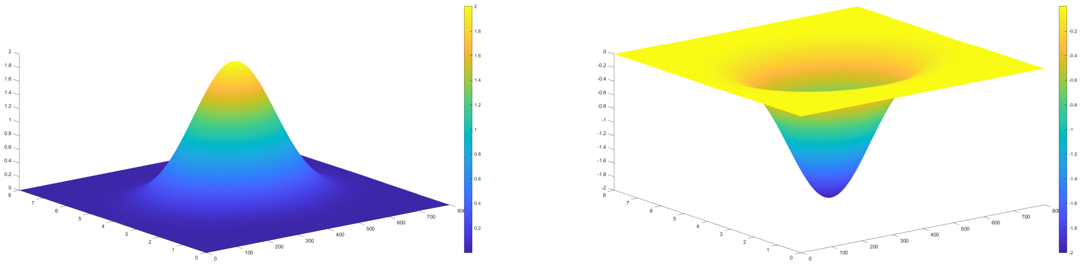

(a) Repulsive Potential Field **(b)** Attractive Potential Field

Figure 1-5: Different types of Artificial Potential Fields (APF)

total potential of the surrounding area of the AV to find the minimum potential path to reach the goal while avoiding obstacles. The authors of [35] use a linear state-space model linearized at the current state of the AV with small angle approximations as the model for the nominal MPC. It uses a road potential to keep the vehicle within the boundaries of the road along with an obstacle potential for collision avoidance to find the minimum potential path. The artificial potential field thus defined at the given time step is added as a cost to the objective function of the MPC problem along with a stage cost to combine local path planning and collision avoidance.

Of the above-discussed strategies to combine path planning and tracking control, the APF-MPC strategy is the most interesting due to the ability to combine local path planning with collision avoidance. The use of only MPC to generate an optimal path requires a large number of constraints as well as a large horizon to avoid obstacles [36]. This can be solved by the addition of an APF to the MPC optimization problem. While APF provides a continuous risk assessment of surrounding obstacles and works well to avoid obstacles, the MPC helps recursively find the optimal path in the presence of dynamic obstacles and adds the AV dynamics and required constraints of the system and its surroundings. Path planning using APF also has very low computation time [37]. Artificial Potential Fields are easy to generate if the information about the surroundings and the obstacles are available. They also provide a way to define different criteria or modes of operation depending on the shape of the APF.

However, the output of the APF-MPC strategy will not stick to the centre of the lane unless a lateral position reference is given due to the shape of a general road potential used which acts as a penalty function at the road boundaries. The selection of this lateral position reference is generally based on assumptions and is not optimal in nature. This can be solved by finding the optimal lane. As the lane number is an integer, Mixed-Integer Model Predictive Control (MIMPC) is an ideal method to find the optimal lane as it can recursively find the optimal lane at every time step given constraints. Du et. al. [38] uses a hybrid/mixed integer MPC by combining integer valued lane variables with continuous state variables to help lane change manoeuvres. A simplified motion model to reduce computation time. The discrete and continuous variables are combined into logical variables and are used to design logical constraints which are further written as linear inequalities [39].

1-4 Thesis Outline

The previous sections discuss the history of the Autonomous Vehicles (AV) and its functional components, the motivation behind the thesis and the relevant work which has happened in the field to finally propose the basic path of the thesis. This section finalizes and outlines the different tasks to be performed to achieve this goal and the assumptions which are used.

The contributions of the thesis are the design of two algorithm to generate an unified navigation block and their comparison. The steps taken while designing each of these algorithms are:

- **APF-MPC algorithm**
  - Design of a quadratic road potential
  - Design an obstacle potential to keep the problem convex as well as to maintain a given distance between the obstacle and the AV.
  - Design of the APF-MPC problem by using the above-designed road and obstacle potentials
- **MIMPC+APF-MPC algorithm**
  - Design a MIMPC optimal control problem to act as a higher level, strategic decision-making model which decides when lane change and overtake manoeuvres are desirable and feasible.
  - Design a road potential which pushes the vehicle to the centre of that particular lane.
  - Design an obstacle potential to keep the problem convex as well as to keep the vehicle at the correct distance from it.
  - Design a APF-MPC problem by using the above-designed road and obstacle potentials
- Comparison between the paths taken by the APF-MPC vs MIMPC+APF-MPC algorithms

The body of the organized as follows; The fundamentals of autonomous driving that were employed in this study are discussed in detail in Chapter 2. Chapter 3 discussed the design of the APF potentials for the APF-MPC and MIMPC+APF-MPC algorithms. The design of the APF-MPC and MIMPC+APF-MPC algorithms are covered in Chapter 4. Chapter 5 shows the results of each of the algorithms and also the comparison between the APF-MPC with MIMPC+APF-MPC algorithms. The conclusions of the graduation work as well as recommendations for future research are given in Chapter 6.

This thesis also contain a number of appendices at the rear that give information that is too lengthy to be presented as a part of the main body. It includes explanation of certain theory and algorithms as well as large matrices used in this thesis. The thesis is concluded with the bibliography and glossary, which includes a list of abbreviations.

Chapter 2

Autonomous Driving: Basics

A thorough explanation to build on the basic ideas introduced in Chapter 1 is provided in this chapter. Section 2-1 discusses the basic idea of path planning. Section 2-2 discusses the concept of safe driving and the design of the safe distance measure, and the logic behind the lane change manoeuvres. The chapter ends with assumptions made by the thesis in Section 2-3 in addition to those made in Section 1-4.

2-1 Path Planning

The goal of an AV is to navigate from the present position to a goal position while avoiding obstacles. Having obtained the map of the environment and after having localized the OV using sensor fusion, decisions are made on how navigation is achieved. The design of a path so as to achieve collision-free motion in a given environment is defined as path planning. Given below are the steps required for a basic path planning problem [40]

- Define the workspace, $\mathcal{W} \subseteq \mathbb{R}^n$.
- A region occupied by the obstacles, $\mathcal{O} \subset \mathcal{W}$ is identified using sensors. $\mathcal{O}$ can be static or dynamic.
- The systems is designed as a rigid body $\mathcal{A} \subset \mathcal{W}$ or a collection of m links: $\mathcal{A}_1$, $\mathcal{A}_2$, $\ldots$, $\mathcal{A}_m \in \mathcal{W}$.
- The configuration space $\mathcal{C} \subseteq \mathcal{W}$ defines all the locations in $\mathcal{W}$ that the robot can reach. We divide the configuration space based on $\mathcal{O}$ as a region occupied by the obstacles, $C_{\text{obs}} = \mathcal{C} \cap \mathcal{O}$ and a region which the vehicle can safely traverse without collision, $C_{\text{free}} = \mathcal{C} \setminus C_{\text{obs}}$.
- An initial configuration, $q_{\text{i}} \in C_{\text{free}}$ and goal configuration $q_{\text{g}} \in C_{\text{free}}$ is also defined.

The goal is to compute a (continuous) path, $\tau : [0,1] \rightarrow C_{\text{free}}$, such that $\tau(0) = q_{\text{i}}$ and $\tau(1) = q_{\text{g}}$.

Mobile robot navigation can be mainly classified into local planning and global planning [41]. While global planning deals with moving the robot towards a fixed goal, local planning works with the dynamic conditions in the environment to adhere to certain constraints like collision avoidance. Figure 2-1 shows the different classifications of path planning based on algorithm type.

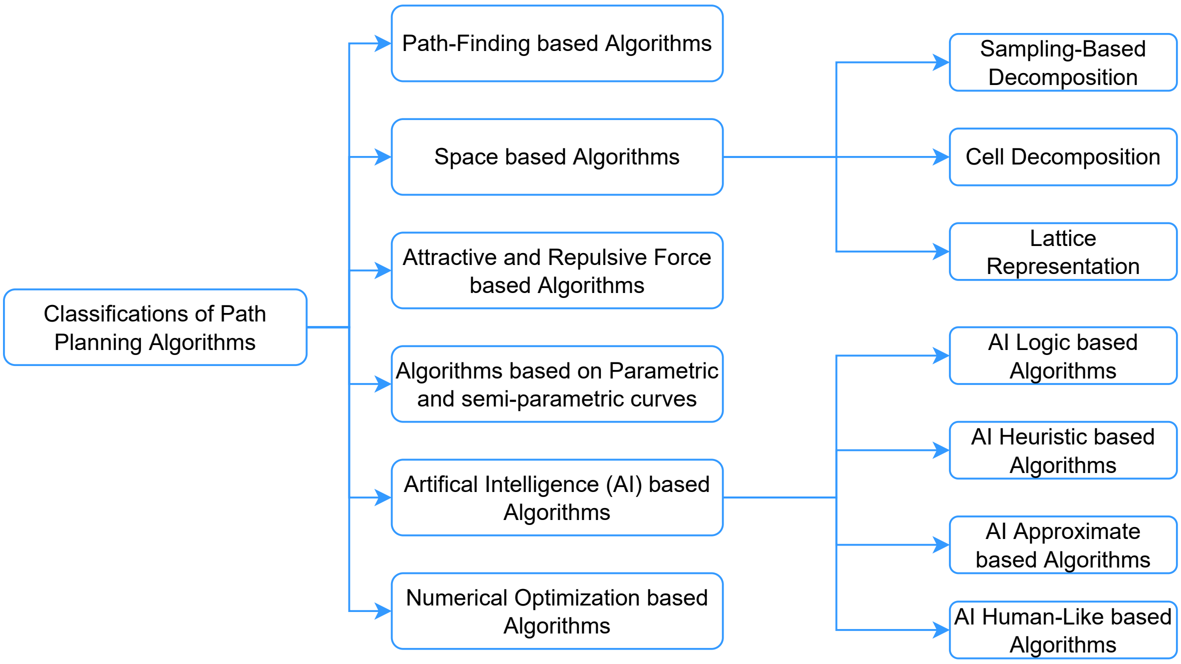

Figure 2-1: Different Classifications of Path Planning Algorithms [10]

The explanation of all the algorithms shown in Figure 2-1 is outside the scope of this thesis; see [10][28].

2-2 Safe Driving

The path generated by the *path planning* block has the following requirements [42]: (1) The path designed must be done so by keeping the dynamics of the AV in mind so that there is low tracking error, (2) The path designed should be collision-free, (3) The path should be designed by keeping in mind the comfort of the passenger. The most important of the above-mentioned requirements for a AV is to maintain the safety of its passengers/goods and to find a path that is collision-free.

However, the idea of safety is not a quantifiable entity but a social construct based on a number of factors such as vehicle capability, driving situations, driving conditions, and many more. The authors of [43] have tried to quantify driving safety based on the idea of severe traffic conflicts. A severe traffic conflict is defined as a traffic situation where a collision is imminent between a set of road users unless no change is made in their present speed and direction. Having identified a number of scenarios of severe traffic conflict, the authors also define a number of safety metrics. These metrics can be divided into two different parts; (1) maintaining a safe distance from the vehicle in front in case lane change is not possible and collision is imminent by braking, (2) Changing its lane to avoid an imminent collision. Figure 2-2 shows the basic flowchart for different vehicle manoeuvres [44].

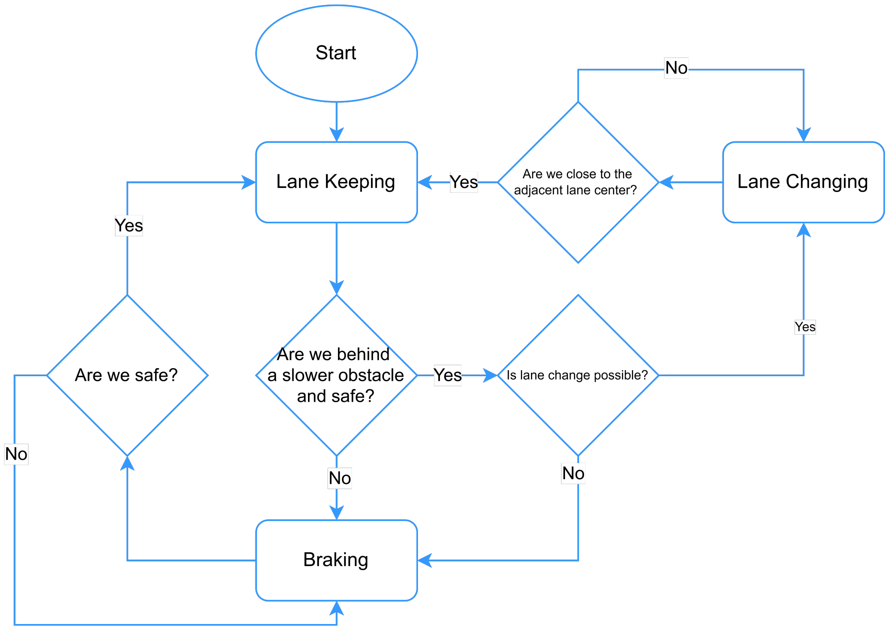

Figure 2-2: Flowchart of different lane change manoeuvres

This thesis used the calculation of the safe distance measure as an identifier to define different vehicle manoeuvres i.e., to decide between lane change or braking manoeuvres. The theory behind the calculation of the safe distance is discussed next.

2-2-1 Safe Distance

There exists a large amount of research on the identification of a safe distance for the following vehicle to maintain from a leading vehicle as a large proportion of accidents occur due to short following distances: 13% in Europe [45] and almost 30% in USA [46]. The design of a safe distance measure derived from the different safety metrics defined in the introduction of Section 2-2 can be used to decide between different manoeuvres to avoid collisions. The safe distance measure should encompass the following properties: (1) the safe distance should be larger than the difference in distance travelled by the following and leading vehicle in case of braking by the leading vehicle and (2) the time taken to detect the deceleration of the leading vehicle should be taken into account. This thesis defines the safe distance measure between the j^{th} OV and the HV as [33]

$$d_{j,\text{safe}} = \underbrace{\frac{v_{x,\text{HV}}^2}{2a_{\text{max,HV}}}}_{\text{A}} - \underbrace{\frac{\left(v_{x,\text{OV}}^j\right)^2}{2a_{x_{\text{min}},\text{OV}^j}}}_{\text{B}} + \underbrace{v_{x,\text{HV}} t_1}_{\text{C}} + \underbrace{d_0}_{\text{D}} \tag{2-1}$$

where $v_{x,\mathrm{HV}}$ is the longitudinal velocity of the HV, $v^j_{x,\mathrm{OV}}$ is the longitudinal velocity of the j^{th} OV, $a_{x_{\min}}$ is the maximum deceleration of the HV, $a_{x_{\min},\mathrm{OV}^j}$ is the maximum deceleration of the j^{th} OV, t_1 is the detection time and d_0 is the minimum distance to be maintained between the HV and an OV. A shows the distance travelled by the HV with maximum deceleration and current longitudinal velocity of the HV, B shows the distance travelled by the OV with maximum deceleration and current longitudinal velocity of the j^{th} OV, C represents the distance travelled by the HV during the time it takes to detect that the OV is decelerating and D is the minimum distance to be maintained between vehicles. This safe distance is then used as a measure to initiate lane changes and to generate reference HV velocity (braking). Table 2-1 shows the constants used in for calculating the safe distance measure where ℓ is

Description	Value	Symbol
Detection time	0	t_1
Minimum HV-OV distance	2ℓ	d_0

Table 2-1: Scalar values of constants used to calculate $d_{j,\mathrm{safe}}$

the length of the vehicle. Let us define a maximum safe distance $d_{\mathrm{safe}_{\max}}$ as the safe distance when the HV is travelling at its maximum longitudinal velocity $v_{\max,\mathrm{HV}}$ and the obstacle is at a standstill.

As the thesis concentrates on local path planning, considering all the OV data when performing the navigation task can increase computation time. The thesis, therefore, only considers vehicles that are within the Region Of Interest (ROI), i.e., the region centred around the HV and extending $d_{\mathrm{ROI}} = 2d_{\mathrm{safe}_{\max}}$ in front of and behind the current longitudinal position of the HV. Figure 2-3 shows the ROI where the black vehicle represents the HV and red vehicles

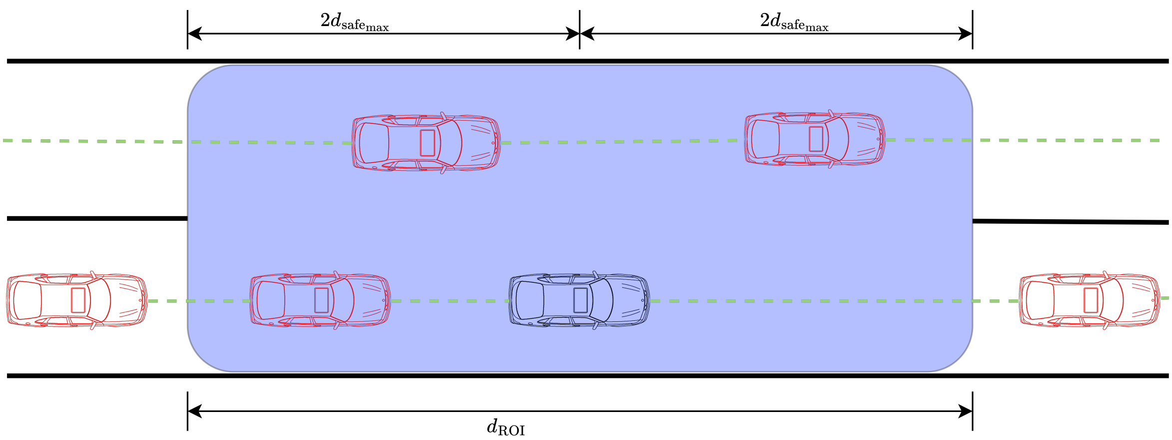

Figure 2-3: Region Of Interest (ROI) of the HV

represents the OV and the blue box represents the ROI. All the OV data within the blue region will be used for the navigation task and the excess data will be discarded.

2-2-2 Lane Change Maneuvers

Lane change manoeuvres are a fundamental behaviour of all vehicles and form the basis of traffic behaviour. AV lane-change manoeuvres are complicated tasks that have to take into account obstacles and environmental facts and require a high-fidelity model of the vehicle to perform. The requirement to change both longitudinal and lateral velocity makes lane change challenging. Lane change manoeuvres can also cause discomfort due to changes in lateral acceleration. The lateral acceleration should be within the range of 0.03 - 0.98m/s^2 for it to be comfortable [47]. Figure 2-4 shows how lane change decisions can be used to avoid collisions in different scenarios where vehicles in shades of black represent the HV and

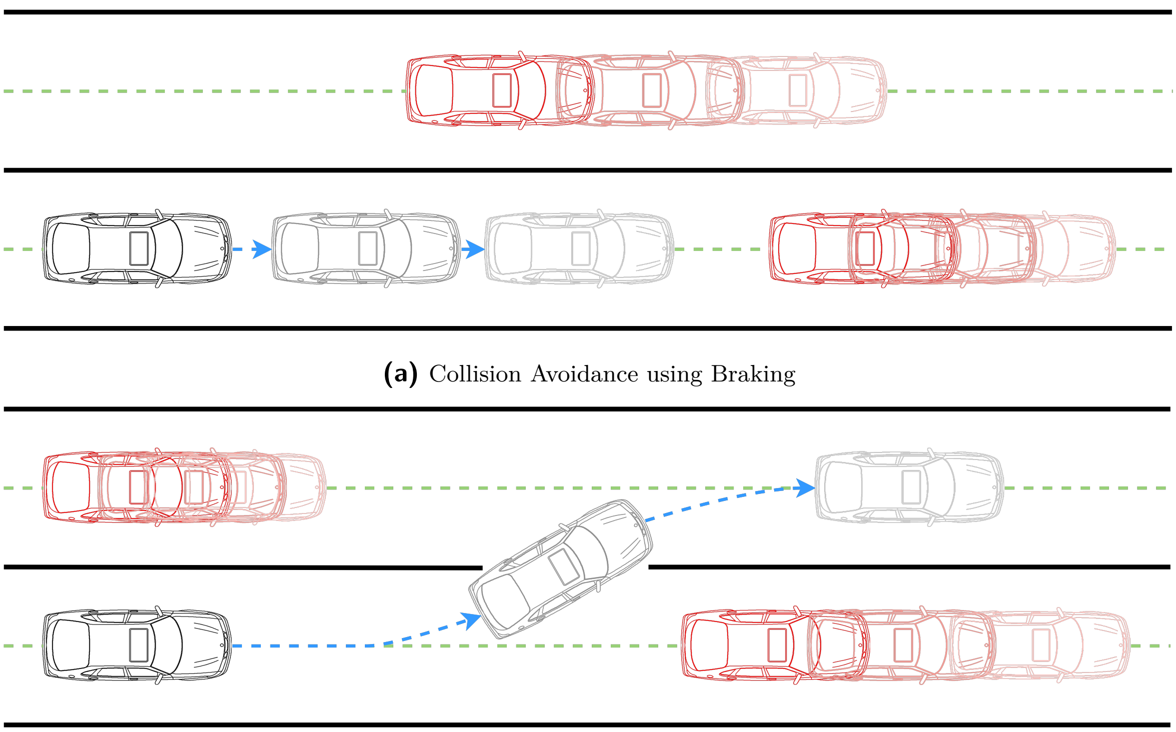

(a) Collision Avoidance using Braking

(b) Collision Avoidance using Lane Change

Figure 2-4: Collision Avoidance in different scenarios

vehicles in shades of red represent the OV with the vehicle colour getting lighter as time moves forward. In Figure 2-4a the vehicle starts braking due to a slow-moving OV in front of the HV and the presence of an OV in the adjacent lane preventing lane change whereas in Figure 2-4b vehicle changes lane to avoid a slow-moving OV in front of the HV. The authors of [48] devised a lane change model based on the safe spacing between vehicles to avoid collisions. This minimum safe spacing can be replaced by the safe distance measure formulated in 2-2-1. However, there are other factors that need to be taken into account along with the safety distance measure to decide if a lane change is safe. Therefore, this thesis uses a binary lane-change safety flag which depicts if the lane change is safe. Table 2-2 defines the different flags used to calculate the safety of a lane change.

Let $\mathrm{OV}_{\mathrm{SL},f}$, $\mathrm{OV}_{\mathrm{AL},f}$ and $\mathrm{OV}_{\mathrm{AL},r}$ represent the vehicles in front of the HV in the same lane,

Flag	Explanation
flag_{LC}	*true* if it is safe to change lane, *false* otherwise
flag_{δ}	*true* if there is an obstacle in front, in the same lane of the HV, *false* otherwise
flag_{ϵ_1}	*true* if there is an obstacle in the adjacent lane and in front of the HV, *false* otherwise
flag_{ϵ_2}	*true* if there is an obstacle in the adjacent lane behind the HV, *false* otherwise

Table 2-2: Definition of flags used to calculate the safety of lane change.

the vehicle in front of the HV in the adjacent lane and the vehicle behind the HV in the adjacent lane respectively. If multiple such vehicles exist within the ROI, the OV with the minimum longitudinal distance is chosen in each case. Let $d_{\text{safe}_{i,j}}$, $X_{\text{OV}_{i,j}}$ and $v_{x,\text{OV}_{i,j}}$ be the safe distance, the longitudinal position and the longitudinal velocity calculated for an obstacle $\text{OV}_{i,j}$ where $i \in \{\text{SL}, \text{AL}\}$ represents if the OV is in the same lane or the adjacent lane of the HV respectively and $j \in \{\text{f}, \text{r}\}$ represents if the OV is in front of or behind the HV respectively. Equation (2-2) lists the multiple logical expressions used to calculate the possibility of a lane change.

$$v_{x,\text{OV}_{\text{SL},f}} - v_{x,\text{HV}} \leq 0 \tag{2-2a}$$

$$X_{\text{OV}_{\text{SL},f}} - X_{\text{HV}} \leq d_{\text{safe}_{\text{SL},f}} + d_0 \tag{2-2b}$$

$$v_{x,\text{OV}_{\text{AL},f}} - v_{x,\text{OV}_{\text{SL},f}} \geq 0 \tag{2-2c}$$

$$X_{\text{OV}_{\text{SL},f}} - X_{\text{OV}_{\text{AL},f}} \leq d_{\text{safe}_{\text{SL},f}} - d_{\text{safe}_{\text{AL},f}} \tag{2-2d}$$

$$X_{\text{HV}} - X_{\text{OV}_{\text{AL},r}} \geq d_{\text{safe}_{\text{AL},r}} + d_0 \tag{2-2e}$$

Table 2-3 explains the different expressions in (2-2). However the values of $d_{\text{safe}_{i,j}}$, $X_{\text{OV}_{i,j}}$ and $v_{x,\text{OV}_{i,j}}$ are undefined when there exists no OV in the $i, j \in \{\{\text{SL}, \text{AL}\}, \{\text{f}, \text{r}\}\}$.

The algorithm to check if a lane change is possible is given by Algorithm 1. The steps of Algorithm 1 is given as follows:

- Line 2 checks if there exists an OV in front of the HV on the same lane. If the condition is true then
  - Line 3 checks if the velocity of the $\text{OV}_{\text{SL},f}$ less than that of the HV. If the condition is true then check if there are OV in the adjacent lane
    - if there are no vehicles in the adjacent lane (Line 4)
      - safe lane change is possible.
    - if $\text{OV}_{\text{AL},f}$ exists but not $\text{OV}_{\text{AL},r}$ (Line 6) then
      - Line 7 checks if the relative longitudinal distance between $\text{OV}_{\text{SL},f}$ and HV is less than the safe distance of $\text{OV}_{\text{SL},f}$ plus constant. This is to make sure that the distance available behind the OV in front of the HV in the adjacent lane is greater so as to not cause a collision.

Equation	**Explanation**
(2-2a)	*true* if the relative velocity of $\text{OV}_{\text{SL},f}$ and HV is greater than zero, *false* otherwise
(2-2b)	*true* if the relative longitudinal distance between $\text{OV}_{\text{SL},f}$ and HV is less than the safe distance of $\text{OV}_{\text{SL},f}$ plus constant, *false* otherwise
(2-2c)	*true* if the relative velocity of $\text{OV}_{\text{AL},f}$ and $\text{OV}_{\text{SL},f}$ is greater than zero, *false* otherwise
(2-2d)	*true* if the relative longitudinal distance between $\text{OV}_{\text{SL},f}$ and $\text{OV}_{\text{AL},f}$ is less than the difference in their safe distances, *false* otherwise
(2-2e)	*true* if the relative longitudinal distance between HV and $\text{OV}_{\text{AL},r}$ is greater than the safe distance of $\text{OV}_{\text{AL},r}$, *false* otherwise

Table 2-3: Logical Expressions used in calculation of flag_{LC}

Algorithm 1: Algorithm to calculate flag_{LC}

Data: HV data, OV data, safe distance measure, $\text{flag}_{\delta}, \text{flag}_{\epsilon_1}, \text{flag}_{\epsilon_2}$

Result: flag_{LC}

1 **begin**
2   **if** $flag_{\delta} = true$ **then**
3   **if** (2-2a)=*true* **then**
4   **if** $flag_{\epsilon_1} = false$ & $flag_{\epsilon_2} = false$ **then**
5   **Set:** $flag_{LC} \leftarrow true$
6   **else if** $flag_{\epsilon_1} = true$ & $flag_{\epsilon_2} = false$ **then**
7   **if** (2-2b)=*true* & (2-2c)=*true* & (2-2d)=*true* **then**
8   **Set:** $flag_{LC} \leftarrow true$
9   **else if** $flag_{\epsilon_1} = false$ & $flag_{\epsilon_2} = true$ **then**
10   **if** (2-2e)=*true* **then**
11   **Set:** $flag_{LC} \leftarrow true$
12   **else if** $flag_{\epsilon_1} = true$ & $flag_{\epsilon_2} = true$ **then**
13   **if** (2-2b)=*true* & (2-2c)=*true* & (2-2d)=*true* & (2-2e)=*true* **then**
14   **Set:** $flag_{LC} \leftarrow true$
15   **else**
16   **Set:** $flag_{LC} \leftarrow false$
17   **else**
18   **Set:** $flag_{LC} \leftarrow false$
19   **else**
20   **Set:** $flag_{LC} \leftarrow false$

- Line 7 checks if the relative velocity of $\text{OV}_{\text{SL},f}$ and $\text{OV}_{\text{SL},f}$ is greater than zero. This is to ensure that the vehicle does not change lanes multiple times.
- Line 7 checks if the relative longitudinal distance between $\text{OV}_{\text{SL},f}$ and

$\mathrm{OV}_{\mathrm{AL},f}$ is less than the difference in their safe distances. This is to make sure that the distance available behind the OV in front of the HV in the adjacent lane is greater so as to not cause a collision.

if the above conditions are true, lane change is allowed.

* if $\mathrm{OV}_{\mathrm{AL},r}$ exists but not $\mathrm{OV}_{\mathrm{AL},f}$, (Line 9) then
  · Line 10 checks if the relative longitudinal distance between HV and $\mathrm{OV}_{\mathrm{AL},r}$ is greater than the safe distance of $\mathrm{OV}_{\mathrm{AL},r}$. This is to prevent rear-end collisions in case the HV has to suddenly apply brakes after a lane change.

  if the above condition is true, lane change is allowed.
* if both $\mathrm{OV}_{\mathrm{AL},f}$ and $\mathrm{OV}_{\mathrm{AL},r}$ exist (Line 12), then
  · Line 13 checks if the relative longitudinal distance between $\mathrm{OV}_{\mathrm{SL},f}$ and HV is less than the safe distance of $\mathrm{OV}_{\mathrm{SL},f}$ plus constant. This is to make sure that the distance available behind the OV in front of the HV in the adjacent lane is greater so as to not cause a collision.
  · Line 13 checks if the relative velocity of $\mathrm{OV}_{\mathrm{SL},f}$ and $\mathrm{OV}_{\mathrm{SL},f}$ is greater than zero. This is to ensure that the vehicle does not change lanes multiple times.
  · Line 13 checks if the relative longitudinal distance between $\mathrm{OV}_{\mathrm{SL},f}$ and $\mathrm{OV}_{\mathrm{AL},f}$ is less than the difference in their safe distances. This is to make sure that the distance available behind the OV in front of the HV in the adjacent lane is greater so as to not cause a collision.
  · Line 13 checks if the relative longitudinal distance between HV and $\mathrm{OV}_{\mathrm{AL},r}$ is greater than the safe distance of $\mathrm{OV}_{\mathrm{AL},r}$. This is to prevent rear-end collisions in case the HV has to suddenly apply brakes after a lane change.

  if the above conditions are true, lane change is allowed.
* if all the above conditions are not true then the lane change is not safe (Line 16).

– if not true then the lane change is not safe (Line 18).

- if not true, the lane change is not safe (Line 20).

The algorithm is designed such that the expressions defined in (2-2) are not checked is a flags representing the presence or absence of $\mathrm{OV}_{\mathrm{SL},f}$, $\mathrm{OV}_{\mathrm{AL},f}$ and $\mathrm{OV}_{\mathrm{AL},r}$ are false, there are no errors.

2-3 Coordinate Systems

The thesis uses two different coordinate frames as seen by the black and blue coordinates systems shown in Figure 2-5. The interpretation of the two distinctly coloured cars is as follows: (1) the black car represents the state of the HV at the start of the control algorithm and (2) the blue car represents the current state of the HV. In addition, two distinct coordinate frames are visible. The black coordinate frame, with the lateral position on the right lane boundary with longitudinal position coinciding with the CoG of the black car and has its x-axis aligned with the longitudinal road direction, represents the global road coordinate

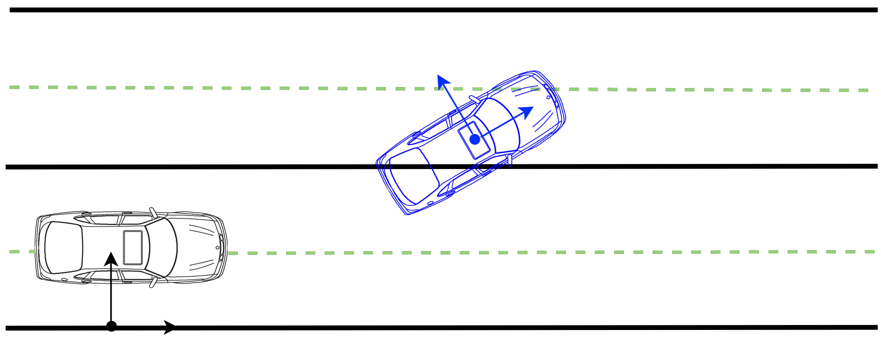

Figure 2-5: Different coordinate frames used.

frame. The blue coordinate frame represents the local HV coordinate frame at the current time and is fixed to the centre of gravity of the blue vehicle. The x and y axes of the local HV coordinate frame are aligned with the direction of the current longitudinal and lateral directions of the HV. The measurements of the longitudinal and lateral position are done in the global road coordinate frame and other states are measured with respect to the local HV coordinate frame.

2-4 Assumptions

Having understood the concept of safe driving and defining measures for collision avoidance and lane changing, we now discuss some simplifying assumptions made during the design of the APF-MPC and the MIMPC+APF-MPC algorithms. The relaxation of these assumptions are considered as future research direction.

- The road is an infinitely long two-lane road with no curvature.
- All vehicles move from left to right on the road.
- A vehicle cannot have negative velocity.
- The size and shape of the OV are the same as that of the HV.
- OV data available to us is deterministic in nature and available at each control loop.
- OV travel at the centre of the lane at a constant speed.
- OV data available only include OV within the ROI.

Chapter 3

Artificial Potential Fields

The APF method works by modelling the AV as a charged particle that moves under an electric field toward an attracting target. Obstacles are represented by particles of opposite charge that repel the AV. The concept was first introduced by Khatib et. al. [27] and has been used widely in robotics for path planning. The APF method assumes that complete information about the surrounding area is available before the start of the algorithm. The basic idea of the APF method begins with the definition of the attractive and repulsive potential, each representing the goal and the obstacles respectively. This chapter is divided into three chapters. Section 3-1 explains the basic idea of an APF method for path planning. Section 3-2 and 3-3 show the formulation of the potentials used further in this thesis.

3-1 Basics: APF

Given n obstacles, let $\mathcal{X} = \left[\begin{smallmatrix} X & Y \end{smallmatrix}\right]^T$, $\mathcal{X}_g = \left[\begin{smallmatrix} X_g & Y_g \end{smallmatrix}\right]^T$ and $\mathcal{X}_{o_j} = \left[\begin{smallmatrix} X_{o_j} & Y_{o_j} \end{smallmatrix}\right]^T$ where $j = 1, 2, 3 \dots n$ be any point under review in the environment, the goal position and the location of the j^{th} obstacle respectively in the 2-D plane. The basic attractive potential U_{att} and the repulsive potential for the j^{th} obstacle U^j_{rep} are defined [27] as

$$U_{\text{att}}(\mathcal{X}) = \frac{1}{2} k_{\text{att}} \parallel \mathcal{X} - \mathcal{X}_g \parallel^2 \tag{3-1}$$

$$U^j_{\text{rep}}(\mathcal{X}) = \begin{cases} \frac{1}{2} k_{\text{rep}} \left(\frac{1}{\rho(\mathcal{X})} - \frac{1}{\rho^j_o} \right)^2 & \text{if } \rho(\mathcal{X}) \leqq \rho^j_o \\ 0 & \text{if } \rho(\mathcal{X}) > \rho^j_o \end{cases} \tag{3-2}$$

where ρ^j_o is the limit distance of the potential field influence defining the maximum distance from its centre within which the obstacle has an influence and $\rho(\mathcal{X})$ is the distance to the obstacle from $\mathcal{X}$. Having defined the attractive and the repulsive fields, the total artificial potential field U_{apf} is given by

$$\begin{aligned} U_{\text{apf}}(\mathcal{X}) &= U_{\text{att}}(\mathcal{X}) + \sum_{j=1}^{n} U_{\text{rep}}^{j}(\mathcal{X}) \\ &= U_{\text{att}}(\mathcal{X}) + U_{\text{rep}}(\mathcal{X}). \end{aligned} \tag{3-3}$$

The environment is therefore assigned a potential value at each point. A gradient descent method is used to find the path through the obstacles. The final path is defined using the attractive force $F_{\text{att}}(\mathcal{X})$ of the goal and the repulsive force for the j^{th} obstacle, $F_{\text{rep}_j}(\mathcal{X})$ is given by

$$\begin{aligned} F_{\text{att}}(\mathcal{X}) &= -\nabla U_{att}(\mathcal{X}) \\ &= -k_{att}\left(\mathcal{X} - \mathcal{X}_g\right) \end{aligned} \tag{3-4}$$

$$\begin{aligned} F_{\text{rep}_j}(\mathcal{X}) &= -\nabla U_{\text{rep}}^{j}(\mathcal{X}) \\ &= \begin{cases} k_{\text{rep}}\left(\frac{1}{\rho(\mathcal{X})} - \frac{1}{\rho_o^j}\right)\frac{1}{\rho(\mathcal{X})^2}\frac{\partial\rho}{\partial\mathcal{X}} & \text{if } \rho(\mathcal{X}) \le \rho_o^j \\ 0 & \text{if } \rho(\mathcal{X}) > \rho_o^j \end{cases} \\ \text{where } \frac{\partial\rho}{\partial\mathcal{X}} &= \begin{bmatrix} \frac{\partial\rho}{\partial X} & \frac{\partial\rho}{\partial Y} \end{bmatrix}^T. \end{aligned} \tag{3-5}$$

The total force applied at $\mathcal{X}$ is given by

$$\begin{aligned} F(\mathcal{X}) &= -\nabla U_{\text{apf}}(\mathcal{X}) \\ &= -\nabla U_{\text{att}}(\mathcal{X}) - \sum_{j=1}^{n} \nabla U_{\text{rep}}(\mathcal{X}) \\ &= F_{\text{att}}(\mathcal{X}) + F_{\text{rep}}(\mathcal{X}). \end{aligned} \tag{3-6}$$

The APF method is widely used as opposed to other strategies because it can consider the issues of collision avoidance and direction estimation at the same time while having a small computational burden. However, traditional APF method suffers from a number of problems [49]:

- Lack of net artificial force at certain locations due to opposing forces from the obstacles and the goal respectively may trap the vehicle in a local minimum.
- goal not being able to be reachable with obstacles nearby due to the repulsive potential of the obstacles greater than that of the attractive potential of the goal.

A number of ideas have been proposed to solve the disadvantages of the APF method. Different repulsive and attractive potential functions have been defined as repulsive potential fields with spherical symmetry like a Gaussian shape do not create local minima [50]. Yang et al. [51] also propose a potential field dependent on the Euclidean distance between the goal and the vehicle to overcome the problem of the goal not being reachable. This thesis uses two different repulsive potentials called the obstacle potential field and the road potential field. Each of these potentials is used to denote a specific kind of obstacle that the HV should avoid.

3-2 Obstacle Potential Field

The obstacle potential represents the task of avoiding other vehicles on the road. Superquadric functions are used to denote every OV on the road as they mimic the shape of the obstacle in the region around it while having spherical symmetry in the region away from it [50, 52]. The Yukawa potential is one such superquadric potential and represents an obstacle as an exponential function of the euclidean distance between the HV and OV. Yukawa potential acts like a penalty function that goes from zero in the region away from the obstacle to infinity at the boundary and within the body of the obstacle. The mathematical expression for the Yukawa potential of the j^{th} obstacle is given by

$$U_{\text{yuk}}^{j}\left(\mathcal{X}, B^{j}\right) = A_{\text{yuk}} \frac{e^{-b_{\text{yuk}}\text{dist}\left(\mathcal{X}, B^{j}\right)}}{\text{dist}\left(\mathcal{X}, B^{j}\right)}. \tag{3-7}$$

where $\text{dist}\left(\mathcal{X}, \zeta\right)$ is a function representing the euclidian distance between the coordinates of $\mathcal{X} = [\, X \; Y \,]^T$ with the closest point in the coordinate set ζ, $\mathcal{X}$ is any point on the global coordinate frame, B^j is the set of points representing the j^{th} obstacle, $j = 1, 2, \ldots, N_{\text{OV}}$ with N_{OV} representing the number of OV within the ROI and A_{yuk} and b_{yuk} are constants and are given in Table 3-1.

Description	**Value**	**Symbol**
Scaling constant of the Yukawa potential	100	A_{yuk}
Constant to control the slope of the Yukawa potential	0.001	b_{yuk}

Table 3-1: Scalar values of constants used to calculate U_{yuk}

The euclidean distance function between the coordinates of $\mathcal{X}$ with the closest point in the coordinate set ζ is defined as

$$\text{dist}\left(\mathcal{X}, \zeta\right) = \min_{b \in \zeta} \|\mathcal{X} - b\| \tag{3-8}$$

$$\text{dist}\left(\mathcal{X}, B^{j}\right) = \min_{b \in B^{j}} \|\mathcal{X} - b\| \tag{3-9}$$

Figure 3-1 shows a Yukawa potential. However, the design of the Yukawa potential has the following problems: (1) The vehicle detects the change in potential due to the obstacle only after it reaches close to the vehicle making it dangerous in case of sudden braking by the obstacle, (2) As the shape of the potential follows the shape of the obstacle, the HV does not get any help to make smooth lane change manoeuvres and maintain a safe distance from the obstacle.

A new obstacle potential is therefore proposed to combat these problems exhibited by the Yukawa potential. First, the negative exponential part of the Yukawa potential is replaced by an inverse logarithm so as to extend the range of influence of the potential. Figure 3-2 shows the comparison between the 2-D versions of the Yukawa potential and the newly designed potential for clarity.

The second improvement is the addition of a wedge-shaped block behind the obstacle for maintaining a safe distance and aid smooth lane changes [1] as seen in Figure 3-3 where blue

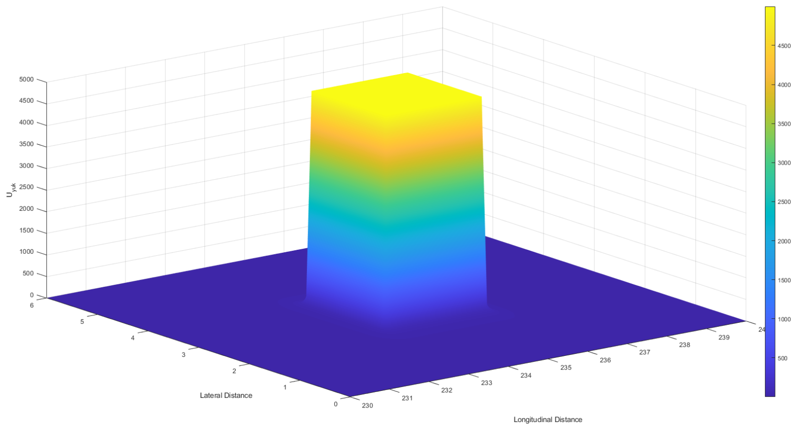

Figure 3-1: Yukawa Potential

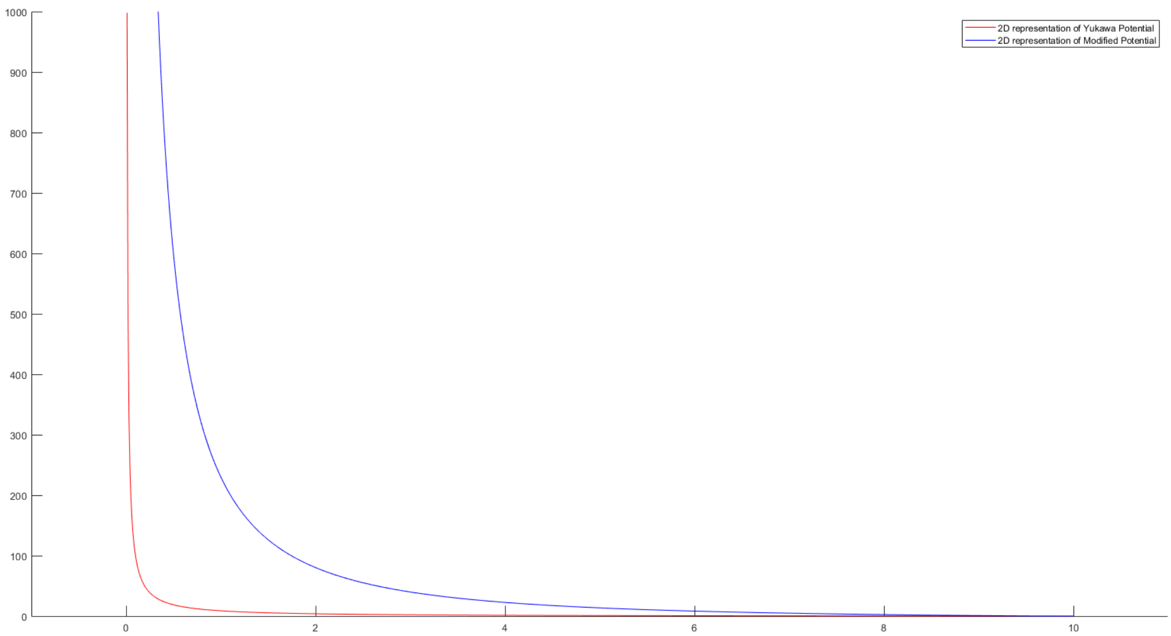

Figure 3-2: Comparison of the curvature of between the 2-D version of the Yukawa potential (in red) and defined obstacle potential (blue)

represents the actual obstacle, grey represents the wedge-shaped block added to maintain a safe distance and to aid lane change. The height of the wedge-shaped block is given by the safe distance measure defined in Section 2-2-1. The mathematical formulation of the new obstacle APF for the j^{th} obstacle is therefore given by

$$U_{\text{obs}}^{j}\left(\mathcal{X}, B^{j}\right) = -\frac{A_{\text{obs}} \ln\left(b_{\text{obs}} \text{dist}\left(\mathcal{X}, B^{j}\right)\right)}{\text{dist}\left(\mathcal{X}, B^{j}\right)} \tag{3-10}$$

where A_{obs} and b_{obs} is a positive constant given in Table 3-2 and B^{j} is is extended to include wedge-shaped block and is dependent on the safe distance of the j^{th} OV.

The orthogonal view of the new obstacle potential is shown in Figure 3-4. This newly designed potential will be referred to as the obstacle APF further in this thesis. It can however be seen

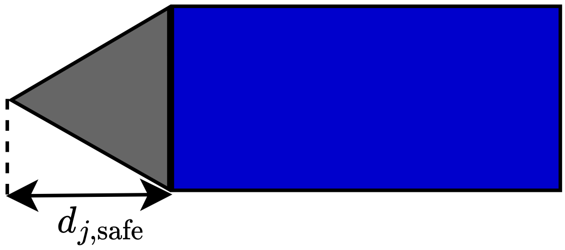

Figure 3-3: Representation of the different parts of the obstacle

Description	Value	Symbol
Scaling constant of the Obstacle APF	1	A_{obs}
Constant to control the slope of the Obstacle APF	0.01	b_{obs}

Table 3-2: Scalar values of constants used to calculate U_{obs}

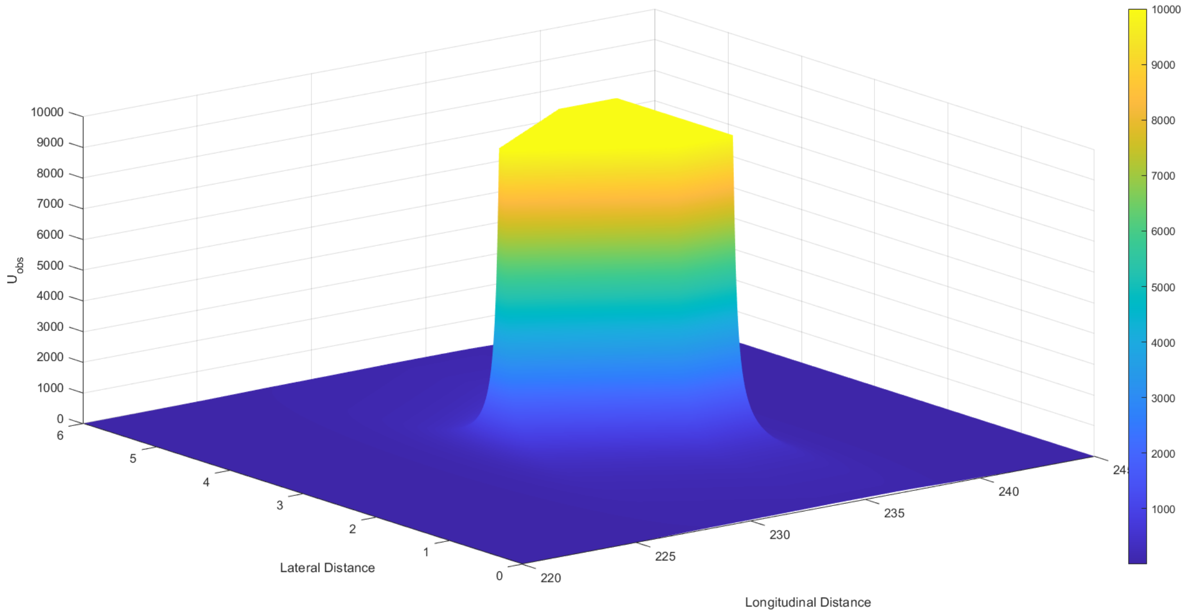

Figure 3-4: 3-D orthogonal representation of the obstacle APF

that the obstacle potential is non-convex in nature and therefore increases the complexity of the control strategy. To reduce computation time and simplify the control strategy, a convex approximation of the obstacle APF is proposed. The idea is to divide the region around the obstacle into regions and define a convex approximation of the obstacle APF in any given region. First, the area around the obstacle is divided into ten different regions as seen in Figure 3-5 where v_i where $i = 1, 2, \ldots, 5$ are the vertices of the j^{th} obstacle and $L_e(\mathcal{X}) := A_e X + B_e Y + C_e$ where $e = 1, 2, \ldots, 10$ are lines which divide the area around the j^{th} obstacle into regions R_e. The upcoming subsections give some basic theory required for the convexification of the obstacle APF.

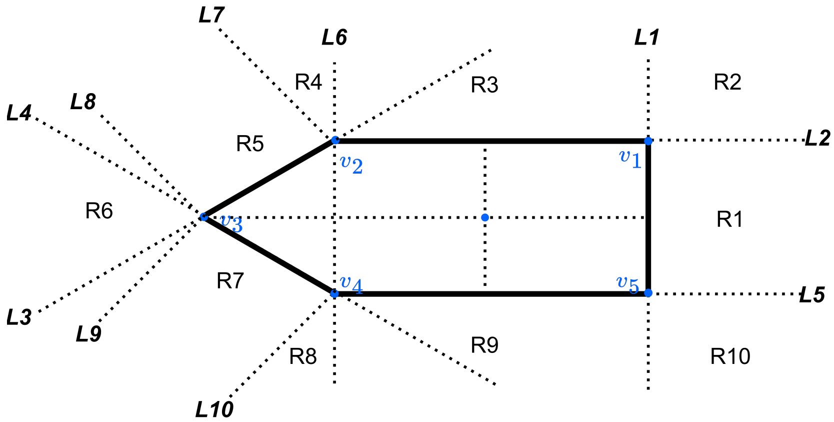

Figure 3-5: Division of the obstacle's surroundings into multiple regions

3-2-1 Location of a point with respect to a line

This subsection defines how to find the location of a point with respect to a line. This is used to find the region R_{HV} around a given OV the HV lies in. Given a line $L(\mathcal{X}) = AX + BY + C$ and $\mathcal{X}_p = [\, X_p \; Y_p \,]^T$ be a point. The idea is to check if the point is above/ in front or below/ behind a given line. Table 3-3 shows the multiple combinations of the line and point and the expression to be used to check the location of the point with respect to the line. For example,

Orientation of the Line	Expression Used
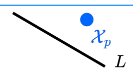	$AX_p + BY_p + C \geq 0$
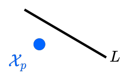	$AX_p + BY_p + C \leq 0$
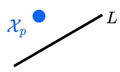	$AX_p + BY_p + C \geq 0$
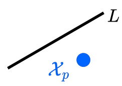	$AX_p + BY_p + C \leq 0$
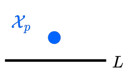	$Y_L - Y_p \leq 0$
	$Y_L - Y_p \geq 0$
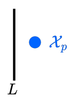	$X_L - X_p \leq 0$
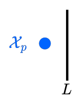	$X_L - X_p \geq 0$

Table 3-3: Expression to be used to check the relative location of $\mathcal{X}_p$ with $L(\mathcal{X})$

it can be checked if a point is above a given line by replacing the coordinates of the point in the line and checking if it is greater than zero and vice versa.

3-2-2 Distance of a Point from a Line Segment

This subsection formulates the minimum distance of a point from a given line segment. Let endpoints of the line segment LS are $\mathcal{X}_{LS_1} = [\, X_{LS_1} \; Y_{LS_1} \,]^T$ and $\mathcal{X}_{LS_2} = [\, X_{LS_2} \; Y_{LS_2} \,]^T$ and $\mathcal{X}_p = [\, X_p \; Y_p \,]^T$ be the point from which we have to find the distance. The basic idea of this formulation comes from the idea of projection of the line segment joining one of the vertices of the LS with $\mathcal{X}_p$ onto LS (using the dot product) and normalizing it. Readers can refer to [53, 54] for more information and the derivation of the equations.

Let t be a variable defined as

$$t = \frac{(X_p - X_{LS_1})\,(X_{LS_2} - X_{LS_1}) + (Y_p - Y_{LS_1})\,(Y_{LS_2} - Y_{LS_1})}{(X_{LS_2} - X_{LS_1})^2 + (Y_{LS_2} - Y_{LS_1})^2}. \tag{3-11}$$

Table 3-4 shows the meaning of different values of t. The minimum distance between X_p and

Orientation of the Line	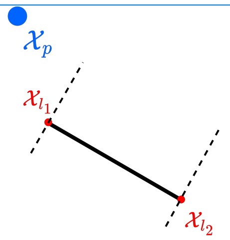	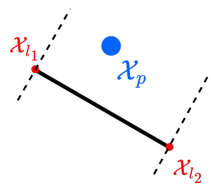	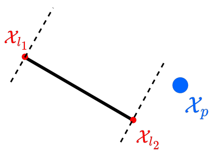
t	$t < 0$	$o \leq t \leq 1$	$t > 1$

Table 3-4: Meaning of different value of t

LS is given by

$$d_{p-ls}\,(\mathcal{X}_p, LS) = \begin{cases} \sqrt{(X_p - X_{LS_1})^2 + (Y_p - yY_{LS_1})^2} & \text{if } t < 0 \\ \sqrt{(X_p - (X_{LS_1} + t\,(X_{LS_2} - X_{LS_1})))^2 + (Y_p - (Y_{LS_1} + t\,(Y_{LS_2} - Y_{LS_1})))^2} & \text{if } 0 \leq t \leq 1 \\ \sqrt{(X_p - X_{LS_2})^2 + (Y_p - Y_{LS_2})^2} & \text{if } t > 1 \end{cases} \tag{3-12}$$

3-2-3 Convex Approximation of the Obstacle APF

This section discusses the method of formulating the convex approximation of the obstacle APF. The basic idea is to first find the region in which the HV lies using the theory explained in Section 3-2-1 and define a region-specific obstacle APF using the theory in Section 3-2-2.

Region Calculation: Let v_1, v_2, v_3, v_4 and v_5 be the vertices of the j^{th} obstacle respectively as shown in Figure 3-6. Table 3-5 shows the logical constraints used to find the region of a given

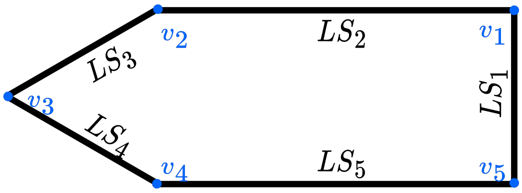

Figure 3-6: Boundaries of the OV

OV that the HV lies in. These expressions are dependent on $\mathcal{X}_{\text{HV}} = [\, x_{\text{HV}} \; y_{\text{HV}} \,]^T$ representing the coordinates of the CoG of the HV and $\mathcal{X}_{v_i} = [\, x_{v_i} \; y_{v_i} \,]^T$ represent the coordinates of the vertices of the j^{th} OV . Let us define R_{HV} as the region around the j^{th} OV that the HV lies in.

Region	**Logical Expression**
R_1	$X_{\text{HV}} - X_{v_1} > 0 \wedge Y_{\text{HV}} - Y_{v_1} \leq 0 \wedge Y_{\text{HV}} - Y_{v_5} > 0$
R_2	$X_{\text{HV}} - X_{v_1} \geq 0 \wedge Y_{\text{HV}} - Y_{v_1} > 0$
R_3	$X_{\text{HV}} - X_{v_1} < 0 \wedge Y_{\text{HV}} - Y_{v_1} > 0 \wedge X_{\text{HV}} - X_{v_2} \geq 0$
R_4	$X_{\text{HV}} - X_{v_2} < 0 \wedge A_7 X_{\text{HV}} + B_7 Y_{\text{HV}} + C_7 \geq 0$
R_5	$A_3 X_{\text{HV}} + B_3 Y_{\text{HV}} + C_3 > 0 \wedge A_7 X_{\text{HV}} + B_7 Y_{\text{HV}} + C_7 < 0 \wedge A_8 X_{\text{HV}} + B_8 Y_{\text{HV}} + C_8 \geq 0$
R_6	$A_8 X_{\text{HV}} + B_8 Y_{\text{HV}} + C_8 < 0 \wedge A_9 X_{\text{HV}} + B_9 Y_{\text{HV}} + C_9 \geq 0$
R_7	$A_4 X_{\text{HV}} + B_4 Y_{\text{HV}} + C_4 < 0 \wedge A_9 X_{\text{HV}} + B_9 Y_{\text{HV}} + C_9 < 0 \wedge A_{10} X_{\text{HV}} + B_{10} Y_{\text{HV}} + C_{10} \geq 0$
R_8	$X_{\text{HV}} - X_{v_4} \leq 0 \wedge A_{10} X_{\text{HV}} + B_{10} Y_{\text{HV}} + C_{10} < 0$
R_9	$X_{\text{HV}} - X_{v_1} \leq 0 \wedge X_{\text{HV}} - x_{v_4} > 0 \wedge Y_{\text{HV}} - Y_{v_5} < 0$
R_{10}	$X_{\text{HV}} - X_{v_1} > 0 \wedge Y_{\text{HV}} - Y_{v_1} \leq 0$

Table 3-5: Logical expressions to check the region around an OV the HV lies in.

Euclidian Distance Calculation: Let LS_1, LS_2, LS_3, LS_4 and LS_5 be the line segments between v_5 and v_1, v_1 and v_2, v_2 and v_3, v_3 and v_4 and v_4 and v_5 respectively as shown in Figure 3-6 representing the boundaries of the j^{th} OV.

The minimum distance of the CoG of the HV from the j^{th} OV in a given region is equal to the distance between the CoG of the HV and the boundary of the j^{th} OV in the respective region. Therefore, the distance function $\text{dist}\,(\mathcal{X}, B^j)$ used in (3-10) is replaced with the distance function $d_{p-ls}\,(\mathcal{X}_p, LS_l)$ formulated in (3-12) in the region R_{HV} to generate a convex obstacle APF for each region where LS_l is the line segment representing the boundary of the

j^{th} obstacle bordering R_{HV} with $l = 1, 2, \ldots, 5$. The convex obstacle APF for the j^{th} obstacle for then becomes

$$U^{j,l}_{\text{obs}_{\text{conv}}} \left(\mathcal{X}_{\text{HV}}, LS_l\right) = -\frac{A_{\text{obs}} \ln \left(b_{\text{obs}} d_{p-ls} \left(\mathcal{X}_{\text{HV}}, LS_l\right)\right)}{d_{p-ls} \left(\mathcal{X}_{\text{HV}}, LS_l\right)} \tag{3-13}$$

Table 3-6 shows the line segment representing the nearest boundary of the j^{th} OV for each region around the OV. If the HV is in regions R_1, R_3, R_5, R_7 and R_9, the closest distance

Region	Closest Line Segment
Region 1 and Region 2	LS_1
Region 3 and Region 4	LS_2
Region 5 and Region 6	LS_3
Region 7 and Region 8	LS_4
Region 9 and Region 10	LS_5

Table 3-6: Line Segment used to calculate $d_{p-ls}\left(\mathcal{X}_p, LS_l\right)$ based on region

will be the minimum distance between X_{HV} and the closest point on the corresponding line segment whereas if the HV is in regions R_2, R_4, R_6, R_8 and R_{10}, the closest distance will be the minimum distance between the CoG of the HV and the closest endpoint of the corresponding line segment. Figure 3-7 show the physical representation of $d_{p-ls}\left(\mathcal{X}_p, LS_l\right)$ when the HV is in R_1 and R_2 respectively.

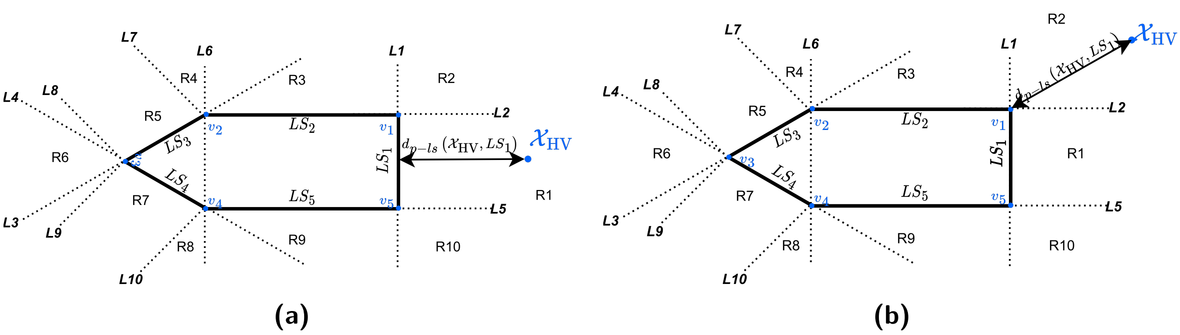

Figure 3-7: Distance between the CoG of the HV and the closest point on the OV for (a) R_1 and (b) R_2

The algorithm that describes the process used to calculate the convex approximation of the j^{th} obstacle APF, $U^{j,l}_{\text{obs}_{\text{conv}}} \left(\mathcal{X}_{\text{HV}}, LS_l\right)$ is given by Algorithm 2.

Algorithm 2: Algorithm to calculate the convex approximation of the obstacle APF

Data: $\mathcal{X}_{\text{HV}}$, A_{obs}, b_{obs}, A_e, B_e, C_e, $\mathcal{X}_{v_i}$, $\mathcal{X}_{1,LS_l}$, $\mathcal{X}_{2,LS_l}$

Result: $U^{j,l}_{\text{obs}_{\text{conv}}}\left(\mathcal{X}_{\text{HV}}, LS_l\right)$

begin

  R_{HV}=`CalculateHVRegion(`$\mathcal{X}_{HV}$, A_e, B_e, C_e, $\mathcal{X}_{v_i}$`)`

  switch *region* **do**

    case R_{HV}== R_1 **do**

      $d_{p-ls}\left(\mathcal{X}_{\text{HV}}, LS_1\right)$= `CalculateDist(`*region*, $\mathcal{X}_{HV}$, $\mathcal{X}_{1,LS_1}$, $\mathcal{X}_{2,LS_1}$`)` break

    case R_{HV}== R_2 **do**

      $d_{p-ls}\left(\mathcal{X}_{\text{HV}}, LS_1\right)$= `CalculateDist(`*region*, $\mathcal{X}_{HV}$, $\mathcal{X}_{1,LS_1}$, $\mathcal{X}_{2,LS_1}$`)` break

      $\vdots$

    case R_{HV}== R_{10} **do**

      $d_{p-ls}\left(\mathcal{X}_{\text{HV}}, LS_5\right)$= `CalculateDist(`*region*, $\mathcal{X}_{HV}$, $\mathcal{X}_{1,LS_5}$, $\mathcal{X}_{2,LS_5}$`)` break

  $U^{j,l}_{\text{obs}_{\text{conv}}}\left(\mathcal{X}_{\text{HV}}, LS_l\right) = -\frac{A_{\text{obs}} \ln\left(b_{\text{obs}} d_{p-ls}(\mathcal{X}_{\text{HV}}, LS_l)\right)}{d_{p-ls}(\mathcal{X}_{\text{HV}}, LS_l)}$

where $\mathcal{X}_{v_i}$ are the coordinates of the vertices of the j^{th} OV, $\mathcal{X}_{1,LS_l}$ and $\mathcal{X}_{2,LS_l}$ are the coordinates of the endpoints of line segment LS_l, $R_{\text{HV}} = R_1, R_2, \ldots, R_{10}$ is the current region in which the HV lies in, *CalculateHVRegion* is a function used to calculate the current region around the OV in which $\mathcal{X}_{\text{HV}}$ lies and *CalculateK* is a function to generate the correct value of $d_{p-ls}\left(\mathcal{X}_p, LS_l\right)$ to be used in (3-13) to generate the obstacle APF based on the current region. The algorithms for these function definitions are given in Appendix B. The algorithm works as follows:

- Calculate the region around the OV which the HV lies in using the *CalculateHVRegion* function. The input to the *CalculateHVRegion* function is the position of the CoG of the HV, the heading angle of the HV, the vertices of the obstacle APF and the data about the lines dividing the area around the OV into regions. The algorithm of the *CalculateHVRegion* function is described by Algorithm 5.
- A switch case is used to calculate the correct value of $d_{p-ls}\left(\mathcal{X}_{\text{HV}}, LS_l\right)$ using the *CalculateDist* function described by Algorithm 6. The closest boundary of the OV is selected based on Table 3-6. The input to the *CalculateDist* function is the position of the CoG of the HV, the heading angle of the HV, the vertices of the obstacle APF and the data about the lines dividing the area around the OV into regions.
- The obtained value of $d_{p-ls}\left(\mathcal{X}_{\text{HV}}, LS_l\right)$ is used to obtain the convex approximation of the j^{th} obstacle potential, $U^{j,l}_{\text{obs}_{\text{conv}}}\left(\mathcal{X}_{\text{HV}}, LS_l\right)$ by replacing $\text{dist}\left(\mathcal{X}, \zeta\right)$ used in (3-10) with $d_{p-ls}\left(\mathcal{X}_p, LS_l\right)$.

Figure 3-8 shows the contours of the obstacle APF before and after approximation. It can be seen that the contours follow each other well.

The obtained convex approximation of the obstacle APF can be further simplified with the help of a quadratic approximation of the obstacle APF obtained as the output of Algorithm 2. Let us define a function $quad\left(U\right)$ used to calculate the quadratic Taylor-series approximation of any potential U. Appendix A shows the definition of $quad\left(U\right)$. The quadratic Taylor-series

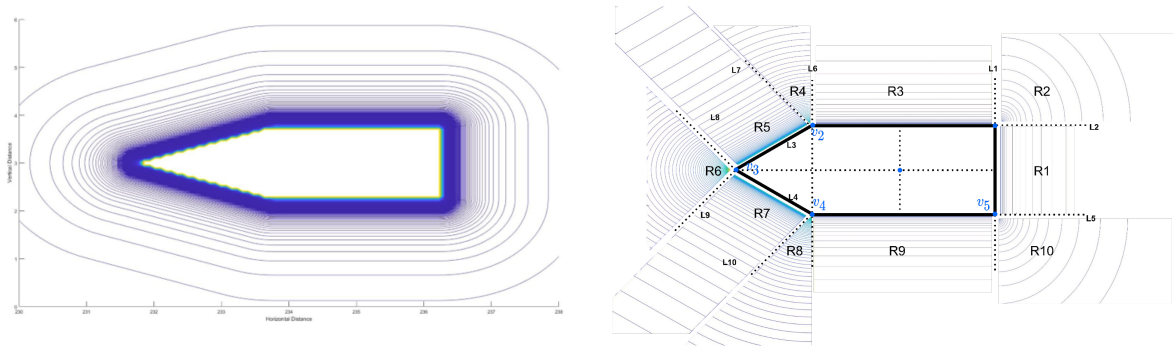

(a) **(b)**

Figure 3-8: Contour of the obstacle APF for (a) the obstacle APF, (b) the convex approximation of the obstacle APF for all the regions

approximation of the convex approximation of the j^{th} obstacle APF can therefore represented as

$$quad\left(U^{j,l}_{\text{obs}_{\text{conv}}}\left(\mathcal{X}_{\text{HV}}, LS_l\right)\right)$$

The total obstacle APF is defined as the sum of the quadratic Taylor-series approximation of the convex approximation of all obstacle APF and is represented as

$$U_o\left(\mathcal{X}_{\text{HV}}\right) = \sum_{j=1}^{N_{\text{OV}}} quad\left(U^{j,l}_{\text{obs}_{\text{conv}}}\left(\mathcal{X}_{\text{HV}}, LS_l\right)\right) \tag{3-14}$$

3-3 Road Potential Field

The road potential field is used to keep the HV away from the edges of the road to ensure safe driving within the road boundaries. The road APF therefore has two important requirements: (1) to keep the HV from leaving the road boundaries and (2) to prevent the HV to drive very close to the road boundary. Road potentials are an integral part of any APF based collision avoidance algorithms. This thesis uses simple definitions of road potential to reduce the complexity of the control strategy. The two different formulations of the road potential used in the thesis are defined in the following subsections.

3-3-1 Road APF for APF-MPC algorithm

The road APF for the APF-MPC algorithm is a basic road potential which fulfils the two requirements of the road potential. The road potential is given by a combination of penalty functions at each of the road boundaries. The mathematical expression for the road potential field is expressed as [1]

$$U_r\left(\mathcal{X}\right) = \frac{1}{2}\eta\sum_i\left(\frac{1}{Y - Y_i^{\text{road}}}\right)^2 \tag{3-15}$$

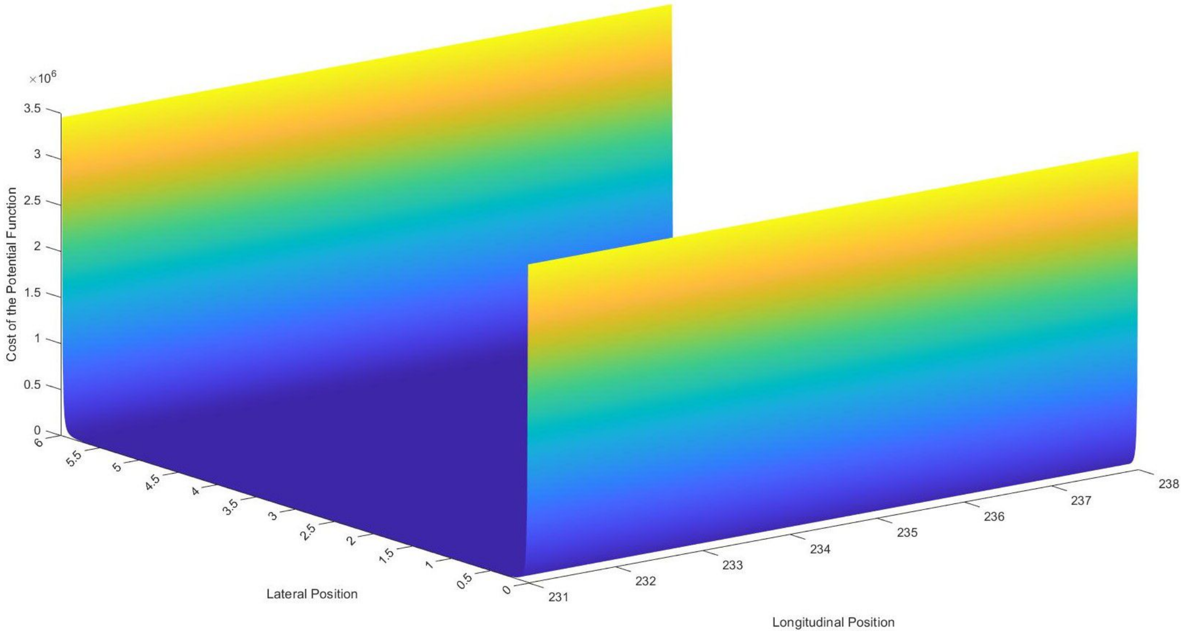

Figure 3-9

Figure 3-10: Orthogonal View of the Road Potential $U_r(\mathcal{X})$

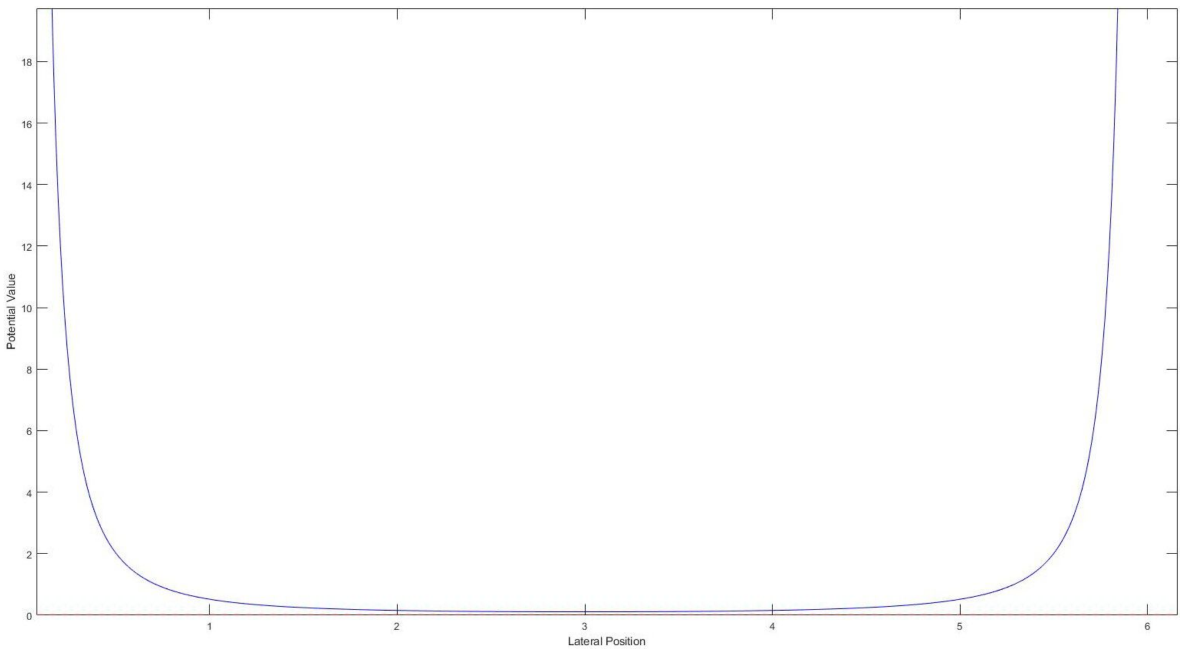

Figure 3-11: Side View of Quadratic Road Potential $U_r(\mathcal{X})$

where Y_i^{road} is the lateral position of the road boundaries in global road coordinates, $i \in \{1, 2\}$ and η is a scaling factor. Table 3-7 shows the values of constants used in (3-16). Figure 3-10 shows the 3-D orthogonal view of the road potential.

This road potential however does not keep the vehicle in the lane centre as the potential is

Description	Value	Symbol
Scaling constant of the Road APF for APF-MPC algorithm	1	η
Right lane boundary	0	Y_1
Left lane boundary	6	Y_2

Table 3-7: Scalar values of constants used to calculate $U_r\left(\mathcal{X}_{\text{HV}}\right)$

not zero away from the edges of the road as seen in Figure 3-11. The road potential slopes such that there is a minimum at the centre of the road. This road potential is approximated to a quadratic potential around the CoG of the HV by a Taylor series approximation defined in Appendix A to simplify the MPC optimal control problem. The quadratic road potential for the APF-MPC algorithm is therefore given by

$$U_{r_{quad}}\left(\mathcal{X}\right) = quad\left(U_r\left(\mathcal{X}\right)\right) \tag{3-16}$$

3-3-2 Road APF for MIMPC+APF-MPC algorithm

The road APF for the MIMPC+APF-MPC algorithm is a road potential that generates a convex potential which is skewed towards the centre of a given lane. The road potential is a combination of two basic potentials; (1) a road potential which goes to infinity on the edges of the road and is almost flat elsewhere (3-16) and (2) a LINear EXponential (LINEX) loss function [55] to skew it towards the centre of the given lane. The combined mathematical expression is given by

$$U_{L_*,r}\left(\mathcal{X}\right) = \underbrace{b_{r,*}\left(e^{a_{r,*}(Y-Y_{\text{lane}})} - a_{r,*}\left(Y - Y_{\text{lane}}\right) - 1\right)}_{\text{LINEX Loss Function}} + \underbrace{\frac{1}{2}\eta\sum_i\left(\frac{1}{Y - Y_i^{\text{road}}}\right)^2}_{\text{Penalty Function}} \tag{3-17}$$

where $a_{r,*}$ and $b_{r,*}$ are constants used to tune the shape of the road potential where $* \in \{0,1\}$

Lane	Description	Value	Symbol
Lane 0	Rate of Change of Skew for the LINEX loss function	-2	$a_{r,*}$
	Scaling Factor for the LINEX loss function	1×10^5	$b_{r,*}$
	Centre of the lane	1.5	Y_{lane}
Lane 1	Rate of Change of Skew for the LINEX loss function	2	$a_{r,*}$
	Scaling Factor for the LINEX loss function	1×10^5	$b_{r,*}$
	Centre of the lane	4.5	y_{lane}

Table 3-8: Scalar values of constants used to calculate $U_{L_*,r}\left(\mathcal{X}_{\text{HV}}\right)$

defines if the road potential is for Lane 0 or Lane 1, Y_{lane} is the lateral position of the given lane centre, Y_i^{road} is the lateral position of the road boundaries in global road coordinates, $i \in \{1, 2\}$ and η is a scaling factor. Table 3-8 shows the values of the different constants used in (3-17) for both lanes.

Figure 3-12a and Figure 3-12b show the orthogonal view of the skewed road potential when the selected lane is Lane 0 or Lane 1 respectively. This road potential is approximated to a

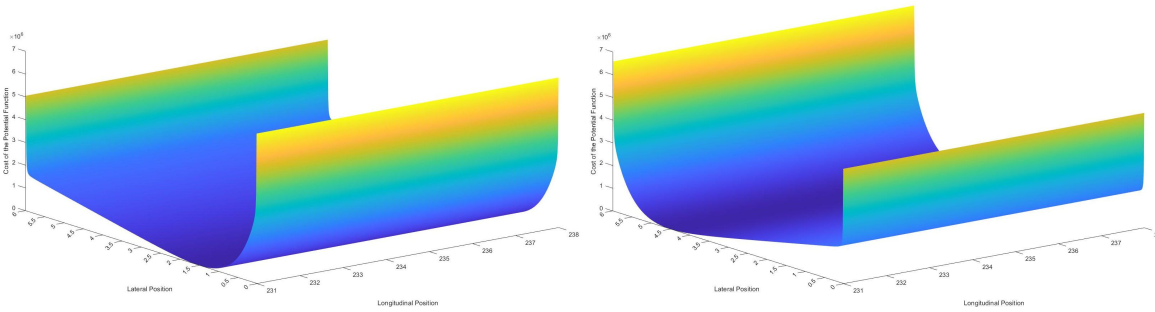

(a) **(b)**

Figure 3-12: Orthogonal View of Quadratic Road Potential (a) $U_{L_0,r}\left(\mathcal{X}_{\mathsf{HV}}\right)$, (b) $U_{L_1,r}\left(\mathcal{X}_{\mathsf{HV}}\right)$

quadratic potential around the CoG of the HV by a Taylor series approximation defined in Appendix A to simplify the MPC optimal control problem. The quadratic road potential for the MIMPC+APF-MPC algorithm is therefore given by

$$U_{L_*,r_{quad}}\left(\mathcal{X}\right) = quad\left(U_{L_*,r}\left(\mathcal{X}\right)\right) \tag{3-18}$$

Chapter 4

Vehicle Control System (VCS)

The race to provide increasingly better systems for driver support has led to competition between automotive manufacturers. This is true even for autonomous vehicles with manufacturers competing with increasingly better features. However, it is to be kept in mind that each of these subsystems has to be integrated into a single module to coordinate with each other to provide high performance of the AV.

Vehicle Control System performs the task of integrating the different goals of the subsystems into a single task and effectively finding a set of actuator inputs to help fulfil these goals. These tasks include but are not limited to energy efficiency, passenger comfort, reference tracking etc. These tasks can be pre-programmed like the bounds for acceleration or jerk which can lead to discomfort of the passengers or can be generated onboard like the path to track generated by the path planner for the vehicle controller to follow. An AV can however only give a certain number of control inputs to track these goals. These inputs for an autonomous ground vehicle are the throttle and the steering angle. VCS also have to deal with both longitudinal and lateral control.

MPC is an optimization-based control strategy which has been widely used in the design on VCS due to its incorporation of the model and constraints of the system and its surroundings, support for multi-input multi-output and the wide range of problems it can solve [56][57]. This chapter is divided as follows; Section 4-1 discusses the formulation of MPC for standard MPC and MIMPC. Section 4-2 introduces the system models used in the APF-MPC and MIMPC+APF-MPC control strategies respectively. Section 4-3 and Section 4-4 expand upon the formulation of the different vehicle models in each strategy and formulates the APF-MPC and MIMPC+APF-MPC control strategies respectively.

4-1 Model Predictive Control (MPC)

Model Predictive Control (MPC) is a control strategy in which the control input to be applied to the system is attained by solving a finite horizon optimal control problem online by using the current state of the system as its initial state. The design of MPC is divided into two parts: (1) the system model defined based on the mathematical model of the system to be controlled and (2) the optimization problem used to attain the desired control input. Figure 4-1 shows the basic block diagram of MPC control strategy and its interaction with the system under consideration. The system model predicts the system's response to a set of control

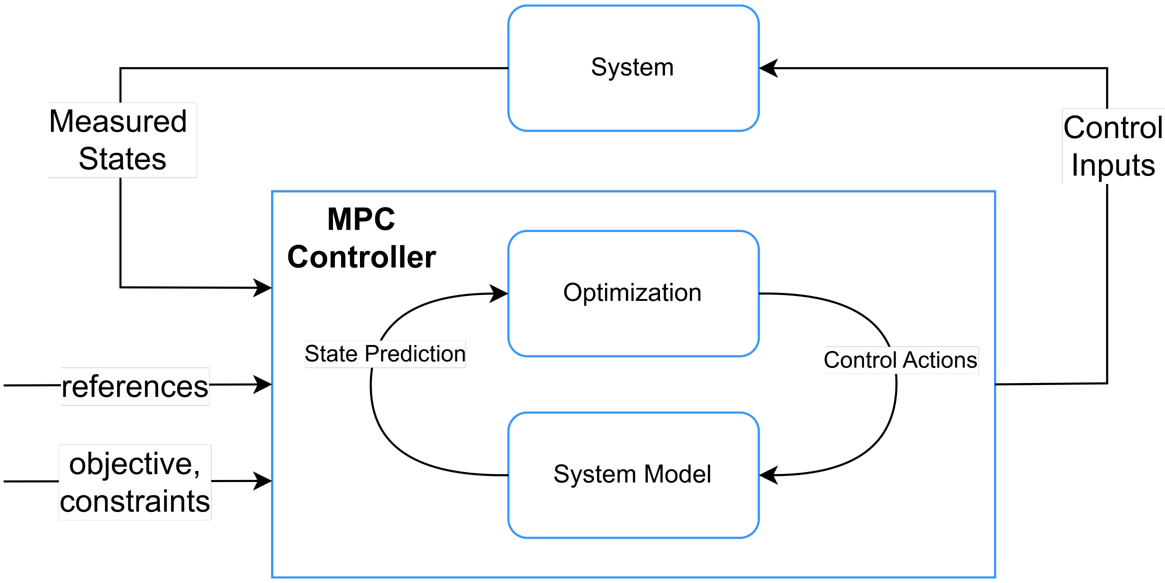

Figure 4-1: Block diagram of Model Predictive Control (MPC)[11]

inputs. The set of control inputs represents the control inputs given to the actual system over a finite number of steps. The number of steps represents the prediction horizon of the MPC problem. The optimization defines the cost function and the constraints as a function of the above-mentioned set of control inputs. The cost function obtains the state closest to the reference state by optimizing over the set of control inputs.

Having been first introduced almost half a century ago as Model Predictive Heuristic Control by Richalet, J et.al. [58], MPC has spread its presence over most industries due to ease of implementation, its ability to accurately handle nonlinear dynamics and to cope with hard constraints on controls and states.

If the principles behind the system to be modelled are known, the prediction model is derived using differential equations for the continuous time systems and difference equations for discrete-time systems. Some systems which are a function of both continuous and discrete-time variables are written as hybrid systems. The authors in [59] discuss the different hybrid systems used with MPC. If the system is a black box and only the input/output data is available, then the model of the system is developed using system identification. Multiple system models which can be identified from input-output data are shown in [60]. MPC can be classified into standard MPC and MIMPC depending on the presence of integer variables in the system model, cost or constraints. The next two subsections discuss the basic theory of standard MPC and MIMPC respectively.

Let $k = 1, 2, \dots N_p$ represent the prediction steps of the MPC optimal control problem, $q = 1, 2, \dots \infty$ represent the number of loops outside the MPC optimal control problem and the generalized notation $h_{q+k|q}$ indicate the value of the variable h at loop number q and prediction step k based on the value of h from loop zero to q. This notation is followed throughout the thesis. The prediction horizon of the MPC problem is denoted by N_p.

4-1-1 Standard MPC Formulation

In this section, we consider the case when all variables associated with the optimal control problem are real-valued. The general form of a discrete-time prediction model with initial state $\mathbf{x}_{q|q}$ is given by

$$\mathbf{x}_{q+k|q} = f(\mathbf{x}_{q+k-1|q}, \mathbf{u}_{q+k-1|q}) \tag{4-1}$$

where $\mathbf{x}_{q+k-1|q} \in \mathbb{R}^n$ is the state vector, $\mathbf{u}_{q+k-1|q} \in \mathbb{R}^m$ is the input vector, $f(\mathbf{x}_{q+k-1|q}, \mathbf{u}_{q+k-1|q})$ is the state equation and $x_{q+k|q}$ represents the successor state. The k steps forward solution of (4-1) is denoted as $\mathbf{x}_{q+k-1|q} = \phi\left(q+k-1; \mathbf{x}_{q|q}, \boldsymbol{u}_{q+k-1}\right)$ where $\boldsymbol{u}_{q+k-1} = \{\mathbf{u}_{q+0|q}, \mathbf{u}_{q+1|q}, \ldots, \mathbf{u}_{q+k-1|q}\}$ is the set of inputs which lead the system from $\mathbf{x}_{q|q}$ to $\mathbf{x}_{q+k}$. The case when (4-1) is a linear time-invariant system is given by

$$\mathbf{x}_{q+k|q} = A\mathbf{x}_{q+k-1|q} + B\mathbf{u}_{q+k-1|q} \tag{4-2}$$

where $A \in \mathbb{R}^{n\times n}$ is the state transition matrix and $B \in \mathbb{R}^{n\times m}$ is the input matrix

The optimization problem consisting of the objective function, the system dynamics, the system constraints and the terminal constraints is given by

$$\mathbb{P}_{N_p}\left(\mathbf{x}_{q|q}\right) := \begin{cases} \min\limits_{\boldsymbol{u}_{q+N_p-1}} & V_{N_p}\left(\mathbf{x}_{q|q}, \boldsymbol{u}_{q+N_p-1}\right) \\ \text{s.t.} & \mathbf{x}_{q+k|q} = A\mathbf{x}_{q+k-1|q} + B\mathbf{u}_{q+k-1|q} \\ & \mathbf{x}_{q+k|q} \in \mathbb{X}_{q+k} \\ & \mathbf{u}_{q+k-1|q} \in \mathbb{U}_{q+k-1} \\ & \mathbf{x}_{q+N_p+1|q} \in \mathbb{X}_f \end{cases} \tag{4-3}$$

where $\mathbb{X}_{q+k} \subseteq \mathbb{R}^n$ is the state constraint, $\mathbb{U}_{q+k-1} \subseteq \mathbb{R}^m$ is the input constraint, $\mathbf{x}_{q+N_p+1|q}$ is state of the system after N_p prediction steps, $\mathbb{X}_f \subseteq \mathbb{R}^n$ is the terminal constraint and $V_{N_p}\left(\mathbf{x}_{q|q}, \boldsymbol{u}_{q+N_p-1|q}\right)$ is the objective function given by

$$V_{N_p}\left(\mathbf{x}_{q|q}, \boldsymbol{u}_{q+N_p-1}\right) = \sum_{k=1}^{N_p}\{\underbrace{V_s(\mathbf{x}_{q+k-1|q}, \mathbf{u}_{q+k-1|q})}_{\text{stage cost}}\} + \underbrace{V_{\mathrm{f}}(\mathbf{x}_{q+N_p+1})}_{\text{terminal cost}}. \tag{4-4}$$

where $\mathbb{X}_{q+k}$ is convex, closed set $\forall\ q, k$, $\mathbb{U}_{q+k-1}$ is a convex and compact set at $\forall\ q, k$ and each of them contains the origin. The objective function encodes performance and safety requirements that have to be optimized under the given constraints. Equation (4-4) shows how the objective cost function of an MPC problem is divided. V_s is the stage cost is the cost associated with the input-state pair at each prediction step and V_f is the terminal cost which is the cost associated with the state after the final prediction step of the MPC optimal control problem. The system constraints include state, input, output and state-input constraints.

As the constrained optimization problem leads to a non-linear control law, proving closed-loop stability is done using the Lyapunov theory. The objective function can be used as the Lyapunov function if a terminal equality constraint $\mathbb{X}_f = 0$ is added to the stage cost [61]. This idea has then been extended with the addition of a terminal constraint set containing the origin, $\mathbf{x}_{q+N_p+1|q} \in \mathbb{X}_f \subset \mathbb{X}_{q+k}$ and the addition of terminal cost to the stage cost. The sufficient conditions for proving closed-loop stability and recursive feasibility of a constrained MPC problem when terminal cost or constraints are added to the objective function [62] are: (1) the terminal constraint set is a subset of the state constraint set and is closed, (2) A locally stabilizing controller is employed within the terminal set (3) the terminal constraint set is positively invariant for the locally stabilizing controller employed and (4) the terminal cost function is a local Lyapunov function in the terminal constraint set.

4-1-2 Mixed Integer MPC Formulation

MIMPC is an extension of the standard MPC algorithm when the problem contains discrete variables along with continuous variables. A specific form of the MIMPC system model which integrates continuous and logical variables called MLD systems was discussed in [39] and is given by [59]

$$\begin{aligned} \mathbf{x}_{q+k|q} &= A_1\mathbf{x}_{q+k-1|q} + B_1\mathbf{u}_{q+k-1|q} + B_2\Delta_{q+k-1|q} + B_3\mathbf{z}_{q+k-1|q} \\ E_2\Delta_{q+k-1|q} + E_3\mathbf{z}_{q+k-1|q} &\leq E_4\mathbf{x}_{q+k-1|q} + E_1\mathbf{u}_{q+k-1|q} + E_5 \end{aligned} \tag{4-5}$$

where $\mathbf{x} = \begin{bmatrix} \mathbf{x}_c \ \mathbf{x}_d \end{bmatrix}^{\mathrm{T}} \in \mathbb{R}^{n_c} \times \mathbb{B}^{n_d}$ is the system state, $\mathbf{u} = \begin{bmatrix} \mathbf{u}_c \ \mathbf{u}_d \end{bmatrix}^{\mathrm{T}} \in \mathbb{R}^{m_c} \times \mathbb{B}^{m_d}$ is the system input, $\Delta \in \mathbb{B}^{r_d}$ is the set of logical variables and $\mathbf{z} \in \mathbb{B}^{r_c}$ is the set of compound variables which represent the product between the logical variables and the system states and inputs. $\mathbf{x}_c$ and $\mathbf{u}_c$ represent the continuous state and input variables and $\mathbf{x}_d$ and $\mathbf{u}_d$ represent the integer/discrete state and input variable. The matrices $A_1 \in \mathbb{R}^{(n_c+n_d)\times(n_c+n_d)}$, $B_1 \in \mathbb{R}^{(n_c+n_d)\times(m_c+m_d)}$, $C_1 \in \mathbb{R}^{(p_c+p_d)\times(n_c+n_d)}$, $D_1 \in \mathbb{R}^{(p_c+p_d)\times(m_c+m_d)}$, $B_2 \in \mathbb{R}^{(n_c+n_d)\times(r_d)}$ and $D_2 \in \mathbb{R}^{(p_c+p_d)\times(r_d)}$, $B_3 \in \mathbb{R}^{(n_c+n_d)\times(r_c)}$,and $D_3 \in \mathbb{R}^{(p_c+p_d)\times(r_c)}$ are real constant matrices respectively and E_5 is a scalar vector.

The solution of (4-5) is represented as

$$\begin{aligned} \mathbf{x}_{q+k-1|q} =& \phi\left(q+k-1; \mathbf{x}_{q|q}, \boldsymbol{u}_{q+k-1}, \boldsymbol{\Delta}_{q+k-1}, \boldsymbol{z}_{q+k-1}\right) \\ =& A_1^{(q+k-1)}\mathbf{x}_{q|q} + \mathcal{C}^{\boldsymbol{u}}_{q+k-1}\boldsymbol{u}_{q+k-1} + \mathcal{C}^{\boldsymbol{\Delta}}_{q+k-1}\boldsymbol{\Delta}_{q+k-1} + \mathcal{C}^{\boldsymbol{z}}_{q+k-1}\boldsymbol{z}_{q+k-1} \end{aligned} \tag{4-6}$$

where $\boldsymbol{u}_{q+k-1} = \{\mathbf{u}_{q+0|q}, \mathbf{u}_{q+1|q}, \ldots, \mathbf{u}_{q+k-1|q}\}$, $\boldsymbol{\Delta}_{q+k-1} = \left\{\Delta_{q+0|q}, \Delta_{q+1|q}, \ldots, \Delta_{q+k-1|q}\right\}$ and $\boldsymbol{z}_{q+k-1} = \left\{\mathbf{z}_{q+0|q}, \mathbf{z}_{q+1|q}, \ldots, \mathbf{z}_{q+k-1|q}\right\}$ are the set of inputs, logical variables and compound variables which lead the system from $\mathbf{x}_0$ to $\mathbf{x}_{q+k}$ and

$$\begin{aligned} \mathcal{C}^{\boldsymbol{u}}_{q+k-1} &:= \begin{bmatrix} B_1 & A_1B_1 & \cdots & A_1^{q+k-1}B_1 \end{bmatrix} \\ \mathcal{C}^{\Delta}_{q+k-1} &:= \begin{bmatrix} B_2 & AB_2 & \cdots & A^{q+k-1}B_2 \end{bmatrix} \\ \mathcal{C}^{z}_{q+k-1} &:= \begin{bmatrix} B_3 & AB_3 & \cdots & A^{q+k-1}B_3 \end{bmatrix} \end{aligned} \tag{4-7}$$

The optimization problem for MIMPC consisting of the linear or quadratic objective function, linear system dynamics and linear system constraints is given by

$$\mathbb{P}_{N_p}\left(\mathbf{x}_{q|q}\right) =: \begin{cases} \min\limits_{\boldsymbol{u}_{q+N_p-1},\boldsymbol{\Delta}_{q+N_p-1},\boldsymbol{z}_{q+N_p-1}} & V_{N_p}\left(\mathbf{x}_{q|q}, \boldsymbol{u}_{q+N_p-1}, \boldsymbol{\Delta}_{q+N_p-1}, \boldsymbol{z}_{q+N_p-1}\right) \\ \text{s.t.} & \mathbf{x}_{q+k|q} = A_1\mathbf{x}_{q+k-1|q} + B_1\mathbf{u}_{q+k-1|q} + B_2\Delta_{q+k-1|q} \\ & \qquad +B_3\mathbf{z}_{q+k-1|q}, \\ & E_2\Delta_{q+k-1|q} + E_3\mathbf{z}_{q+k-1|q} \leq E_4\mathbf{x}_{q+k-1|q} \\ & \qquad +E_1\mathbf{u}_{q+k-1|q} + E_5, \end{cases} \tag{4-8}$$

where $V_{N_p}\left(\mathbf{x}_{q|q}, \boldsymbol{u}_{q+N_p-1}, \boldsymbol{\Delta}_{q+N_p-1}, \boldsymbol{z}_{q+N_p-1}\right)$ is the objective function given by

$$V_{N_p}\left(\mathbf{x}_{q|q}, \boldsymbol{u}_{q+N_p-1}, \boldsymbol{\Delta}_{q+N_p-1}, \boldsymbol{z}_{q+N_p-1}\right) = \sum_{k=1}^{N_p} V_s\left(\mathbf{x}_{q+k-1|q}, \mathbf{u}_{q+k-1|q}, \Delta_{q+k-1|q}, \mathbf{z}_{q+k-1|q}\right) \tag{4-9}$$

4-2 Vehicle Model

The design of a vehicle model used in MPC should be done carefully as it plays a major role in the formulation of the control law. The vehicle model in an MPC based control strategy is used to predict the future states of the system given a set of control inputs over the prediction horizon. The mathematical model of a vehicle may consist of vehicle kinematics and/or vehicle dynamics. There are multiple representations of both the vehicle kinematics and dynamics, each with different levels of complexity [63].

Multiple vehicle models are used in this thesis with each to be used for different parts of the control algorithm. Section 4-3-1 describes the mathematical model as the combination of the kinematic vehicle model [64] and the non-linear bicycle model [65], linearized at the current state as the HV and is used in the APF-MPC algorithm. A simplified continuous dynamics which follows the Forward-Euler for vehicle velocity is used to denote the HV in the MIMPC algorithm along with a binary vehicle lane variable as seen in Section 4-4-1. The motion of the obstacles is represented by a Constant Velocity (CV) model is discussed in Section 4-3-2.

4-3 APF-MPC Control Strategy

The design of the APF-MPC control strategy brings together the advantages of the APF such as obstacle avoidance and that of MPC and integrates path planning and vehicle control as explained in Section 1-3.

The APF-MPC algorithm uses standard MPC methods as discussed in Section 4-1-1. The formulation of the algorithm is divided into; (1) the formulation of the system model of the HV, (2) the design of the tracking model of the OV, (3) the selection of the time period and the prediction horizon, (4) the formulation of the state and input constraints, (5) the design of the reference trajectories, and (6) the formulation of the cost/ objective function of the APF-MPC algorithm.

4-3-1 HV Model (APF-MPC)

The vehicle model for the APF-MPC algorithm uses both the kinematic vehicle model representing the motion of the HV in the global road coordinate frame [64, 66] and the non-linear bicycle model representing the interaction between the longitudinal and lateral dynamics of a vehicle [65]. The bicycle model also called a single-track model is a commonly used vehicle dynamics model due to its balance between the representation of actual system dynamics and model complexity. It is called a bicycle model/single track as the left and right wheels (seen in grey) are assumed to behave equally and therefore combined to be represented as a two-wheel model (seen in black) as seen in Figure 4-2. where ℓ_f and ℓ_r is the distance between

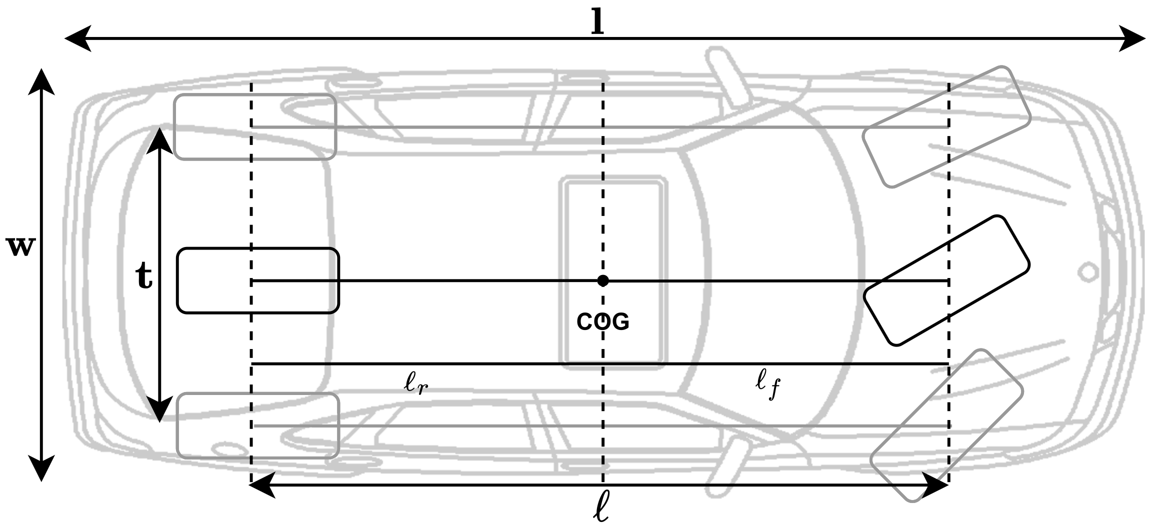

Figure 4-2: 4-wheel model (grey) vs bicycle model (black)

the CoG and the front and rear wheel axles respectively, wheelbase $\ell = \ell_f + \ell_r$ and the track $\mathbf{t}$ are vehicle dimensions of the vehicle chassis, and $\mathbf{l}$ and $\mathbf{w}$ are the length and width of the vehicle.

The states of the vehicle model are the longitudinal and lateral position of the HV with respect to the global road coordinate $X_{\text{HV}}, Y_{\text{HV}} \in \mathcal{Y}_x := [0, Y_{\max}]$ respectively, the lateral and longitudinal velocity of the HV $v_{x,\text{HV}} \in \mathcal{V}_x := [0, v_{x,\max}], v_{y,\text{HV}} \in \mathcal{V}_y := [-v_{y,\max}, v_{y,\max}]$, the yaw angle $\theta_{\text{HV}} \in \mathcal{T} := [-\theta_{\max}, \theta_{\max}]$ and the rate of change of yaw angle $\dot{\theta}_{\text{HV}} \in \mathcal{R} := [-r_{\max}, r_{\max}]$. The control inputs to the system are defined as the vehicle longitudinal acceleration $a_{x,\text{HV}} \in \mathcal{A}_x := [-a_{x,\max}, a_{x,\max}]$ and the steering wheel angle $\delta_{\text{HV}} \in \mathcal{D} := [-\delta_{\max}, \delta_{\max}]$. Figure 4-3 shows the free-body diagram of the bicycle model

where F_{l_f} and F_{l_r} are the longitudinal tire forces on the front and the rear wheel, F_{c_f} and F_{c_r} are the lateral tire forces on the front and the rear wheel, v_f and v_r are the velocities at the front and the rear wheel respectively, α_f and α_r are the slip angles at the front and the rear wheel respectively, m is the mass of the vehicle and $F = m\ a_{x,\text{HV}}$ is the external longitudinal force applied to the CoG due the acceleration input.

The kinematics of the vehicle is represented as the combination of a translation and rotation

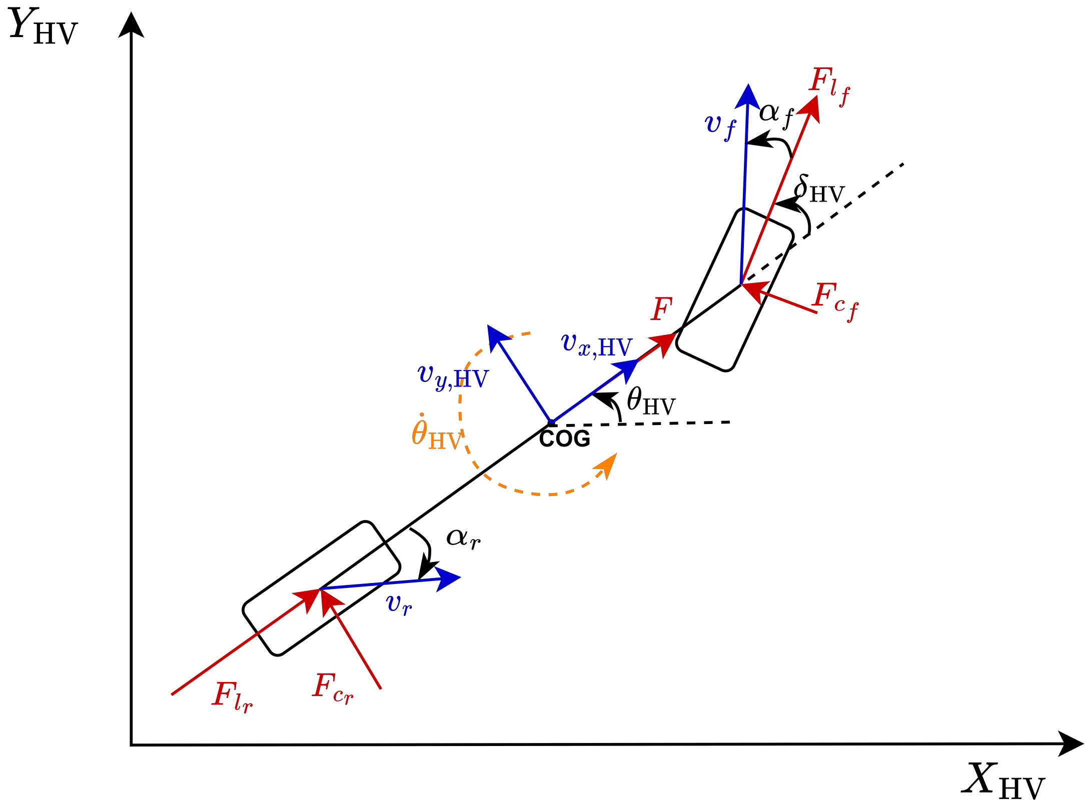

Figure 4-3: Free body diagram of the bicycle model of the HV

of the local HV coordinates to the stationary global road coordinate and are given by [66]

$$\begin{aligned}\dot{X}_{\text{HV}} &= v_{x,\text{HV}} \cos(\theta_{\text{HV}}) - v_{y,\text{HV}} \sin(\theta_{\text{HV}}) \\ \dot{Y}_{\text{HV}} &= v_{x,\text{HV}} \sin(\theta_{\text{HV}}) + v_{y,\text{HV}} \cos(\theta_{\text{HV}})\end{aligned} \tag{4-10}$$

The equations denoting the mathematical model of the non-linear bicycle model representing the HV dynamics are derived from the free body diagram shown in Figure 4-3 using Newton's laws of motion and are given by [67, 68]

$$\begin{aligned}\dot{v}_{x,\text{HV}} &= \dot{\theta}_{\text{HV}} v_{y,\text{HV}} + \frac{2F_{x_f}}{m} + \frac{2F_{x_r}}{m} + a_{x,\text{HV}} \\ \dot{v}_{y,\text{HV}} &= -\dot{\theta}_{\text{HV}} v_{x,\text{HV}} + \frac{2F_{y_f}}{m} + \frac{2F_{y_r}}{m} \\ \ddot{\theta}_{\text{HV}} &= \frac{\ell_f F_{y_f}}{I_z} - \frac{\ell_r F_{y_r}}{I_z}\end{aligned} \tag{4-11}$$

where I_z is the inertia of the vehicle over the axis passing through the CoG of the HV perpendicular to the X-Y plane, and the forces $F_{x_f}, F_{x_r}, F_{y_f}, F_{y_r}$ represent the forces applied on the CoG of the HV due to the longitudinal and lateral tire forces and are given by

$$\begin{aligned}F_{x_*} &= F_{l_*} \cos(\delta_{*,\text{HV}}) - F_{c_*} \sin(\delta_{*,\text{HV}}) \\ F_{y_*} &= F_{l_*} \sin(\delta_{*,\text{HV}}) + F_{c_*} \cos(\delta_{*,\text{HV}})\end{aligned} \tag{4-12}$$

where $* \in [f, r]$. As the thesis assumes that only the front wheels of the vehicle are controllable using the steering angle, $\delta_{r,\text{HV}} = 0$ and $\delta_{f,\text{HV}} = \delta_{\text{HV}}$. The longitudinal tire force F_{l_*} and lateral tire force F_{c_*} can be generally represented as

$$\begin{aligned} F_{l_*} &= f_l(\alpha_*, \mu, s, F_z) \\ F_{c_*} &= f_c(\alpha_*, \mu, s, F_z) \end{aligned} \tag{4-13}$$

where μ is the friction coefficient of the road, s is the slip ratio describing the ratio of the difference between the wheel velocity (the longitudinal velocity of the vehicle based on the angular velocity of the wheel) and the measured longitudinal velocity with the latter and F_z is the vertical load of the HV. This thesis assumes that the wheels do not slip on the road and therefore the longitudinal tire forces of the vehicle are assumed to be zero. The lateral tire forces are given by

$$\begin{aligned} F_{c_f} &= -C_f \alpha_f \\ F_{c_r} &= -C_r \alpha_r \end{aligned} \tag{4-14}$$

where C_f and C_r are the stiffness parameters of the front and rear wheels. Under small angle assumptions, the tire slip angles can be denoted as

$$\begin{aligned} \alpha_f &= \delta_{\text{HV}} - \frac{v_{y_{\text{HV}}} + l_f \dot{\theta}_{\text{HV}}}{v_{x_{\text{HV}}}} \\ \alpha_r &= \frac{v_{y_{\text{HV}}} - l_r \dot{\theta}_{\text{HV}}}{v_{x_{\text{HV}}}} \end{aligned} \tag{4-15}$$

By substituting (4-12)-(4-15) in (4-11) the non-linear bicycle model with linear tire response is given by

$$\begin{aligned} \dot{v}_{x,\text{HV}} &= \dot{\theta}_{\text{HV}} v_{y,\text{HV}} + \left(\frac{2C_f}{m}\right)\left(\delta_{\text{HV}} - \frac{v_{y,\text{HV}} + \ell_f \dot{\theta}_{\text{HV}}}{v_{x,\text{HV}}}\right)\sin\delta_{\text{HV}} + a_{x,\text{HV}} \\ \dot{v}_{y,\text{HV}} &= -\dot{\theta}_{\text{HV}} v_{x,\text{HV}} - \left(\frac{2C_f}{m}\right)\left(\delta_{\text{HV}} - \frac{v_{y,\text{HV}} + \ell_f \dot{\theta}_{\text{HV}}}{v_{x,\text{HV}}}\right)\cos\delta_{\text{HV}} - \left(\frac{2C_r}{m}\right)\left(\frac{v_{y,\text{HV}} - \ell_r \dot{\theta}_{\text{HV}}}{v_{x,\text{HV}}}\right) \\ \ddot{\theta}_{\text{HV}} &= -\left(\frac{\ell_f C_f}{I_z}\right)\left(\delta_{\text{HV}} - \frac{v_{y,\text{HV}} + \ell_f \dot{\theta}_{\text{HV}}}{v_{x,\text{HV}}}\right)\cos\delta_{\text{HV}} + \left(\frac{\ell_r C_r}{I_z}\right)\left(\frac{v_{y,\text{HV}} - \ell_r \dot{\theta}_{\text{HV}}}{v_{x,\text{HV}}}\right) \end{aligned} \tag{4-16}$$

The final state equation of the HV with states $\mathbf{x}_{\text{HV}} = \begin{bmatrix} v_{x,\text{HV}} & X_{\text{HV}} & Y_{\text{HV}} & v_{y,\text{HV}} & \dot{\theta}_{\text{HV}} & \theta_{\text{HV}} \end{bmatrix}^{\mathrm{T}}$ and inputs $\mathbf{u}_{\text{HV}} = \begin{bmatrix} a_{x,\text{HV}} & \delta_{\text{HV}} \end{bmatrix}^{\mathrm{T}}$ is given by

$$\dot{\mathbf{x}}_{\text{HV}} = \begin{bmatrix} \dot{v}_{x,\text{HV}} \\ \dot{X}_{\text{HV}} \\ \dot{Y}_{\text{HV}} \\ \dot{v}_{y,\text{HV}} \\ \ddot{\theta}_{\text{HV}} \\ \dot{\theta}_{\text{HV}} \end{bmatrix} = \begin{bmatrix} \dot{\theta}_{\text{HV}} v_{y,\text{HV}} + \left(\frac{2C_f}{m}\right)\left(\delta_{\text{HV}} - \frac{v_{y,\text{HV}} + \ell_f \dot{\theta}_{\text{HV}}}{v_{x,\text{HV}}}\right)\sin\delta_{\text{HV}} + a_{x,\text{HV}} \\ v_{x,\text{HV}}\cos(\theta_{\text{HV}}) - v_{y,\text{HV}}\sin(\theta_{\text{HV}}) \\ v_{x,\text{HV}}\sin(\theta_{\text{HV}}) + v_{y,\text{HV}}\cos(\theta_{\text{HV}}) \\ -\dot{\theta}_{\text{HV}} v_{x,\text{HV}} - \left(\frac{2C_f}{m}\right)\left(\delta_{\text{HV}} - \frac{v_{y,\text{HV}} + \ell_f \dot{\theta}_{\text{HV}}}{v_{x,\text{HV}}}\right)\cos\delta_{\text{HV}} - \left(\frac{2C_r}{m}\right)\left(\frac{v_{y,\text{HV}} - \ell_r \dot{\theta}_{\text{HV}}}{v_{x,\text{HV}}}\right) \\ -\left(\frac{\ell_f C_f}{I_z}\right)\left(\delta_{\text{HV}} - \frac{v_{y,\text{HV}} + \ell_f \dot{\theta}_{\text{HV}}}{v_{x,\text{HV}}}\right)\cos\delta_{\text{HV}} + \left(\frac{\ell_r C_r}{I_z}\right)\left(\frac{v_{y,\text{HV}} - \ell_r \dot{\theta}_{\text{HV}}}{v_{x,\text{HV}}}\right) \\ \theta_{\text{HV}} \end{bmatrix} \tag{4-17}$$

The continuous time output equation is defined as

$$\mathbf{y}_{\mathrm{HV}} = \begin{bmatrix} v_{x,\mathrm{HV}} \\ v_{y,\mathrm{HV}} \\ \dot{\theta}_{\mathrm{HV}} \\ \theta_{\mathrm{HV}} \end{bmatrix} = \underbrace{\begin{bmatrix} 1 & 0 & 0 & 0 & 0 & 0 \\ 0 & 0 & 0 & 0 & 0 & 0 \\ 0 & 0 & 0 & 1 & 0 & 0 \\ 0 & 0 & 0 & 0 & 1 & 0 \\ 0 & 0 & 0 & 0 & 0 & 1 \end{bmatrix}}_{C_c} \mathbf{x}_{\mathrm{HV}} \tag{4-18}$$

Description	Value	Symbol
Distance between the CoG of the HVand the front axle	1.7	ℓ_f
Distance between the CoG of the HV and the rear axle	1.7	ℓ_r
Wheelbase of the HV	3.4	ℓ
Track of the HV	1.2	$\mathbf{t}$
Length of the HV	4.5	$\mathbf{l}$
Width of the HV	1.8	$\mathbf{w}$
Stiffness coefficient of the front wheel of the HV	98 389	C_f
Stiffness coefficient of the rear wheel of the HV	198 142	C_r
Mass of the HV	1900	m
Inertial coefficient of the HV	2865.61	I_z

Table 4-1: Value of different constants of the HV model (APF-MPC)[12, 13, 14]

Let the current state of the system in loop q be given by $\mathbf{x}(q) = \mathbf{x}_{q|q}$ and the current input to the system in loop q be $\mathbf{u}(q) = \mathbf{u}_{q|q}$. The linearized model of the HV at the current state and input is written as

$$\begin{aligned} \dot{\mathbf{x}}_{\mathrm{HV}} &= A_{\mathrm{HV}}\mathbf{x}_{\mathrm{HV}} + B\mathbf{u}_{\mathrm{HV}} \\ \mathbf{y}_{\mathrm{HV}} &= C_{\mathrm{HV}}\mathbf{x}_{\mathrm{HV}} \end{aligned} \tag{4-19}$$

The expansions of A_{HV}, A_{HV} and A_{HV} are given in Appendix C.

As the implementation of the APF-MPC controller needs a discrete-time controller, the model obtained above is discretized. As the input to the system model between two steps of an MPC algorithm is piecewise constant, an ZOH method is used to discretize the model [69]. The selection of a sampling time T is discussed in Section 4-3-3. Therefore, the discrete-time state-space model of the HV obtained at each loop is given by

$$\begin{aligned} \mathbf{x}_{\mathrm{HV}_{q+k|q}} &= A_{d,\mathrm{HV}}\mathbf{x}_{\mathrm{HV}_{q+k-1|q}} + B_{d,\mathrm{HV}}\mathbf{u}_{\mathrm{HV}_{q+k-1|q}} \\ \mathbf{y}_{\mathrm{HV}_{q+k|q}} &= C_{d,\mathrm{HV}}\mathbf{x}_{\mathrm{HV}_{q+k|q}} \end{aligned} \tag{4-20}$$

where the discrete-time matrices are calculated as

$$\begin{aligned}A_{d,\mathrm{HV}} &= e^{A_{\mathrm{HV}}T} \\ B_{d,\mathrm{HV}} &= B_{\mathrm{HV}} \int_0^T e^{A_{\mathrm{HV}}T} dT \\ C_{d,\mathrm{HV}} &= C_{\mathrm{HV}}\end{aligned} \tag{4-21}$$

Let us define the vehicle state and input at $q = 0$ as

$$\begin{aligned}\mathbf{x}_{\mathrm{HV}_{base}} &= \begin{bmatrix} v_{x,\mathrm{HV}_{base}} & X_{\mathrm{HV}_{base}} & Y_{\mathrm{HV}_{base}} & v_{y,\mathrm{HV}_{base}} & \dot{\theta}_{\mathrm{HV}_{base}} & \theta_{\mathrm{HV}_{base}} \end{bmatrix}^T \\ \mathbf{u}_{\mathrm{HV}_{base}} &= \begin{bmatrix} a_{x,\mathrm{HV}_{base}} & \delta_{\mathrm{HV}_{base}} \end{bmatrix}^T\end{aligned} \tag{4-22}$$

and the maximum total velocity $v_{\mathrm{tot,max}}$ of the HV. Let the coordinates of the CoG of the HV in loop q and prediction step k be represented as $\mathcal{X}_{\mathrm{HV}_{q+k|q}} = [\, X_{\mathrm{HV}_{q+k|q}} \; Y_{\mathrm{HV}_{q+k|q}} \,]^T$

4-3-2 OV Model

Prediction models are important because they allow for the accurate calculation of the optimal value of the system input given constraints and the objective function. Though the inclusion of these models helps predict the system's future trajectories, there is a need to predict the trajectories of the OV around the HV to generate vehicle inputs that can avoid collisions. The prediction model used to track the evolution of the OV is called as a motion model. A Constant Velocity (CV) motion model is used in this thesis due to its simplicity. The CV motion model is a linear motion model which assumes that the system acceleration is zero. The state transition equation of the CV model is given by

$$\mathbf{x}_{\mathrm{OV}_{q+k|q}} = \underbrace{\begin{bmatrix} 1 & T & 0 & 0 \\ 0 & 1 & 0 & 0 \\ 0 & 0 & 1 & T \\ 0 & 0 & 0 & 1 \end{bmatrix}}_{C_{\mathrm{OV}}} \mathbf{x}_{\mathrm{OV}_{q+k-1|q}} \tag{4-23}$$

where $\mathbf{x}_{\mathrm{OV}} = [\, X_{\mathrm{OV}} \; v_{x,\mathrm{OV}} \; Y_{\mathrm{OV}} \; v_{y,\mathrm{OV}} \,]^{\mathrm{T}}$ are the states of all the OV and T is the sampling time of the MPC control algorithm. X_{OV} and Y_{OV} are the longitudinal and lateral position and $v_{y,\mathrm{OV}}$ and $v_{y,\mathrm{OV}}$ are the longitudinal and lateral velocities of the OV.

$$\mathbf{x}_{\mathrm{OV}_{q+k-1|q}} = \begin{bmatrix} X_{\mathrm{OV}_{q+k-1|q}} \\ v_{x,\mathrm{OV}_{q+k-1|q}} \\ Y_{\mathrm{OV}_{q+k-1|q}} \\ v_{y,\mathrm{OV}_{q+k-1|q}} \end{bmatrix} \tag{4-24}$$

4-3-3 Sampling Period and Horizon Length

The selection of the sampling period and horizon length while designing a generalized MPC optimal control problem should be chosen based on the control task it performs. The selection of these two parameters should obtain good control performance while keeping the computation cost low. Long horizons and small sampling time can help achieve the best performance [70] but this can lead to a very heavy computational load. The selection of the sampling time must also take into account practical considerations such as the frequency of data obtained from the perception block as well the speed of the bus used. While RADAR systems work in the frequency range of 24-79 Hz [71], cameras and LiDAR systems operate at a higher frequency. The frequency of obtaining data after being processed by the perception block is, therefore, slower than 24 Hz. The sampling period is therefore limited by these factors. A sampling time of 0.1 s or a sampling period of 10 Hz is therefore selected.

The selection of the horizon length is a complicated task that varies based on traffic scenarios. The horizon length can be equated to the amount of time a driver takes to respond to an obstacle and to react to it. The authors in [72] studied the response time of participants driving in a simulator in a cut-in scenario. An average response time of 1.05s with a standard deviation of 0.43 s was seen. A similar study by [73] analyzes the response time of drivers in real-time traffic for a braking scenario. The response time of the participants was between 0.433-1 s. Therefore a horizon length of 1 s is chosen with a sampling time of 0.1 s with 10 prediction steps.

Description	Value	Symbol
Sampling time	0.1	T
Prediction horizon	10	N_p

Table 4-2: Constants of the APF-MPC control strategy

4-3-4 Constraints

The constraints in the APF-MPC optimization problem are designed to take into account the limits of the vehicle actuators, the comfort of the human passengers, the limits in terms of road boundaries and rules of traffic and are integrated into the optimization problem to generate a safe and comfortable path for the HV to follow. The constraints are

- The constraint on the longitudinal velocity of the HV is given by the

$$v_{x_{\min}} \leq v_{x,\mathrm{HV}_{q+k|q}} \leq v_{x_{\max}} \tag{4-25}$$

  where the minimum value of the longitudinal velocity of the HV $v_{x_{\min}}$ is zero as the vehicle cannot move in the reverse direction as assumed in Section 1-4 and $v_{x_{\max}}$ is the maximum longitudinal velocity of the HV and is calculated as [74]

$$v_{x_{\max}} = v_{\mathrm{tot,max}} \cos \beta_{\max} \tag{4-26}$$

  where $\beta_{\max}$ is the maximum vehicle sideslip angle.

- The constraint on the lateral position of the HV is given by

$$y_{\text{min}} \leq Y_{\text{HV}_{q+k|q}} \leq y_{\text{max}} \tag{4-27}$$

where y_{max} and y_{min} are the lateral position of the road boundaries.

- The constraint on the lateral velocity of the HV is given by the

$$v_{y_{\text{min}}} \leq v_{y,\text{HV}_{q+k|q}} \leq v_{y_{\text{max}}} \tag{4-28}$$

where is $v_{y_{\text{max}}}$ is the maximum lateral velocity of the HV and $v_{y_{\text{min}}}$ is the minimum value of the lateral velocity of the HV is equal to $-v_{y_{\text{max}}}$. The maximum lateral velocity is given by [74]

$$v_{y_{\text{max}}} = v_{\text{tot,max}} \sin \beta_{\text{max}} \tag{4-29}$$

- The constraint of the rate of change of heading angle of the HV is given by

$$\dot{\theta}_{\text{min}} \leq \dot{\theta}_{\text{HV}_{q+k|q}} \leq \dot{\theta}_{\text{max}} \tag{4-30}$$

where is $\dot{\theta}_{\text{max}}$ is the maximum yaw rate of the HV and $\dot{\theta}_{\text{min}}$ is the minimum yaw rate of the HV is equal to $-\dot{\theta}_{\text{max}}$. The maximum yaw rate is a function of the friction coefficient of the road μ and the longitudinal velocity of the host vehicle and is given by

$$\dot{\theta}_{\text{max}} = \frac{\mu g}{v_{x,\text{HV}_{q+k|q}}} \tag{4-31}$$

where g is the acceleration due to gravity.

- The constraint on the HV heading angle is given by

$$\theta_{\text{min}} \leq \theta_{\text{HV}_{q+k|q}} \leq \theta_{\text{max}} \tag{4-32}$$

where is θ_{max} is the maximum yaw rate of the HV and θ_{min} is the minimum yaw rate of the HV is equal to $-\theta_{\text{max}}$.

- The constraint on the longitudinal acceleration of the HV is given by the

$$a_{x_{\text{min}}} \leq a_{x,\text{HV}_{q+k-1|q}} \leq a_{x_{\text{max}}} \tag{4-33}$$

where $a_{x_{\text{max}}}$ is the maximum acceleration and $a_{x_{\text{min}}}$ is the maximum deceleration of the HV. The maximum acceleration of the car is a function of the friction coefficient of the road. Assuming a wet road for better traction, the maximum acceleration/ deceleration of the car is given by

$$a_{x_{\text{max}}} = -a_{x_{\text{min}}} = \mu g \tag{4-34}$$

- The constraint on the steering angle of the HV is given by

$$\delta_{\text{min}} \leq \delta_{\text{HV}_{q+k-1|q}} \leq \delta_{\text{max}} \tag{4-35}$$

where is δ_{max} is the maximum yaw rate of the HV and δ_{min} is the minimum yaw rate of the HV is equal to $-\delta_{\text{max}}$. The maximum steering wheel angle is given by [74]

$$\delta_{\text{max}} = \frac{\ell \mu g}{v^2_{x,\text{HV}_{q+k|q}}} \tag{4-36}$$

These constraints are grouped together for loop q and prediction step k and the group of linear constraints are of the form

$$A_{\text{ineq,APF-MPC}_{q+k}} \underbrace{\begin{bmatrix} \mathbf{x}_{\text{HV}_{q+k|q}} \\ \mathbf{u}_{\text{HV}_{q+k-1|q}} \end{bmatrix}}_{\psi_{\text{APF-MPC}_{q+k|q}}} \leq b_{\text{ineq,APF-MPC}_{q+k}} \tag{4-37}$$

and the extension of $\psi_{\text{APF-MPC}_{q+k|q}}$ over the prediction horizon be defined as

$$\Psi_{\text{APF-MPC}_{q+N_p|q}} = \begin{bmatrix} \psi_{\text{APF-MPC}_{q+1|q}} & \psi_{\text{APF-MPC}_{q+2|q}} & \dots & \psi_{\text{APF-MPC}_{q+N_p|q}} \end{bmatrix} \tag{4-38}$$

Description	**Value**	**Symbol**
Maximum total velocity	41.667	$v_{\text{tot,max}}$
Maximum vehicle sideslip angle	$\frac{3}{180}\pi$	β_{max}
Friction coefficient	0.4	μ
Acceleration due to gravity	9.86	g
Maximum yaw rate	$\frac{5}{180}\pi$	θ_{max}

Table 4-3: Constants to calculate the constraints of the APF-MPC control strategy

4-3-5 Reference Trajectories

The calculation of reference values for output $\mathbf{y}_{\text{HV}}$ and input $\mathbf{u}_{\text{HV}}$ is discussed below where the outputs and inputs are as defined in (4-20).

The output reference at loop q and prediction step k $\mathbf{y}_{\text{HV,ref}_{q+k|q}}$ consisting of reference values for all the output variables as defined in (4-18)is given by

$$\mathbf{y}_{\text{HV,ref}_{q+k|q}} = \begin{bmatrix} v_{x,\text{HV,ref}_{q+k|q}} \\ v_{y,\text{HV,ref}_{q+k|q}} \\ \dot{\theta}_{\text{HV,ref}_{q+k|q}} \\ \theta_{\text{HV,ref}_{q+k|q}} \end{bmatrix} \tag{4-39}$$

where $v_{x,\text{HV,ref}_{q+k|q}}$ is the longitudinal velocity reference, $v_{y,\text{HV,ref}_{q+k|q}}$ is the lateral velocity reference, $\dot{\theta}_{\text{HV,ref}_{q+k|q}}$ is the reference for rate of change of the heading angle and $\theta_{\text{HV,ref}_{q+k|q}}$ is the reference for heading angle at loop q and prediction step k.

The design of the longitudinal velocity reference $v_{x,\text{HV,ref}_{q+k|q}}$ depends on the five aspects; (1) longitudinal position $X_{\text{OV}_{\text{SL},f_{q+k|k}}}$, longitudinal velocity $v_{x,\text{OV}_{\text{SL},f_{q+k|k}}}$, safe distance measure

$d_{\text{safe}_{\text{SL},f_{q+k|k}}}$ of $\text{OV}_{\text{SL},f}$, (2) the maximum safe distance $d_{\text{safe}_{\max}}$ as defined in Section 2-2-1, (3) flags $\text{flag}_{\delta_{q+k|k}}$ and $\text{flag}_{\text{LC}_{q+k|k}}$ as defined in Section 2-2-2, (4) longitudinal position $X_{\text{HV}_{q+k|k}}$ and longitudinal velocity $v_{x,\text{HV}_{q+k|k}}$ the HV and (5) longitudinal vehicle velocity at $q = 0$ $v_{x,\text{HV}_{base}}$ as defined in (4-22).

Let the equations in (4-40) represent the logical expressions to be used to calculate $v_{x,\text{HV},\text{ref}_{q+k|q}}$. These expressions are used to ensure the safety of the vehicle to prevent collision due to sudden deceleration of $\text{OV}_{\text{SL},f}$ when the lane change is not possible. Equation (4-40a) checks if the velocity of the HV is less than that of $\text{OV}_{\text{SL},f}$. Equation (4-40b) checks if the relative distance between the HV and $\text{OV}_{\text{SL},f}$ is greater than the maximum safe distance plus a term dependent on their relative velocity to always maintain a distance greater than the maximum safe distance to have enough time to react to any sudden deceleration.

$$v_{x,\text{HV}_{q+k|k}} - v_{\text{OV}_{\text{SL},f_{q+k|k}}} \leq 0 \tag{4-40a}$$

$$X_{\text{OV}_{\text{SL},f_{q+k|q}}} - X_{\text{HV}_{q+k|k}} \leq d_{\text{safe}_{\max}} + 2N_pT\left(v_{x,\text{HV}_{q+k|k}} - v_{\text{OV}_{\text{SL},f_{q+k|k}}}\right) \tag{4-40b}$$

Algorithm 3 shows the algorithm used to obtain the correct longitudinal velocity reference.

Algorithm 3: Algorithm to calculate $v_{x,\text{HV},\text{ref}_{q+k|q}}$

Data: $X_{\text{HV}_{q+k|k}}$, $v_{x,\text{HV}_{q+k|k}}$, $x_{\text{OV}_{\text{SL},f_{q+k|k}}}$ and $v_{\text{OV}_{\text{SL},f_{q+k|k}}}$, $d_{\text{safe}_{\text{SL},f_{q+k|k}}}$, $d_{\text{safe}_{\max}}$, $\text{flag}_{\delta_{q+k|k}}$, $\text{flag}_{\text{LC}_{q+k|k}}$, $v_{x,\text{HV}_{base}}$

Result: $v_{x,\text{HV},\text{ref}_{q+k|q}}$

begin
- **if** $\mathit{flag}_\delta \leftarrow \mathit{true}$ **then**
  - **if** $\mathit{flag}_{LC} \leftarrow \mathit{false}$ & (4-40a) $\leftarrow$ *true* & (4-40b) $\leftarrow$ *true* **then**
    - **Set:** $v_{x,HV,ref_{q+k|q}} = v_{OV_{SL,f_{q+k|k}}}$
  - **else**
    - **Set:** $v_{x,HV,ref_{q+k|q}} = v_{x,HV_{base}}$
- **else**
  - **Set:** $v_{x,HV,ref_{q+k|q}} = v_{x,HV_{base}}$

The working of Algorithm 3 is as follows: The algorithm

- sets the reference velocity equal to the velocity of $\text{OV}_{\text{SL},f}$ if
  - if $\text{OV}_{\text{SL},f}$ exists
  - if Algorithm 1 decides that lane change is not possible.
  - if the velocity of the $\text{OV}_{\text{SL},f}$ is greater than $v_{x,\text{HV}_{q+k|k}}$
  - if the distance between the HV and $\text{OV}_{\text{SL},f}$ is greater than the maximum safe distance plus a term based on the relative velocity
- else the reference velocity is set as $v_{x,\text{HV}_{base}}$.

- checks if $\text{OV}_{\text{SL},f}$ exists. If yes

  - checks if
    - if lane change is not possible (Algorithm 1)
    - if the velocity of the $\mathrm{OV}_{\mathrm{SL},f}$ is greater than $v_{x,\mathrm{HV}_{q+k|k}}$
    - if the distance between the HV and $\mathrm{OV}_{\mathrm{SL},f}$ is greater than the maximum safe distance plus a term based on the relative velocity

    if all the above conditions are true then sets the reference velocity equal to the velocity of $\mathrm{OV}_{\mathrm{SL},f}$
  - else sets the reference velocity equal to the velocity of $v_{x,\mathrm{HV}_{base}}$
- if no then sets the reference velocity equal to the velocity of $v_{x,\mathrm{HV}_{base}}$

The idea behind the algorithm is to maintain a distance greater than that of the maximum safety distance from $\mathrm{OV}_{\mathrm{SL},f}$ if the lane change is not possible and if the velocity of $\mathrm{OV}_{\mathrm{SL},f}$ is greater than that of the HV which can lead to a collision if the HV does not decelerate. The idea behind checking in two steps rather than using a single if statement is due to the fact that the longitudinal position $X_{\mathrm{OV}_{\mathrm{SL},f_{q+k|k}}}$, longitudinal velocity $v_{x,\mathrm{OV}_{\mathrm{SL},f_{q+k|k}}}$, safe distance measure $d_{\mathrm{safe}_{\mathrm{SL},f_{q+k|k}}}$ of $\mathrm{OV}_{\mathrm{SL},f}$ are undefined when $\mathrm{flag}_\delta = 0$.

The lateral velocity reference $v_{y,\mathrm{HV},\mathrm{ref}_{q+k|q}}$ is given by [75]

$$v_{y,\mathrm{HV},\mathrm{ref}_{q+k|q}} = v_{x,\mathrm{HV},\mathrm{ref}_{q+k|q}} \tan\beta_{ss} \tag{4-41}$$

where β_{ss} is the steady state vehicle side slip angle defined as the angle between the longitudinal direction of the local HV coordinate frame and the direction of movement of the host vehicle and is given by

$$\beta_{ss} = 2\rho\left(\ell_r - \frac{m\ell_f v_{x,\mathrm{HV}_{q+k|k}}^2}{\ell C_r}\right) \tag{4-42}$$

where ρ is the curvature of the path taken by the HV and is given by [76]

$$\rho = \frac{1}{\sqrt{\ell_r^2 + \ell^2 \cot\delta_{\mathrm{HV}_{q+k|k}}}} \tag{4-43}$$

As only straight roads are considered in this thesis, and with the assumption that the vehicle changes heading angle for only a very short period of time when it changes lanes, the heading angle reference $\theta_{\mathrm{HV},\mathrm{ref}_{q+k|q}}$ is assumed to be zero. This also leads to the yaw rate reference $\dot{\theta}_{\mathrm{HV},\mathrm{ref}_{q+k|q}}$ to be set as zero.

$$\begin{aligned}\theta_{\mathrm{HV},\mathrm{ref}_{q+k|q}} &= 0\\ \dot{\theta}_{\mathrm{HV},\mathrm{ref}_{q+k|q}} &= 0\end{aligned} \tag{4-44}$$

The input reference at loop q and prediction step k is given by $\mathbf{u}_{\mathrm{HV},\mathrm{ref}_{q+k|q}}$ consists of reference values for all the input variables of the APF-MPC prediction model and is given as

$$\mathbf{u}_{\mathrm{HV},\mathrm{ref}_{q+k-1|q}} = \begin{bmatrix} a_{x,\mathrm{HV},\mathrm{ref}_{q+k-1|q}} \\ \delta_{\mathrm{HV},\mathrm{ref}_{q+k-1|q}} \end{bmatrix} \tag{4-45}$$

As the number of changes in reference vehicle velocity is very low while travelling on a highway due to a low number of interactions with OV, the longitudinal acceleration $a_{x,\mathrm{HV,ref}_{q+k-1|q}}$ reference is taken as zero to avoid erratic behaviour due to transient changes in reference acceleration. As this thesis assumes a straight road, the HV is driving a straight line in the majority of driving situations, the reference steering wheel angle $\delta_{\mathrm{HV,ref}_{q+k-1|q}}$ to be zero.

$$\begin{aligned} a_{x,\mathrm{HV,ref}_{q+k-1|q}} &= 0 \\ \delta_{\mathrm{HV,ref}_{q+k-1|q}} &= 0 \end{aligned} \tag{4-46}$$

Description	**Value**	**Symbol**
Maximum safe distance	230	$d_{\mathrm{safe}_{\max}}$
Length of Region Of Interest around the HV	460	d_{ROI}

Table 4-4: Constants to calculate the references of the APF-MPC control strategy

4-3-6 Objective Function

The objective function of a generic MPC algorithm is used to fulfil the required goals of the control task and depends on the problem domain. The objective function generally consists of multiple costs each corresponding to a particular goal.

The integration of the planning and vehicle control blocks is achieved by the addition of weighted obstacle APF for all the obstacles (3-14) and road APF (3-16) as terms to the MPC objective function. Quadratic approximations of the obstacle potential is used to reduce the computation time. The objective function used for the APF-MPC algorithm of a single step of the MPC optimal control problem for loop number q and prediction step k is given by

$$\begin{aligned} V_{k,\text{APF-MPC}}\left(\mathbf{x}_{q|q}, \psi_{\mathrm{APF-MPC}_{q+k|q}}\right) = &\underbrace{\| \mathbf{y}_{\mathrm{HV}_{q+k|q}} - \mathbf{y}_{\mathrm{HV,ref}_{q+k|q}} \|^2_{W_{\mathbf{y}}}}_{\text{A}} \\ &+ \underbrace{\| \mathbf{u}_{\mathrm{HV}_{q+k-1|q}} - \mathbf{u}_{\mathrm{HV,ref}_{q+k-1|q}} \|^2_{W_{\mathbf{u}}}}_{\text{B}} + \underbrace{\| \mathbf{u}_{\mathrm{HV}_{q+k-1|q}} - \mathbf{u}_{\mathrm{HV}_{q+k-2|q}} \|^2_{W_{\tilde{\mathbf{u}}}}}_{\text{C}} \\ &+ \underbrace{U_o\left(\mathcal{X}_{\mathrm{HV}_{q+k|q}}\right) W_o}_{\text{D}} + \underbrace{U_{r_{quad}}\left(\mathcal{X}_{\mathrm{HV}_{q+k|q}}\right) W_r}_{\text{E}} \end{aligned} \tag{4-47}$$

where W_* where $* \in \{\mathbf{y}, \mathbf{u}, \tilde{\mathbf{u}}, o \text{ and } r\}$ represents the weights on the output, input, rate of change of vehicle input, the obstacle potential and the road potential respectively, $\mathbf{y}_{\mathrm{HV,ref}}$ and $\mathbf{u}_{\mathrm{HV,ref}}$ are the reference values for output and input variables respectively and $\| \Gamma \|^2_{W_*} = \Gamma^T W_* \Gamma$ where Γ is a variable vector. The different costs associated with the objective function are given as follows: A represents the cost used to keep selected vehicle states close to their respective reference values, B represents the cost used to keep the vehicle inputs close to their

Description	Value	Symbol
Weight on the output variables	$\begin{bmatrix} 5 & 0 & 0 & 0 \\ 0 & 1 & 0 & 0 \\ 0 & 0 & 1 & 0 \\ 0 & 0 & 0 & 1000 \end{bmatrix}$	$W_{\mathbf{y}}$
Weight on the input variables	$\begin{bmatrix} 0 & 0 \\ 0 & 1000 \end{bmatrix}$	$W_{\mathbf{u}}$
Weight on the rate of change of input variables	$\begin{bmatrix} 0 & 0 \\ 0 & 100 \end{bmatrix}$	$W_{\tilde{\mathbf{u}}}$
Weight on the total approximated obstacle potential	0.25	W_o
Weight on the road potential	0.1	W_r

Table 4-5: Weights of the objective function of the APF-MPC control strategy

reference value, (C) represents the cost on the rate of change of vehicle inputs, (D) represents the total potential of all the obstacles and (E) is the cost of the total road potential. As the costs are convex and quadratic in nature, the computation load of the optimization problem is low even with the additional approximations of the obstacle potentials.

Figure 4-4 shows the flowchart of the APF-MPC algorithm. The algorithm starts by receiving

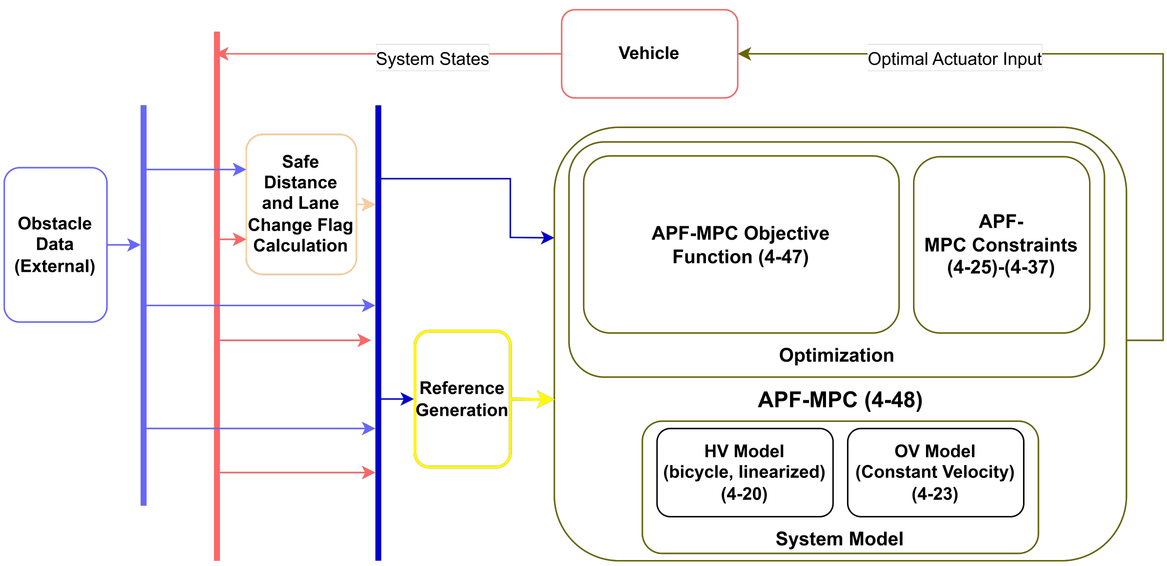

Figure 4-4: Flowchart of the APF-MPC Control Strategy

the position and velocity data from all the OV within the ROI as well as the states of the HV. This data is used to calculate the safe distance measures for all OV as discussed in Section

2-2-1 and the lane change flag as discussed in Section 2-2-2. The OV data, the calculated safe distance measures and flag_{LC} are given as input to the reference generation block which generates the required references. The values of the calculated safe distance measures and flag_{LC} remain do not change for a given loop q. The generation of the convex obstacle potential and its quadratic approximation along with the quadratic approximation of the road potential occurs at each prediction step k whereas the linearization of the HV model every loop q.

The reference data along with OV data, HV data, and the safe distance measures are given as the input to the APF-MPC block which solves the optimal control problem. The final APF-MPC optimization problem for a given loop q is given by

$$\mathbb{P}_{\text{APF}-\text{MPC},N_p}\left(\mathbf{x}_{q|q}, \mathbf{x}_{\text{OV}_{q|q}}\right) := \begin{cases} \min\limits_{\Psi_{\text{APF}-\text{MPC}_{q+N_p|q}}} & \sum\limits_{k=1}^{N_p} V_{k,\text{APF-MPC}}\left(\mathbf{x}_{q|q}, \psi_{\text{APF}-\text{MPC}_{q+k|q}}\right) \\ \text{s.t.} & \mathbf{x}_{\text{HV}_{q+k|q}} = A_{d,\text{HV}}\mathbf{x}_{\text{HV}_{q+k-1|q}} + B_{d,\text{HV}}\mathbf{u}_{\text{HV}_{q+k-1|q}} \\ & \quad \text{with } \mathbf{x}_{\text{HV}}(q) = \mathbf{x}_{q|q} \\ & \mathbf{x}_{\text{OV}_{q+k|q}} = C_{\text{OV}}\mathbf{x}_{\text{OV}_{q+k-1|q}} \text{with } \mathbf{x}_{\text{OV}}(q) = \mathbf{x}_{\text{OV}_{q|q}} \\ & A_{\text{ineq},\text{APF}-\text{MPC}_{q+k}}\psi_{\text{APF}-\text{MPC}_{q+k|q}} \leq b_{\text{ineq},\text{APF}-\text{MPC}_{q+k}} \end{cases} \tag{4-48}$$

where $\mathbf{x}_{\text{OV}_{q|q}}$ is the state of the OV in loop q. The generated optimized vehicle input is then given as input to the vehicle actuators.

4-4 MIMPC+APF-MPC Control Strategy

The MIMPC+APF-MPC control strategy uses MIMPC and APF-MPC algorithms successively in a loop to produce a safe path. While the MIMPC uses a hybrid model with MLD constraints to generate an optimal lane to travel in, the APF-MPC algorithm takes this optimal lane as an input to design a road potential unique to the optimal lane generated to change lanes while avoiding obstacles. This section is divided into three subsections: Section 4-4-1 shows the MIMPC algorithm along with defining logical constraints to select the optimal lane based on OV data, Section 4-4-2 extends the APF-MPC algorithm defined in Section 4-3 to work with the lane input. The final MIMPC+APF-MPC control strategy is discussed in Subsection 4-4-3.

4-4-1 MIMPC

The basic idea of an MIMPC optimal control problem has been discussed in Section 4-1-2. The MIMPC optimal control problem is based on the framework developed in [39] for a system with linear dynamics with both real and integer-valued variables conditioned on a set of logical constraints which are a function of both logical and real-valued variables. The idea is to rewrite these logical constraints as a set of linear inequalities and therefore to write the overall MIMPC optimal control problem to be solved using an MIQP solver.

The formulation of the algorithm is divided into: (1) the formulation of the system model of the HV, (2) the formulation of the tracking model of the OV. The model defined in Section 4-3-2 is used as the tracking model, (3) the time period and the prediction horizon of the MIMPC and APF-MPC parts of the MIMPC+APF-MPC control strategy are the same as discussed in Section 4-3-3, (4) the design of the reference trajectories and (5) the formulation of the MLD constraints as well as the state and input constraints, the formulation of the cost/ objective function of the APF-MPC algorithm.

HV Model (MIMPC)

The vehicle model used for the MIMPC algorithm represents the evolution of the longitudinal velocity $v_{\mathrm{HV}} \in \mathcal{V} := [0, v_{\max}]$ of the HV. The vehicle evolution is controlled by the longitudinal system acceleration $a_{\mathrm{HV}} \in \mathcal{A} := [-a_{\max}, a_{\max}]$. Both v_{HV} and a_{HV} are continuous decision variables. The evolution of the velocity is denoted by a Forward-Euler scheme and is given as

$$v_{\mathrm{HV}_{q+k|q}} = v_{\mathrm{HV}_{q+k-1|q}} + T a_{\mathrm{HV}_{q+k-1|q}} \tag{4-49}$$

where T is a predefined time period.

The system dynamics also contains discrete decision variable l_{HV} used to select the lane on which the HV travels. As this thesis works with a road with only two lanes, $l_{\mathrm{HV}} \in \mathbb{B}$ is represented as a binary variable. The value of T is given by the sampling time of the MPC algorithm and is discussed further in this chapter.

Let us define the velocity metric $v_{j,\mathrm{HV}_{q+k|q}}$, distance metric $d_{j,\mathrm{HV}_{q+k|q}}$ and $l_{j,\mathrm{HV}_{q+k|q}}$ lane metric which represents the relative velocity, the relative longitudinal distance and the lane difference between the host and the j^{th} obstacle vehicle and are defined as

$$v_{j,\mathrm{HV}_{q+k|q}} = v^{j}_{x,\mathrm{OV}_{q+k|q}} - v_{\mathrm{HV}_{q+k|q}} \tag{4-50a}$$

$$d_{j,\mathrm{HV}_{q+k|q}} = d_{j,\mathrm{HV}_{q+k-1|q}} + \tau v_{j,\mathrm{HV}_{q+k|q}} \text{ where } d_{j,\mathrm{HV}_{q|q}} = X^{j}_{\mathrm{OV}_{q|q}} \tag{4-50b}$$

$$l_{j,\mathrm{HV}_{q+k|q}} = l_{j_{q+k|q}} - l_{\mathrm{HV}_{q+k|q}} \tag{4-50c}$$

Let us also define $\mathrm{flag}_{\mathrm{LC}_{q|q}}$ as the lane change flag and $l_{j,\mathrm{HV}_{q|q}}$ as the current lane of the HV for loop q.

Reference Trajectories

This section discusses the generation of the reference trajectories used in the MIMPC part of the MIMPC+APF-MPC control strategy. References on the the velocity of the the HV $v_{\mathrm{HV}_{q+k|q}}$ and the acceleration input $a_{\mathrm{HV}_{q+k-1|q}}$ are used in this thesis.

The velocity reference of the MIMPC part of the MIMPC+APF-MPC control strategy $v_{\mathrm{HV,ref}_{q+k|q}}$ is set using the same procedure as $v_{x,\mathrm{HV,ref}_{q+k|q}}$ as discussed in Section 4-3-5 (Algorithm 3). The acceleration reference $a_{\mathrm{HV,ref}_{q+k-1|q}}$ is set to zero because the number of changes in reference velocity are low due to low interaction between HV and OV while driving on a highway and to reduce transient changes in reference acceleration.

$$\begin{aligned} v_{\mathrm{HV,ref}_{q+k|q}} &= v_{x,\mathrm{HV,ref}_{q+k|q}} \\ a_{\mathrm{HV,ref}_{q+k-1|q}} &= 0 \end{aligned} \tag{4-51}$$

Constraints

Two different sets of constraints are used in the MIMPC algorithm. There are boundary constraints for the continuous and binary variables and MLD constraints

Boundary constraints: Boundary constraints are used to limit the maximum and minimum value of the continuous and discrete variables and are given by

$$v_{\min} \leq v_{\mathrm{HV}_{q+k|q}} \leq v_{\max} \tag{4-52a}$$

$$a_{\min} \leq a_{\mathrm{HV}_{q+k-1|q}} \leq a_{\max} \tag{4-52b}$$

$$l_{\mathrm{HV}_{q+k|q}} \in \mathbb{B} := \{0, 1\} \tag{4-52c}$$

The values of $v_{\max}$, $v_{\min}$, $a_{\max}$ and $a_{\min}$ are equal to the values of $v_{x,\max}$, $v_{x,\min}$, $a_{x,\max}$ and $a_{x,\min}$ defined in Section 4-3-5. The value of l_{HV} is binary as this thesis uses a two-lane road.

MLD constraints: Mixed-Logical Dynamical (MLD) constraints are constraints based on logical expressions. These expressions are functions of the continuous and integer variables used by the hybrid model representing the HV. Each of these logical expressions can be rewritten as a set of linear inequalities and therefore the MIMPC optimization problem can be converted into a MIQP problem.

Three logical constraints are defined to fulfil a certain role. The first logical constraint is used to maintain the longitudinal safety of the host vehicle i.e, have a relative distance between the HV and the OV in the same lane in-front of the HV to be greater than a given safe distance (Equation (4-53a)). The second and third logical constraints are used to not let the HV not change lanes when $\mathrm{flag}_{\mathrm{LC}} = 0$ (Equation (4-53b)-(4-53c)). These constraints are mathematically written as

$$\underbrace{[l_{j,\mathrm{HV}_{q+k|q}} = 0]}_{\alpha_{1,j_{q+k|k}}=1} \wedge \underbrace{[d_{j,\mathrm{HV}_{q+k|q}} \geq 0]}_{\alpha_{2,j_{q+k|k}}=1} \implies [d_{j,\mathrm{HV}_{q+k|q}} \geq d_{j,\mathrm{safe}_{q|q}}] \tag{4-53a}$$

$$\underbrace{[l_{j,\mathrm{HV}_{q+k|q}} = 0]}_{\alpha_{1,j_{q+k|k}}=1} \implies [l_{\mathrm{HV}_{q+k|q}} - l_{\mathrm{HV}_{q+k-1|q}} = \mathrm{flag}_{\mathrm{LC}_{q|q}}] \tag{4-53b}$$

$$\underbrace{[l_{j,\mathrm{HV}_{q+k|q}} = 1]}_{\alpha_{3,j_{q+k|k}}=1} \implies [l_{\mathrm{HV}_{q+k|q}} - l_{\mathrm{HV}_{q+k-1|q}} = -\mathrm{flag}_{\mathrm{LC}_{q|q}}] \tag{4-53c}$$

Let us now define $\alpha_{1,j_{q+k|k}} = 1$, $\alpha_{2,j_{q+k|k}} = 1$ and $\alpha_{3,j_{q+k|k}} = 1$ which can be written as

$$[\alpha_{1,j_{q+k|k}} = 1] \implies [l_{j,\mathrm{HV}_{q+k|q}} \leq 0] \wedge [l_{j,\mathrm{HV}_{q+k|q}} \geq 0] \tag{4-54a}$$

$$[\alpha_{2,j_{q+k|k}} = 1] \implies [d_{j,\mathrm{HV}_{q+k|q}} \geq 0] \tag{4-54b}$$

$$[\alpha_{2,j_{q+k|k}} = 1] \implies [l_{j,\mathrm{HV}_{q+k|q}} \leq 1] \wedge [l_{j,\mathrm{HV}_{q+k|q}} \geq 1] \tag{4-54c}$$

Let us further define logical variables to obtain a one-on-one logical representation of each logical expression defined in (4-54) as

$$[\beta_{1,j_{q+k|k}} = 1] \implies [l_{j,\mathrm{HV}_{q+k|q}} \leq 0] \tag{4-55a}$$

$$[\beta_{2,j_{q+k|k}} = 1] \implies [l_{j,\mathrm{HV}_{q+k|q}} \geq 0] \tag{4-55b}$$

$$[\beta_{3,j_{q+k|k}} = 1] \implies [l_{j,\mathrm{HV}_{q+k|q}} \leq 1] \tag{4-55c}$$

$$[\beta_{4,j_{q+k|k}} = 1] \implies [l_{j,\mathrm{HV}_{q+k|q}} \geq 1] \tag{4-55d}$$

Each of these logical expressions can be written as a set of linear inequalities using the relationships provided in Table 4-6. Therefore the equations in (4-54) can be written as

Representation	Logical Implication	System of Inequaties
$\mathcal{S}_{\geq}(\delta, f(x), c)$	$[\delta = 1] \iff [f(x) \geq c]$	$\begin{cases} (c-m)\,\delta \leq f(x) - m \\ (M-c-\epsilon)\,\delta \geq f(x) - c + \epsilon \end{cases}$
$\mathcal{S}_{\leq}(\delta, f(x), c)$	$[\delta = 1] \iff [f(x) \leq c]$	$\begin{cases} (M-c)\,\delta \leq M - f(x) \\ (c+\epsilon-m)\,\delta \geq \epsilon + c - f(x) \end{cases}$
$\mathcal{S}_{\wedge}(\delta, \rho, \gamma)$	$[\delta = 1] \iff [\rho = 1] \wedge [\gamma = 1]$	$\begin{cases} -\rho + \delta \leq 0 \\ -\gamma + \delta \leq 0 \\ \rho + \gamma - \delta \leq 1 \end{cases}$
$\mathcal{S}_{\vee}(\delta, \rho, \gamma)$	$[\delta = 1] \iff [\rho = 1] \vee [\gamma = 1]$	$\begin{cases} \rho - \delta \leq 0 \\ \gamma - \delta \leq 0 \\ -\rho - \gamma + \delta \leq 1 \end{cases}$
$\mathcal{S}_{\Rightarrow}(g, f(x), \delta)$	$[\delta = 0] \Rightarrow [g = 0], [\delta = 1] \Rightarrow [g = f(x)]$	$\begin{cases} m\delta \leq g \leq M\delta \\ -M(1-\delta) \leq g - f(x) \leq -m(1-\delta) \end{cases}$

Table 4-6: Basic Logical Implications and associated system inequalities ($f : \mathbb{R} \to \mathbb{R}$ Linear Function, $M = \max_{x \in X} f(x)$, $m = \min_{x \in X} f(x)$, X Compact Set, $c \in \mathbb{R}$, $\epsilon > 0, \delta, \rho, \gamma \in \mathbb{B}$) [15]

$$\text{(4-54a)} \implies \begin{cases} \mathcal{S}_{\leq}\left(\beta_{1,j_{q+k|k}}, l_{j,\mathrm{HV}_{q+k|q}}, 0)\right) \\ \mathcal{S}_{\geq}\left(\beta_{2,j_{q+k|k}}, l_{j,\mathrm{HV}_{q+k|q}}, 0)\right) \\ \mathcal{S}_{\wedge}\left(\alpha_{1,j_{q+k|k}}, \beta_{1,j_{q+k|k}}, \beta_{2,j_{q+k|k}}\right) \end{cases} \tag{4-56a}$$

$$\text{(4-54b)} \implies \mathcal{S}_{\geq}\left(\alpha_{2,j_{q+k|k}}, d_{j,\mathrm{HV}_{q+k|q}}, 0\right), \tag{4-56b}$$

$$\text{(4-54c)} \implies \begin{cases} \mathcal{S}_{\leq}\left(\beta_{3,j_{q+k|k}}, l_{j,\mathrm{HV}_{q+k|q}}, 1)\right) \\ \mathcal{S}_{\geq}\left(\beta_{4,j_{q+k|k}}, l_{j,\mathrm{HV}_{q+k|q}}, 1)\right) \\ \mathcal{S}_{\wedge}\left(\alpha_{3,j_{q+k|k}}, \beta_{3,j_{q+k|k}}, \beta_{4,j_{q+k|k}}\right) \end{cases} \tag{4-56c}$$

Using the above definitions the equations in (4-53) can be written as

$$\alpha_{1,j_{q+k|k}} \alpha_{2,j_{q+k|k}} \left(d_{j,\mathrm{HV}_{q+k|q}} - d_{j,\mathrm{safe}_{q|q}}\right) \geq 0 \tag{4-57a}$$

$$\alpha_{1,j_{q+k|k}} \left(l_{\mathrm{HV}_{q+k|q}} - l_{\mathrm{HV}_{q+k-1|q}} - \mathrm{flag}_{\mathrm{LC}_{q|q}}\right) = 0 \tag{4-57b}$$

$$\alpha_{1,j_{q+k|k}}\left(l_{\mathrm{HV}_{q+k|q}} - l_{\mathrm{HV}_{q+k-1|q}} + \mathrm{flag}_{\mathrm{LC}_{q|q}}\right) = 0 \tag{4-57c}$$

As the expressions in (4-57) are nonlinear in the vehicle state and the defined logical variables, new logical variables are defined to make the equations in (4-57) linear inequalities. The relationship defined for the product of these variables are

- Variables which are combinations of two logical variable,

  $$\phi_1 := \phi_2\phi_3.$$

  where ϕ_2 and ϕ_3 are logical variables. Then the variable can be written as a set of inequalities given by

  $$\mathcal{S}_{\wedge}\left(\phi_1, \phi_2, \phi_3\right).$$

- Variables which are combinations of a logical and a continuous variable,

  $$\phi_1 := \phi_2\phi_3.$$

  where ϕ_2 is a logical variable and ϕ_3 is a continuous variable dependent on the state of the vehicle. Then the variable can be written as a set of inequalities given by

  $$\mathcal{S}_{\Rightarrow}\left(\phi_1, \phi_3, \phi_2\right).$$

By further introducing variables $\gamma_{1,j_{q+k|q}}$, $\gamma_{2,j_{q+k|q}}$, $\gamma_{3,j_{q+k|q}}$, $\gamma_{4,j_{q+k|q}}$, $\gamma_{5,j_{q+k|q}}$ and $\gamma_{6,j_{q+k|q}}$ to represent the product between two MLD variables or between an MLD variables and a system variable, the equations in (4-57) can be rewritten as

$$\gamma_{2,j_{q+k|q}} - \gamma_{1,j_{q+k|q}} d_{j,\mathrm{safe}_{q|q}} \geq 0 \tag{4-58a}$$

$$\gamma_{3,j_{q+k|q}} - \gamma_{4,j_{q+k|q}} - \alpha_{1,j_{q+k|q}} \mathrm{flag}_{\mathrm{LC}_{q|q}} \geq 0 \tag{4-58b}$$

$$\gamma_{5,j_{q+k|q}} - \gamma_{6,j_{q+k|q}} + \alpha_{2,j_{q+k|q}} \mathrm{flag}_{\mathrm{LC}_{q|q}} \geq 0 \tag{4-58c}$$

where $\gamma_{1,j_{q+k|q}}$, $\gamma_{2,j_{q+k|q}}$, $\gamma_{3,j_{q+k|q}}$, $\gamma_{4,j_{q+k|q}}$, $\gamma_{5,j_{q+k|q}}$ and $\gamma_{6,j_{q+k|q}}$ can be expanded as

$$\gamma_{1,j_{q+k|q}} := \alpha_{1,j_{q+k|q}}\alpha_{2,j_{q+k|q}} \Longrightarrow \mathcal{S}_{\wedge}\left(\gamma_{1,j_{q+k|q}}, \alpha_{1,j_{q+k|q}}, \alpha_{2,j_{q+k|q}}\right), \tag{4-59a}$$

$$\gamma_{2,j_{q+k|q}} := \gamma_{1,j_{q+k|q}} d_{j,\mathrm{HV}_{q+k|q}} \Longrightarrow \mathcal{S}_{\Rightarrow}\left(\gamma_{2,j_{q+k|q}}, d_{j,\mathrm{HV}_{q+k|q}}, \gamma_{1,j_{q+k|q}}\right), \tag{4-59b}$$

$$\gamma_{3,j_{q+k|q}} := \alpha_{1,j_{q+k|q}} l_{\mathrm{HV}_{q+k|q}} \Longrightarrow \mathcal{S}_{\Rightarrow}\left(\gamma_{3,j_{q+k|q}}, l_{\mathrm{HV}_{q+k|q}}, \alpha_{1,j_{q+k|q}}\right), \tag{4-59c}$$

$$\gamma_{4,j_{q+k|q}} := \alpha_{1,j_{q+k|q}} l_{\mathrm{HV}_{q+k-1|q}} \Longrightarrow \mathcal{S}_{\Rightarrow}\left(\gamma_{4,j_{q+k|q}}, l_{\mathrm{HV}_{q+k-1|q}}, \alpha_{1,j_{q+k|q}}\right), \tag{4-59d}$$

$$\gamma_{5,j_{q+k|q}} := \alpha_{2,j_{q+k|q}} l_{\mathrm{HV}_{q+k|q}} \Longrightarrow \mathcal{S}_{\Rightarrow}\left(\gamma_{5,j_{q+k|q}}, l_{\mathrm{HV}_{q+k|q}}, \alpha_{2,j_{q+k|q}}\right), \tag{4-59e}$$

$$\gamma_{6,j_{q+k|q}} := \alpha_{2,j_{q+k|q}} l_{\mathrm{HV}_{q+k-1|q}} \Longrightarrow \mathcal{S}_{\Rightarrow}\left(\gamma_{6,j_{q+k|q}}, l_{\mathrm{HV}_{q+k-1|q}}, \alpha_{2,j_{q+k|q}}\right), \tag{4-59f}$$

By defining M_l and m_l as the maximum and minimum values of $l_{j,\mathrm{HV}_{q+k|q}}$ and $l_{j,\mathrm{HV}_{q+k-1|q}}$ and M_l and m_l as the maximum and minimum values $d_{j,\mathrm{HV}_{q+k|q}}$ respectively in their respective domains, the equations in (4-56), (4-58) and (4-59) can be written as linear inequalities.

The total number of MLD constraints are given by $39N_{\text{OV}} + 3$ where 39 represents the total number of linear inequalities obtained after converting the logical constraints with 3 boundary constraints.

The linear inequalities representing the MLD constraints together with boundary constraints are grouped together for loop q and prediction step k and are written as

$$A_{\text{ineq,MIMPC}_{q+k}} \psi_{\text{MIMPC}_{q+k|q}} \leq b_{\text{ineq,MIMPC}_{q+k}} \tag{4-60}$$

where

$$\psi_{\text{MIMPC}_{q+k|q}} = \left[\, v_{\text{HV}_{q+k|q}} \; l_{\text{HV}_{q+k|q}} \; a_{\text{HV}_{q+k-1|q}} \; \alpha_{1_{q+k|k}} \; \beta_{1_{q+k|k}} \; \gamma_{1_{q+k|k}} \cdots \gamma_{N_{\text{OV}}{}_{q+k|k}} \,\right]. \tag{4-61}$$

is a variable used to simplify the set of linear inequalities into a compact form where $\alpha_{j_{q+k|k}} = \left[\, \alpha_{1,j_{q+k|k}} \cdots \alpha_{3,j_{q+k|k}} \,\right]$, $\beta_{j_{q+k|k}} = \left[\, \beta_{1,j_{q+k|k}} \cdots \beta_{4,j_{q+k|k}} \,\right]$ and $\gamma_{j_{q+k|k}} = \left[\, \gamma_{1,j_{q+k|k}} \cdots \gamma_{6,j_{q+k|k}} \,\right]$. Let the extension of $\psi_{\text{MIMPC}_{q+k|q}}$ over the prediction horizon be defined as

$$\Psi_{\text{MIMPC}_{N_p}} = \begin{bmatrix} \psi_{\text{MIMPC}_{q+1|q}} & \psi_{\text{MIMPC}_{q+2|q}} & \dots & \psi_{\text{MIMPC}_{q+N_p|q}} \end{bmatrix} \tag{4-62}$$

Objective Function

The objective function for the MIMPC algorithm is a quadratic cost and the different terms of the cost are:

- Cost for reference tracking of the longitudinal velocity of the HV
- Cost for reference tracking of the longitudinal acceleration of the HV
- Cost for the rate of change of input

The total objective function for loop q and prediction step k is given by

$$\begin{aligned} V_{k,\text{MIMPC}}\left(v_{q|q}, d_{q|q}, l_{q|q}, \psi_{\text{MIMPC}_{q+k|q}}\right) &= \underbrace{\| \, v_{\text{HV}_{q+k|q}} - v_{\text{HV,ref}_{q+k|q}} \, \|^2_{W_{\mathbf{v}}}}_{\text{velocity reference tracking}} \\ &+ \underbrace{\| \, a_{\text{HV}_{q+k-1|q}} - a_{\text{HV,ref}_{q+k-1|q}} \, \|^2_{W_{\mathbf{a}}}}_{\text{acceleration reference tracking}} + \underbrace{\| \, a_{\text{HV}_{q+k-1|q}} - a_{\text{HV}_{q+k-2|q}} \, \|^2_{W_{\tilde{\mathbf{a}}}}}_{\text{acceleration increment}} \end{aligned} \tag{4-63}$$

where W_* where $* \in \{\mathbf{v}, \mathbf{a} \text{ and } \tilde{\mathbf{a}}\}$ represents the weights on the velocity, acceleration and rate of change of vehicle acceleration respectively and $v_{\text{HV,ref}}$ and $a_{\text{HV,ref}}$ are the reference values for velocity and acceleration respectively. The references for velocity and acceleration used for the cost function are the same as the reference of longitudinal velocity and longitudinal acceleration used for the cost function in Section 4-3-5. The algorithm of the MIMPC optimal control problem is as follows: (1) Receiving of obstacle data from the perception block, (2) calculation of the safe distance measures for all the obstacles within the ROI with obstacle data and HV data as input, (3) generation of the references for the MIMPC optimal control problem, (4) MIMPC optimal control problem is optimized to find the optimal lane input which includes the objective function, formulation of the MLD and boundary constraints, the

Description	Value	Symbol
Weight on velocity	1	$W_{\mathbf{v}}$
Weight on acceleration	0.01	$W_{\mathbf{a}}$
Weight on the rate of change of acceleration	10	$W_{\tilde{\mathbf{a}}}$

Table 4-7: Weights of the objective function of the MIMPC part of the MIMPC + APF-MPC control strategy

Forward-Euler HV model defined in Section 4-4-1 as well as a CV model for the obstacles defined in Section 4-3-2. The final MIMPC optimization problem for a given loop q is given by

$$\mathbb{P}_{\text{MIMPC},N_p}\left(v_{q|q}, d_{q|q}, l_{q|q}, \mathbf{x}_{\text{OV}_{q|q}}\right) := \begin{cases} \min\limits_{\Psi_{\text{MIMPC}_{N_p}}} & \sum\limits_{k=1}^{N_p} V_{k,\text{MIMPC}}\left(v_{q|q}, d_{q|q}, l_{q|q}, \psi_{\text{MIMPC}_{q+k|q}}\right) \\ \text{s.t.} & v_{\text{HV}_{q+k+1|q}} = v_{\text{HV}_{q+k|q}} + \tau a_{\text{HV}_{q+k|q}} \\ & \text{with } v_{\text{HV}}(q) = v_{q|q} \text{ and } l_{\text{HV}}(q) = l_{q|q} \\ & \mathbf{x}_{\text{OV}_{q+k|q}} = C_{\text{OV}} \mathbf{x}_{\text{OV}_{q+k-1|q}} \text{with } \mathbf{x}_{\text{OV}}(q) = \mathbf{x}_{\text{OV}_{q|q}} \\ & A_{\text{ineq,MIMPC}_{q+k}} \psi_{\text{MIMPC}_{q+k|q}} \leq b_{\text{ineq,MIMPC}_{q+k}} \end{cases} \tag{4-64}$$

4-4-2 APF-MPC algorithm with lane input

The APF-MPC part of the MIMPC + APF-MPC control strategy uses the optimal lane input produced by the MIMPC algorithm in Section 4-4-1 (as a solution to (4-64)) as an input for the APF-MPCalgorithm. The optimal lane is used to select the correct road potential to move the vehicle to the correct lane and to help the vehicle stay in the centre of the lane. The sampling time and horizon length, the constraints, and the references used in the APF-MPC part of the MIMPC + APF-MPC control strategy are the same as discussed in 4-3. However, the objective function is extended to select the correct road potential based on the optimal lane input and is given by

$$\begin{aligned} V_{k,\text{APF-MPC}}\left(\mathbf{x}_{q|q}, \psi_{\text{APF-MPC}_k}, l_{\text{HV,opt}}\right) = & \underbrace{\| \mathbf{y}_{\text{HV}_{q+k|q}} - \mathbf{y}_{\text{HV,ref}_{q+k|q}} \|^2_{W_{\mathbf{y}}}}_{\text{A}} + \underbrace{\| \mathbf{u}_{\text{HV}_{q+k-1|q}} - \mathbf{u}_{\text{HV,ref}_{q+k-1|q}} \|^2_{W_{\mathbf{u}}}}_{\text{B}} \\ & + \underbrace{\| \mathbf{u}_{\text{HV}_{q+k-1|q}} - \mathbf{u}_{\text{HV}_{q+k-2|q}} \|^2_{W_{\tilde{\mathbf{u}}}}}_{\text{C}} + \underbrace{U_o\left(\mathbf{x}_{\text{HV}_{q+k|q}}\right) W_o}_{\text{D}} + \\ & \underbrace{\left(1 - l_{\text{HV,opt}}\right) U_{L_0, r_{quad}}\left(\mathcal{X}_{\text{HV}_{q+k|q}}\right) W_r}_{\text{E}} \\ & + \underbrace{l_{\text{HV,opt}} U_{L_1, r_{quad}}\left(\mathcal{X}_{\text{HV}_{q+k|q}}\right) W_r}_{\text{G}} \end{aligned} \tag{4-65}$$

where $l_{\text{HV,opt}}$ is the optimal lane generated as the output of the MIMPC algorithm, $U_{L0,r_{quad}}\left(\mathcal{X}_{\text{HV}_{q+k|q}}\right)$ is the road potential used if the optimal lane input is zero and $U_{L1,r_{quad}}\left(\mathcal{X}_{\text{HV}_{q+k|q}}\right)$ is the road potential used if the optimal lane input is one and are defined in Section 3-3-2.

Description	**Value**	**Symbol**
Weight on the output variables	$\begin{bmatrix} 50 & 0 & 0 & 0 \\ 0 & 1 & 0 & 0 \\ 0 & 0 & 1 & 0 \\ 0 & 0 & 0 & 1 \end{bmatrix}$	$W_{\mathbf{y}}$
Weight on the input variables	$\begin{bmatrix} 100 & 0 \\ 0 & 100 \end{bmatrix}$	$W_{\mathbf{u}}$
Weight on the rate of change of input variables	$\begin{bmatrix} 100 & 0 \\ 0 & 1000 \end{bmatrix}$	$W_{\tilde{\mathbf{u}}}$
Weight on the total approximated obstacle potential	0.5	W_o
Weight on the road potential	10	W_r

Table 4-8: Weights of the objective function of the APF-MPC part of the MIMPC + APF-MPC control strategy

The algorithm runs as follows: (1) Gathering the OV and HV data, (2) calculation of the safe distance measures for all OV, (3) Calculation of the reference trajectories, (4) start of the APF-MPC optimal control problem with an extended objective which includes road potential based on optimal lane input, combined obstacle potential for all the OV after convexification and quadratic approximation, cost on reference tracking for the input and for selected states, and cost on the rate of change of input (4-65). The optimal control problem of the APF-MPC algorithm for loop q is given by

$$\mathbb{P}_{\text{APF-MPC},N_p}\left(\mathbf{x}_{q|q}, \mathbf{x}_{\text{OV}_{q|q}}, l_{\text{HV,opt}}\right) := \begin{cases} \min\limits_{\Psi_{\text{APF-MPC}_{N_p}}} & \sum\limits_{k=1}^{N_p} V_{k,\text{APF-MPC}}\left(\mathbf{x}_{q|q}, \psi_{\text{APF-MPC}_k}, l_{\text{HV,opt}}\right) \\ \text{s.t.} & \mathbf{x}_{\text{HV}_{q+k|q}} = A_{d,\text{HV}}\mathbf{x}_{\text{HV}_{q+k-1|q}} + B_{d,\text{HV}}\mathbf{u}_{\text{HV}_{q+k-1|q}} \\ & \text{with } \mathbf{x}_{\text{HV}}(q) = \mathbf{x}_{q|q} \\ & \mathbf{x}_{\text{OV}_{q+k|q}} = C_{\text{OV}}\mathbf{x}_{\text{OV}_{q+k-1|q}} \text{with } \mathbf{x}_{\text{OV}}(q) = \mathbf{x}_{\text{OV}_0} \\ & A_{\text{ineq,APF-MPC}_{q+k}}\psi_{\text{APF-MPC}_{q+k|q}} \leq b_{\text{ineq,APF-MPC}_{q+k}} \end{cases} \tag{4-66}$$

where $\mathbf{x}_{\text{OV}_{q|q}}$ is the state of the OV in loop q.

4-4-3 Combining APF-MPC and MIMPC

The MIMPC algorithm and the APF-MPC algorithm are used successively in a loop to generate a set of optimal inputs for the HV. The idea behind combining APF-MPC algorithm with and MIMPC algorithm is to generate a road potential based on the optimal lane output of the MIMPC algorithm. The advantage of the improved road potential is the movement of the HV towards the centre of the optimal lane while taking into account the system dynamics and constraints while also maintaining a safe distance from OV in front. The road potentials for each of the lanes are defined in Section 3-3-2. Figure 4-5 shows the flowchart of the APF-MPC and MIMPC control strategy and how the MIMPC algorithm formulated in Section 4-4-1 is combined with APF-MPC algorithm defined in Section 4-4-2. Algorithm 4 shows

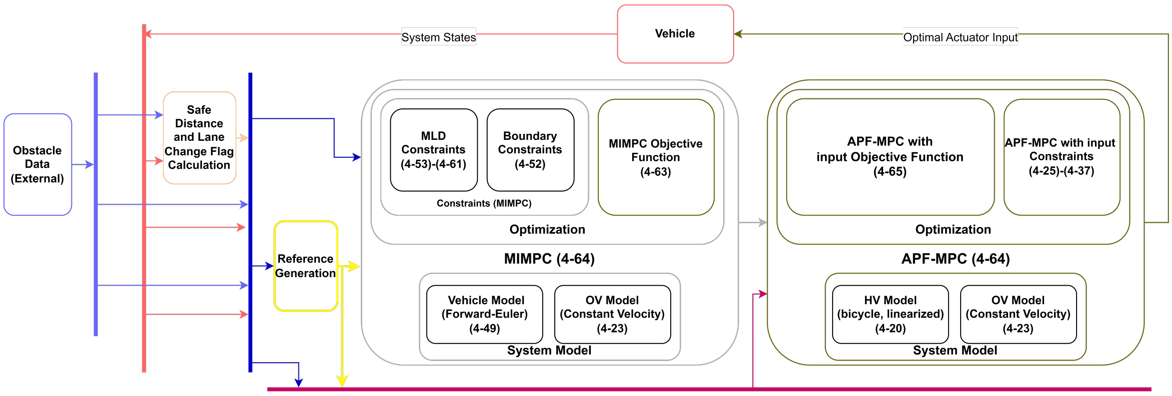

Figure 4-5: Flowchart of the MIMPC+APF-MPC Control Strategy

the basic pseudo code for the The algorithm works as follows: (1) The vehicle takes the

---

Algorithm 4: Algorithm MIMPC+APF-MPC Control Strategy.

Data: $\mathbf{x}_{q|q}, \mathbf{x}_{\text{OV}_{q|q}}, \mathbf{x}_{\text{HV}_{base}}, \mathbf{u}_{\text{HV}_{base}}, T, N_p, v_{\text{tot,max}}$
Result: $\Psi_{\text{APF-MPC}_{N_p}}$

begin
- $\text{flag}_{\text{LC}_{q|q}}$=`CalculateLCFlag` `/* using Algorithm 1 */`
- $d_{j,\mathsf{safe}_{q|q}}, d_{\mathsf{safe}_{\max}}$ = `CalulateSF()` `/* Calculate the Safe Distance Measures for all OV` (2-1) `*/`
- $v_{\mathsf{HV,ref}_{q+k|q}}, a_{\mathsf{HV,ref}_{q+k-1|q}}, \mathbf{y}_{\mathsf{HV,ref}_{q+k|q}}, \mathbf{u}_{\mathsf{HV,ref}_{q+k|q}}$ = `GenerateRefTraj()` `/* Generate Reference Trajectories for MIMPC and APF-MPC algorithms using` (4-39)-(4-46), (4-51) `*/`
- $l_{\text{HV,opt}}$=**Solve:** $\mathbb{P}_{MIMPC,N_p}\left(v_{q|q}, d_{q|q}, l_{q|q}, \mathbf{x}_{OV_{q|q}}\right)$ `/* Generate Optimal Lane` (4-64) `*/`
- $\mathbf{u}_{\text{HV,opt}}$=**Solve:** $\mathbb{P}_{APF-MPC,N_p}\left(\mathbf{x}_{q|q}, \mathbf{x}_{OV_{q|q}}, l_{HV,opt}\right)$ `/* Generate Optimal Input (Acceleration and Steering Angle) for the HV` (4-66) `*/`

HV and OV data to calculate the lane change flag using the *CalculateLCFlag* function as defined by Algorithm 1 and calculate the safe distance measures for all the OV within the ROI represented by the *CalculateSF* function respectively, (2) The reference trajectories for the MIMPC and the APF-MPC algorithm are generated based as discussed in Section 4-4-1 and Section 4-3-5 respectively and is represented by the *GenerateRefTraj* function, (3) the MIMPC optimal control problem is run using the above calculated data along with the HV and OV data to generate the optimal lane, (5) this optimal lane along with the input given to the MIMPC optimal control problem is given as an input to the APF-MPC optimal control problem. This calculates the quadratic approximations of the road and obstacle potentials as defined in Chapter 3 and the optimal input for the HV is generated.

Chapter 5

Simulations and Results

This chapter presents the results of simulations that run the APF-MPC and the MIMPC+APF-MPC control strategies defined in Chapter 4. The simulations were run using the help of the YALMIP toolbox for MATLAB to model the optimization problems.

YALMIP [77] is a MATLAB toolbox specifically designed to model and solve optimization problems using a set of inbuilt or external solvers. The use of YALMIP to solve optimization problems simplifies the development of the optimization problem. Initially introduced to solve Semi-Definite Programming and Linear Matrix Inequalities based optimization problems, YALMIP has evolved to support quadratic and second-order cone problems. This thesis has two different kinds of optimization problems to solve. While the APF-MPC control strategy, as well as the APF-MPC part of the MIMPC+APF-MPC control strategy, are represented by quadratic programming problems with quadratic objective function and linear equality and inequality constraints, the MIMPC part of the MIMPC+APF-MPC control strategy is a MIQP problem. As YALMIP is a toolbox used to simplify the modelling of optimization problems, external solvers are required to solve the quadratic and MIQP based optimization problems.

Gurobi [78] is one such state-of-the-art commercial solver for linear, quadratic and mixed integer programming with advanced resolve methods used to simplify optimization problems. As Gurobi can solve both quadratic programming and mixed integer problems efficiently, it is used as the solver to solve the APF-MPC and the MIMPC+APF-MPC control strategies. Gurobi uses a simplex or parallel barrier algorithm to solve the quadratic programming problem and a branch and bound-based algorithm to solve the MIQP problem.

5-1 Simulation Results

The thesis simulates the APF-MPC and the MIMPC+APF-MPC control strategies in four different scenarios. These scenarios reflect real-world situations an AV will face while driving. These situations are divided into two different categories based on the velocity of the OV

- Scenarios where OV are moving at constant velocity.
  - Single lane change: Single lane change by the HV to avoid an OV in front of it.
  - Deceleration of HV: Deceleration by the HV to avoid collision with vehicles moving at a slower velocity as no lane change is possible
  - Double Lane change: Double lane change by the HV to avoid multiple OV on the road.
- Scenarios where the velocity of the OV changes.
  - Deceleration of the OV: Deceleration of the HV to match the speed of the OV in front to avoid collision in case of sudden deceleration by the OV.

This section compares the APF-MPC and the MIMPC+APF-MPC control strategies by overlapping the results from both on a single graph.

Each of the scenarios above is presented as follows: (1) plot initial states of the HV and all the OV and the length of the road that the simulation is conducted over, (2) plot/s showing the different key points of the simulation in terms of lane change and deceleration/acceleration, and (3) plot showing the path of the HV and OV, the other states of the HV and the flags generated during the simulation after the end of the simulation.

Let us now introduce some general terminology and representation of objects used in the results shown in the upcoming sections.

- The obstacles are represented as a rectangle with a wedge attached to its end as discussed in Figure 3-3. The length of the wedge changes as the velocity of the HV and the respective OV changes over time. The HV and OV in a control strategy are represented as seen in Figure 5-1. However, as the vehicles travel at different velocities at each time instant for each of the control strategies, every plot will contain two different sets of images for the HV and OV respectively.

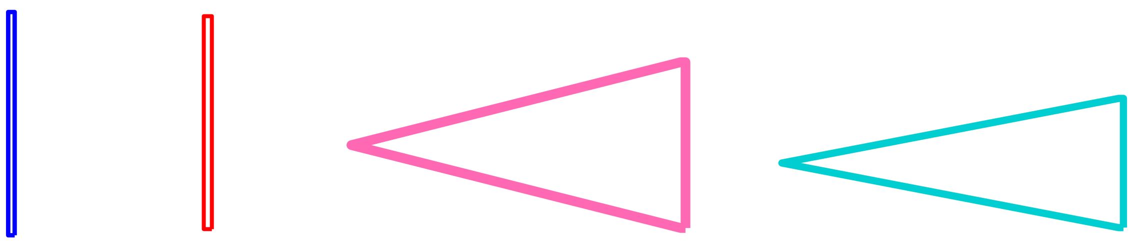

(a) **(b)** **(c)** **(d)**

Figure 5-1: Representation of the (a) HV in the MIMPC+APF-MPC control strategy (b) HV in the APF-MPC control strategy, (c) OV in the MIMPC+APF-MPC control strategy, (d) OV in the APF-MPC control strategy during simulations

- The road selected has different lengths based on the type of simulation. Figure 5-2 shows an empty road with a road of length 1000 m.

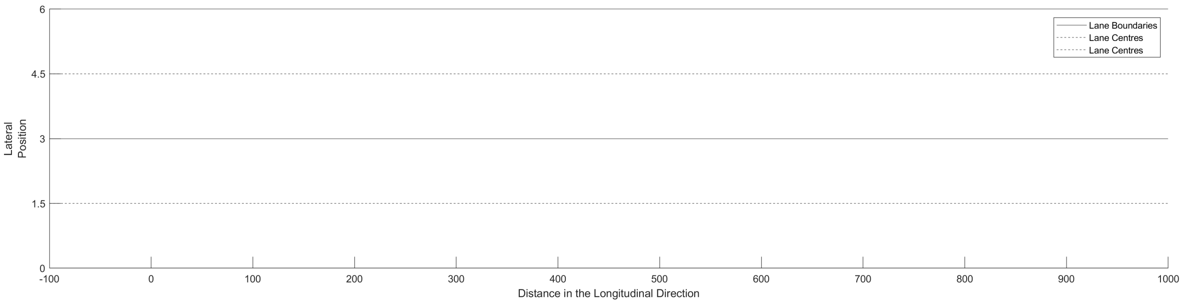

Figure 5-2: Representation of the lane centres and boundaries

- Table 5-1 shows the legend representing the different variables used in this thesis. Some legends represent multiple variables over different plots. For example, the red line represents all the variables representing the HV during the APF-MPC control strategy. It represents the path when the different paths for different strategies are compared, the velocity of the HV when the velocity of the different strategies are compared and so on. As a colour represents one variable at a time within a plot, the chance of confusion is minimal.

Representation	Description	Color	Line Properties
	MIMPC	Green	Solid
	APF-MPC	Red	Solid
	MIMPC+APF-MPC	Blue	Solid
	Lane Boundaries	Black	Solid
	Lane Centers	Black	Dashed
	Reference Data (MIMPC+APF-MPC)	Magenta	Dashed
	OV Data (MIMPC+APF-MPC)	Pink	Solid and Bold
	flag_δ (MIMPC+APF-MPC)	Purple	Solid and Bold
	flag_{LC} (MIMPC+APF-MPC)	Orange	Dashed and Bold
	OV Data (APF-MPC)	Turquoise	Solid and Bold
	Reference Data (APF-MPC)	Dark Green	Dashed
	flag_δ(APF-MPC)	Dodger Blue	Solid and Bold
	flag_{LC} (APF-MPC)	Brown	Dashed and Bold

Table 5-1: Representation of different variable during Simulation

- As the results are a combination of lane changes and braking/accelerating manoeuvres depending on the scenario 5-1, the results are shown as a combination of plots, each of which represents one manoeuvre.

A manoeuvre representing a lane change contains two plots. The first plot shows the path taken by the HV to reach the point before the start of the lane change manoeuvre and the second plot shows the same at the end of the manoeuvre.

A manoeuvre representing the braking/acceleration of the HV also contains two sets of plots, each with two individual plots. The first set plots at the beginning of the manoeuvre and the second set of plots show the plots at the end of the manoeuvre. The two plots within a set are: (1) a plot to show the path taken by the HV to reach the point and (2) a plot to show the velocity at that point.

- The results of both control strategies are shown in each plot to compare the variables for each of the control strategies.

The simulation results in the scenarios discussed are discussed in the introduction of Section 5-1 for the MIMPC+APF-MPC and the APF-MPC control strategies are shown next.

5-1-1 Single Lane Change

A single lane change scenario shows the response of the integrated control strategies designed in this thesis to the presence of an OV in the same lane and in front of the HV with no OV in the adjacent lane. The initial state of the HV at the start of the scenario is given as

$$\mathbf{x}_{\text{HV}_{base}} = \begin{bmatrix} 35 & 0 & 1.5 & 0 & 0 & 0 \end{bmatrix}^T, \; \mathbf{x}_{\text{OV}_{base}} = \begin{bmatrix} 10 & 500 & 1.5 & 0 & 0 & 0 \end{bmatrix}^T \tag{5-1}$$

where $\mathbf{x}_{\text{HV}_{base}}$ and $\mathbf{x}_{\text{OV}_{base}}$ are the base values of the HV and OV at the start of the simulation and the road length is 1000 m. Figure 5-3 show the initials states of the system on the road.

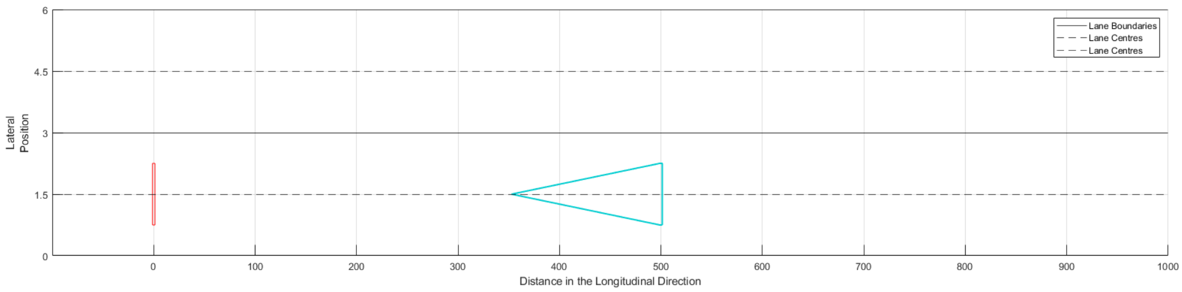

Figure 5-3: Initial state of the HV and OV for the Single Lane Change scenario

The single lane change manoeuvres for the MIMPC + APF-MPC control strategy and the APF-MPC control strategy occur at different points in time. Figure 5-4 shows the instances of the simulations where the lane change manoeuvres start and end for both control strategies.

The following sections explain the reasoning behind the manoeuvres shown in Figure 5-4.

MIMPC + APF-MPC control strategy

Figure 5-4a and Figure 5-4b show the points in the simulation of the MIMPC + APF-MPC control strategy right before and after the HV changes lane. The lane change starts due to

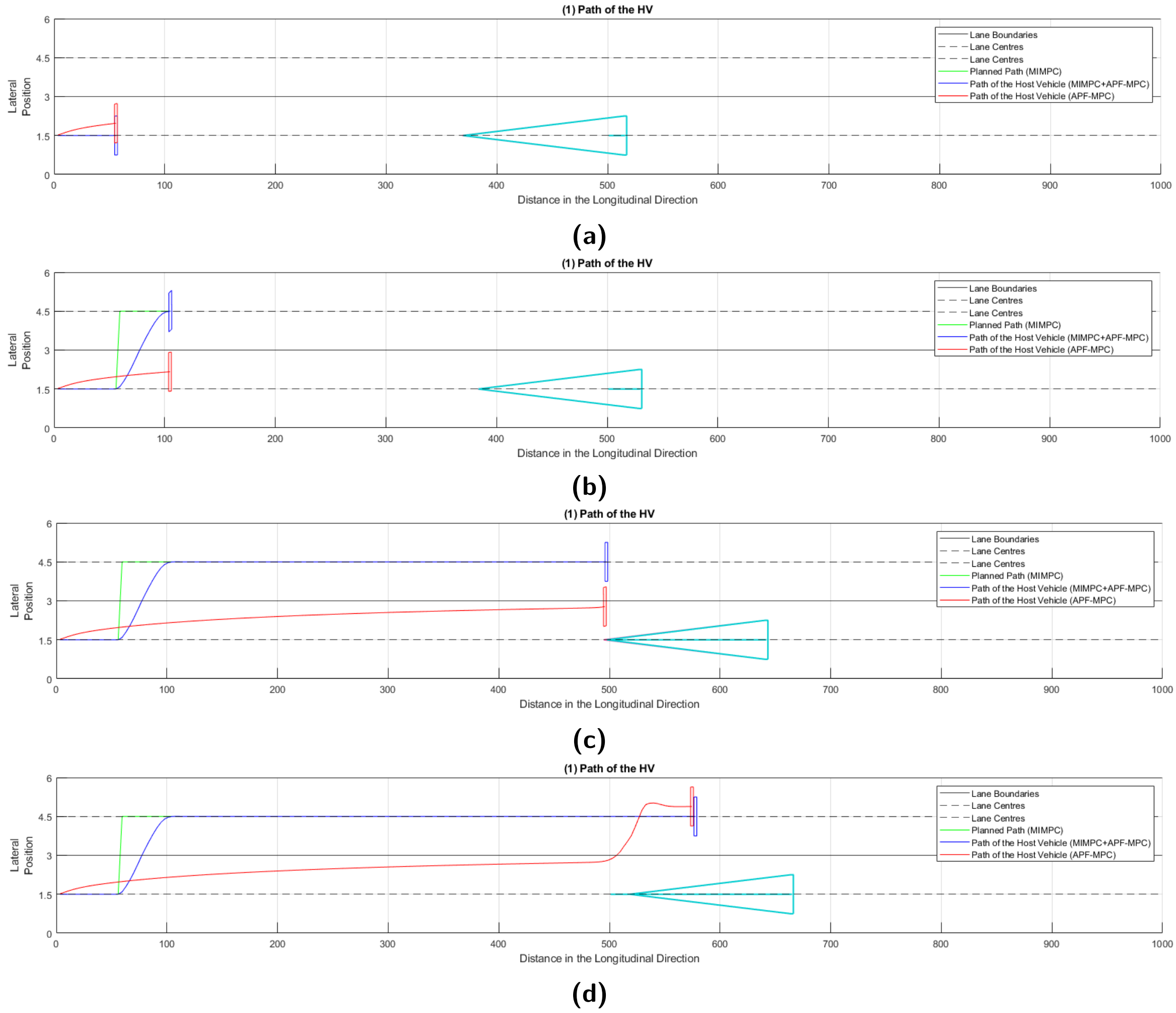

Figure 5-4: Manoeuvres during the simulation of Single Lane Change scenario

Figure	Explanation
5-4a	Start of the lane change for the HV in the MIMPC+APF-MPC control strategy
5-4b	End of the lane change for the HV in the MIMPC+APF-MPC control strategy
5-4c	Start of the lane change for the HV in the APF-MPC control strategy
5-4d	End of the lane change for the HV in the APF-MPC control strategy

Table 5-2: Basic explanation of different sub-figures shown in Figure 5-4

the presence of an OV within the ROI, in the same lane and in front of the HV (Line 2, Algorithm 1). When the HV notices the OV within its ROI, it checks if there exists an OV in the adjacent lane (Line 4-Line 16, Algorithm 1). As there is no OV in the adjacent lane in this scenario, the HV changes lane. The MIMPC part of the MIMPC + APF-MPC control strategy (Equation (4-64)) uses the above data to generate an optimal lane. This lane input is used to select the correct road potential and generate the optimal path to travel in (Equation (4-65)).

APF-MPC control strategy

Figure 5-4c and Figure 5-4d show the points in the simulation of the APF-MPC control strategy before and after the HV changes lane. The HV changes lane very close to the OV unlike that of the MIMPC + APF-MPC control strategy as the lane change and lane keeping characteristics are controlled only with the help of the potential functions defined. The HV drifts to the centre of the road due to the shape of the road potential as shown in Figure 3-11. The HV moves away from the lane centre as it passes the OV in the adjacent lane due to the higher weight of the obstacle potential with respect to the road potential.

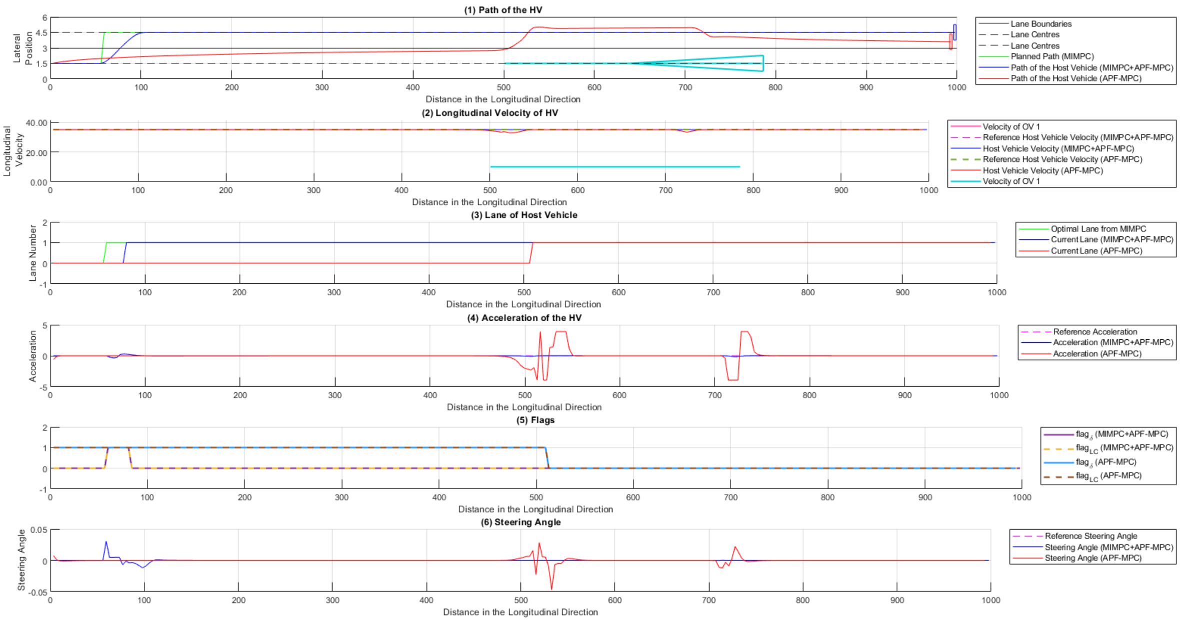

Figure 5-5: Final state of the HV and OV for the Single Lane Change scenario

Figure 5-5 shows the plot of the states of the HV after the end of the simulation of the single lane change scenario. It can be seen from Figure 5-5 (4) that the acceleration of the HV has small spikes when the HV passes by an OV in the adjacent lane. This is due to the influence of the changing regions of OV and happens when entering from a region where $1 \leq t \leq 0$ when calculating the euclidian distance $K_{\text{obs}_{\text{conv}}}$ to a region where $t > 1$ or $t < 0$. This change in acceleration and the influence of the obstacle potential also generates a small change in steering angle as shown in Figure 5-5 (6).

5-1-2 Deceleration of the HV

This section shows the response of the integrated path planning and control algorithms designed in this thesis to the presence of obstacles in both lanes of the road that are moving slower than the base velocity of the HV and, thus no lane change possible. Figure 5-6 shows the initial state of the HV at the start of the scenario and is given as

$$\mathbf{x}_{\mathrm{HV}_{base}} = \begin{bmatrix} 41.6 & 0 & 1.5 & 0 & 0 & 0 \end{bmatrix}^T, \ \mathbf{x}_{\mathrm{OV}_{base}} = \begin{bmatrix} 20 & 600 & 1.5 & 0 & 0 & 0 \\ 20 & 600 & 4.5 & 0 & 0 & 0 \end{bmatrix}^T \tag{5-2}$$

with a simulated road length of 1000 m. The simulation for this section consists of a braking

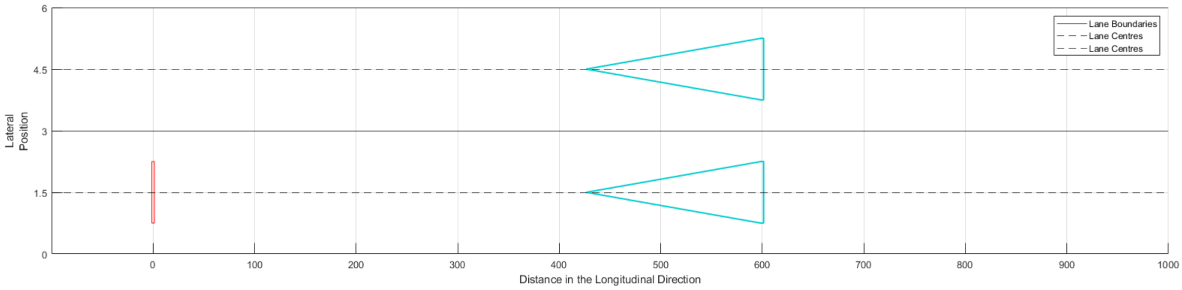

Figure 5-6: Initial state of the HV and OV for the Deceleration of the HV scenario

manoeuvre by the HV behind a pair of slower-moving OV. The braking manoeuvre for each of the control strategies starts and ends at different instances and are shown in Figure 5-7 and 5-8. The simulations are divided into two separate figures due to space limitations. Table 5-3 gives a basic explanation of the different sub-figures shown in Figure 5-7 and 5-8. The

Figure	Explanation
5-7a	Start of braking by the HV in the MIMPC+APF-MPC control strategy
5-7b	Start of braking by the HV in the APF-MPC control strategy
5-7c	Start of braking by the HV in the APF-MPC control strategy
5-8	End of braking by the HV in the MIMPC+APF-MPC control strategy

Table 5-3: Basic explanation of different sub-figures shown in Figure 5-7 and 5-8

following sections explain the reasoning behind the manoeuvres shown in Figure 5-7 and 5-8.

MIMPC + APF-MPC control strategy

Figure 5-7a and Figure 5-8 show the instances in the simulation of the MIMPC + APF-MPC control strategy right before and after the HV starts braking behind the OV. As lane change is not possible due to the presence of an OV in the adjacent lane within a given distance (Line 6-Line 8, Algorithm 1), the velocity reference to the HV changes to the velocity of the OV in front of it in the same lane and the HV starts decelerating (Algorithm 3).

APF-MPC control strategy

Figure 5-7b and Figure 5-7c show the instances in the simulation of the APF-MPC control strategy right before and after the HV start and end of braking behind the OV. The reason

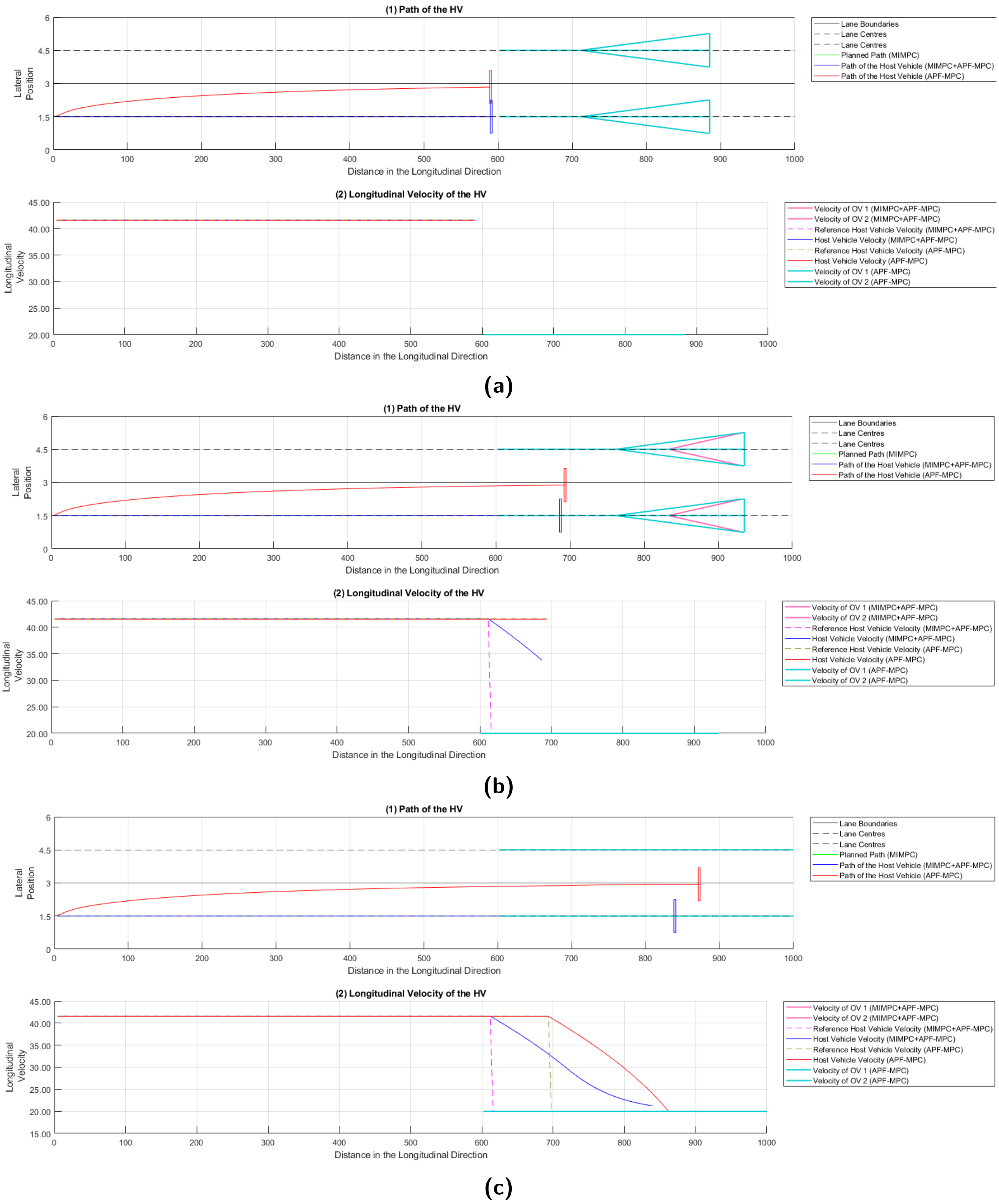

Figure 5-7: Manoeuvres during the simulation of Deceleration of HV scenario- 1

for the deceleration is the same as in the case of the MIMPC + APF-MPC control strategy. However, in this case, the distance between the HV and the OV in front of it before the start of deceleration of the HV is lower than that of the MIMPC + APF-MPC control strategy. This is due to the fact that the MIMPC + APF-MPC control strategy uses logical constraints

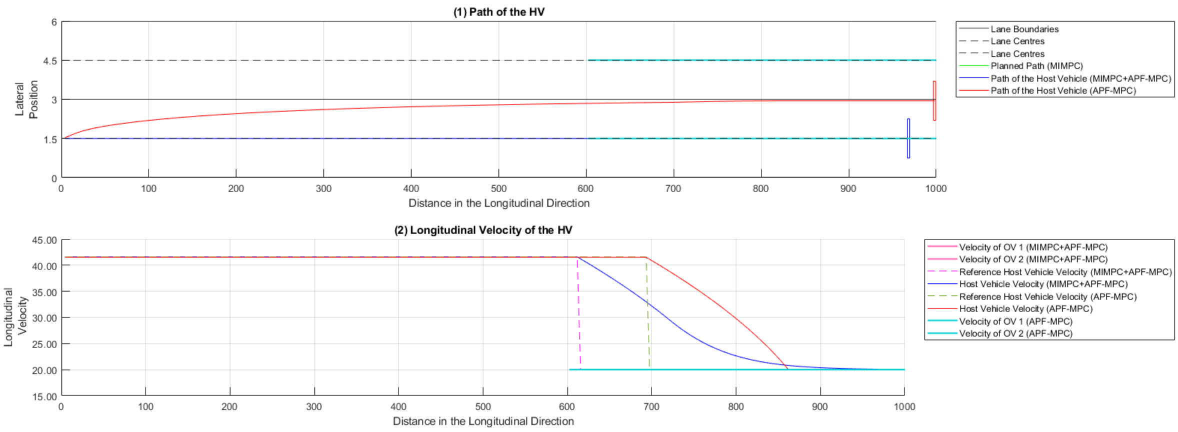

Figure 5-8: Manoeuvres during the simulation of Deceleration of HV scenario-2

to maintain a minimum distance from the OV and change lanes (Equation (4-53)).

Figure 5-9 shows the states of the vehicle after the end of the simulation. It can be seen clearly that the rate of change of acceleration between the two control strategies is very different. Let

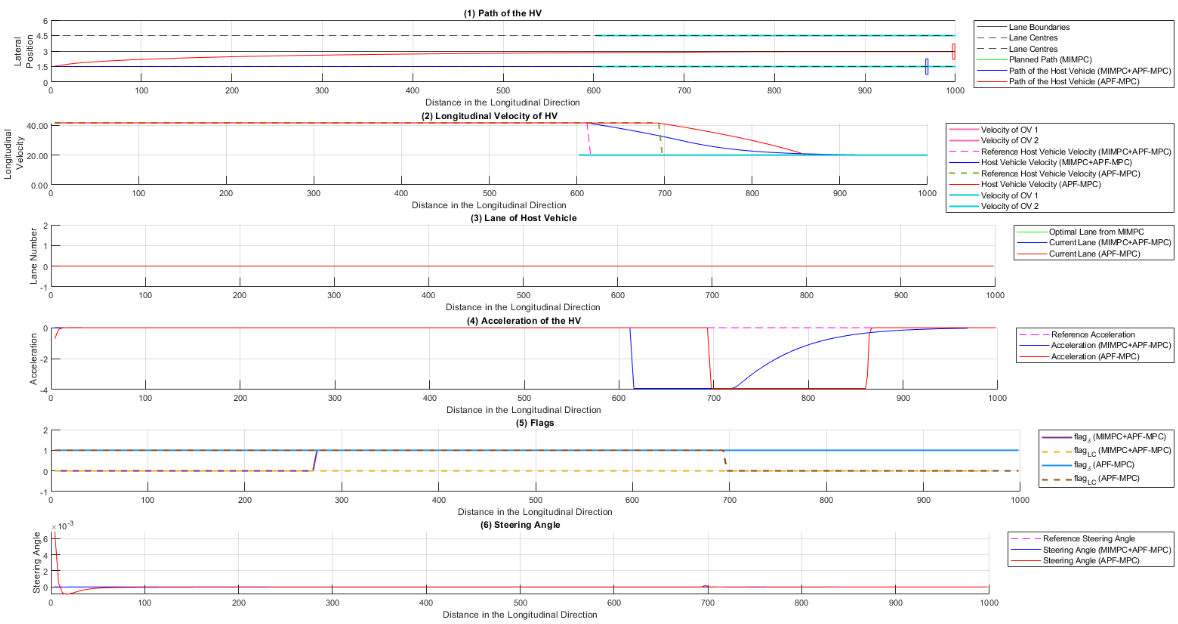

Figure 5-9: Final state of the HV and OV for the Deceleration of the HV scenario

us define rms_{jerk} and $\text{rms}_{\text{accel}}$ as the Root Mean Square (RMS) values of the rate of change of acceleration and acceleration over the simulation and let $q = 1, 2, 3, \ldots, n$ be the total number of loops over the simulated road. Equation (5-3) shows the mathematical equations for calculating rms_{jerk} and $\text{rms}_{\text{accel}}$.

$$\begin{aligned}\text{rms}_{\text{jerk}} &= \sqrt{\frac{1}{n}\sum_{k=1}^{n}\left(a_{x,\text{HV}_{q+k-1|q}} - a_{x,\text{HV}_{q+k-2|q}}\right)^2} \\ \text{rms}_{\text{accel}} &= \sqrt{\frac{1}{n}\sum_{k=1}^{n}\left(a_{x,\text{HV}_{q+k-1|q}}\right)^2}\end{aligned} \tag{5-3}$$

Table 5-4 shows the RMS values of the acceleration and jerk for the control strategies. It can be seen that the MIMPC + APF-MPC control strategy has lower values of RMS jerk and acceleration when compared to the APF-MPC control strategy. This leads to a more comfortable ride for the passengers of the HV.

Root Mean Square	MIMPC + APF-MPC	APF-MPC
$\text{rms}_{\text{accel}}$	1.4689	1.7010
rms_{jerk}	0.2265	0.2883

Table 5-4: RMS values of the acceleration and jerk for the control strategies for simulation of the Deceleration of HV scenario

5-1-3 Double Lane Change

A double-lane change scenario shows a combination of lane change and braking/acceleration manoeuvres in order to perform a double-lane change. This scenario consists of two obstacles whose initial states are shown in Figure 5-10. The initial states of the obstacles and the host

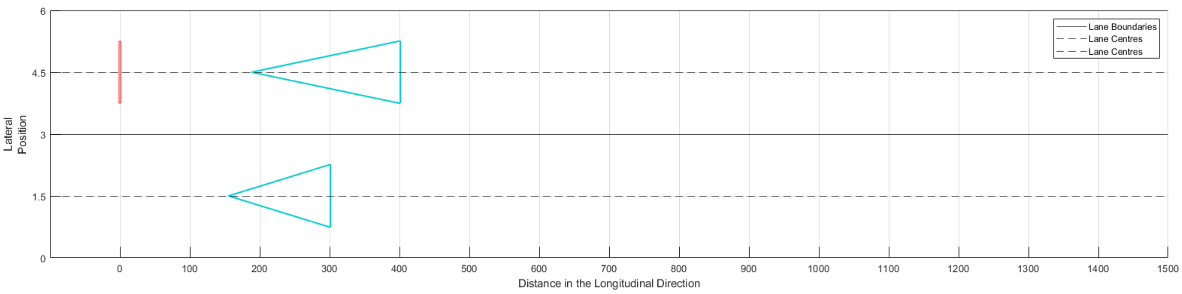

Figure 5-10: Initial state of the HV and OV for the Double Lane Change scenario

vehicle before the start of the simulation are

$$\mathbf{x}_{\text{HV}_{base}} = \begin{bmatrix}41.6 & 0 & 4.5 & 0 & 0 & 0\end{bmatrix}^T, \ \mathbf{x}_{\text{OV}_{base}} = \begin{bmatrix}10 & 400 & 1.5 & 0 & 0 & 0 \\ 25 & 300 & 1.5 & 0 & 0 & 0\end{bmatrix}^T \tag{5-4}$$

with the simulation road length of 1400 m. Figure 5-11, 5-12, 5-13 and 5-14 show the different manoeuvres that the HV performs to avoid obstacles and move forward in order of occurrence.

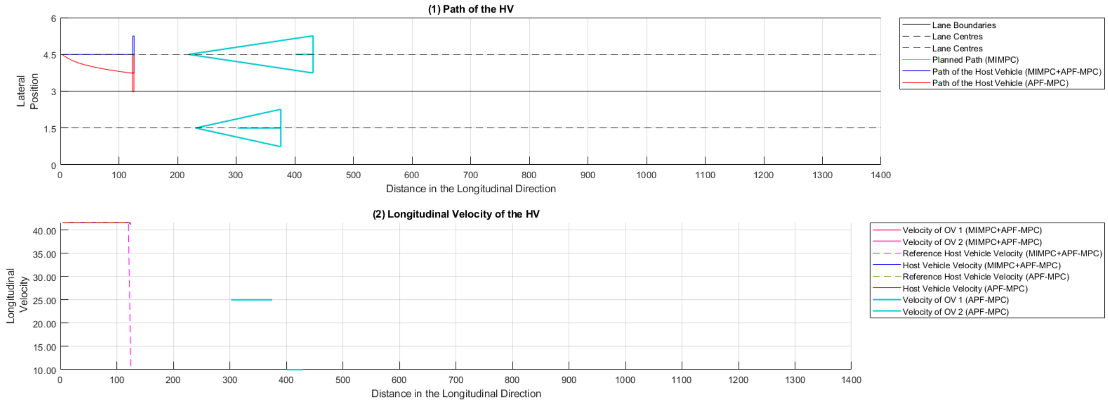

(a)

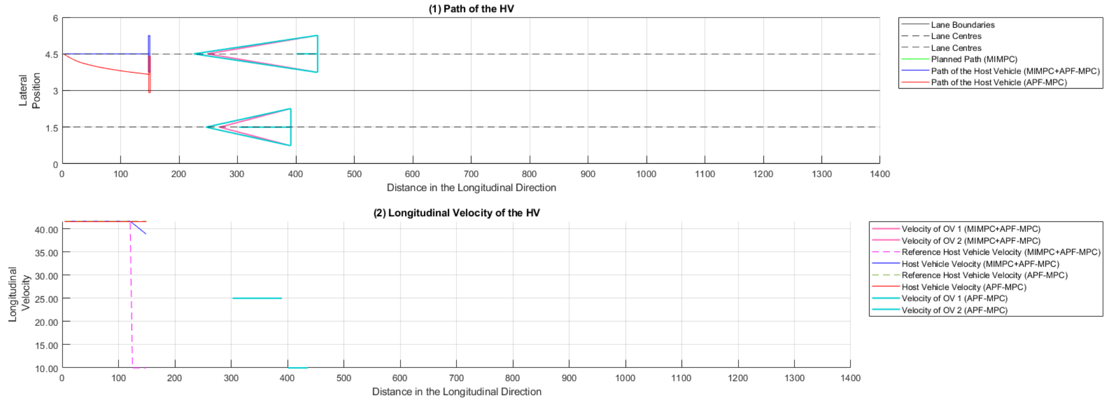

(b)

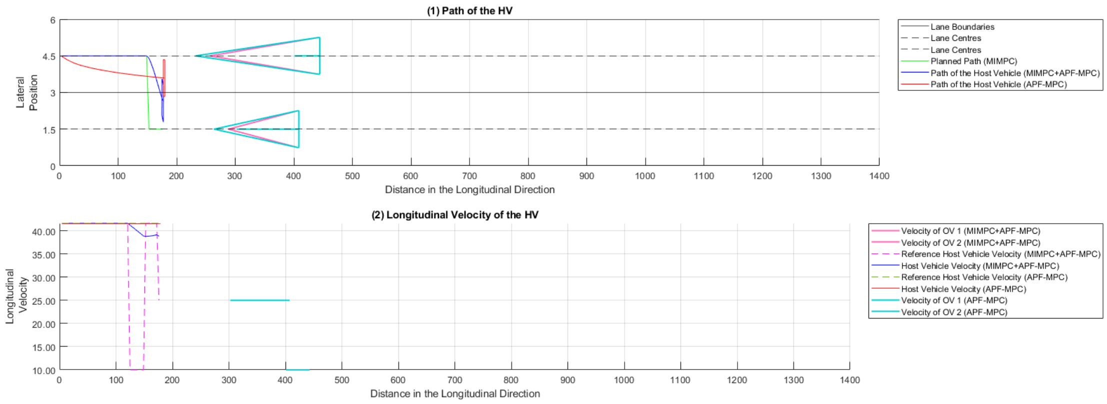

(c)

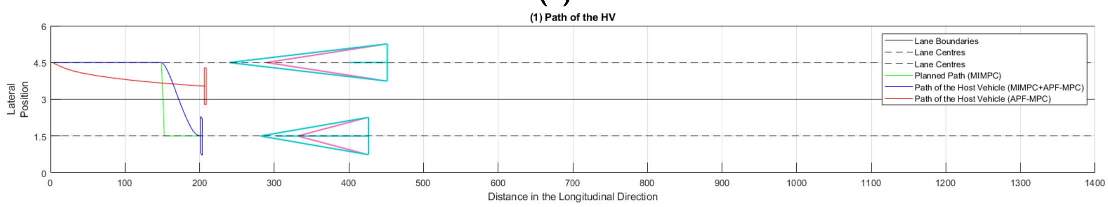

(d)

Figure 5-11: Manoeuvres in the simulation of Double Lane Change scenario-1

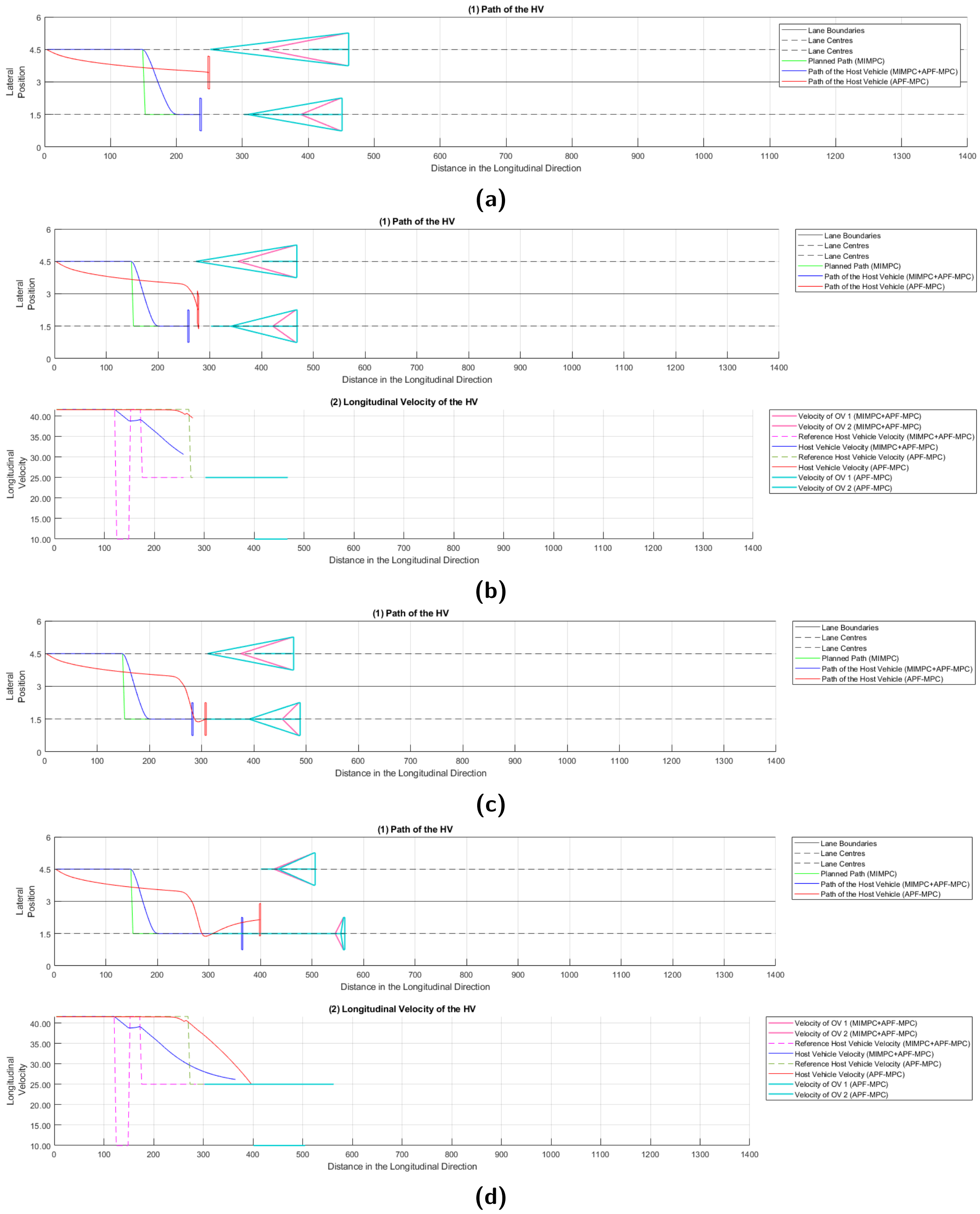

Figure 5-12: Manoeuvres in the simulation of Double Lane Change scenario-2

The key instances are divided into four figures for clear visualization and the basic explanation of a manoeuvre/s represented in each figure is described in Table 5-5. The manoeuvres for the double lane change in the order of occurrence are:

- Deceleration of the HV to match the velocity of the OV in front of the HV in the same lane as lane change is not possible.

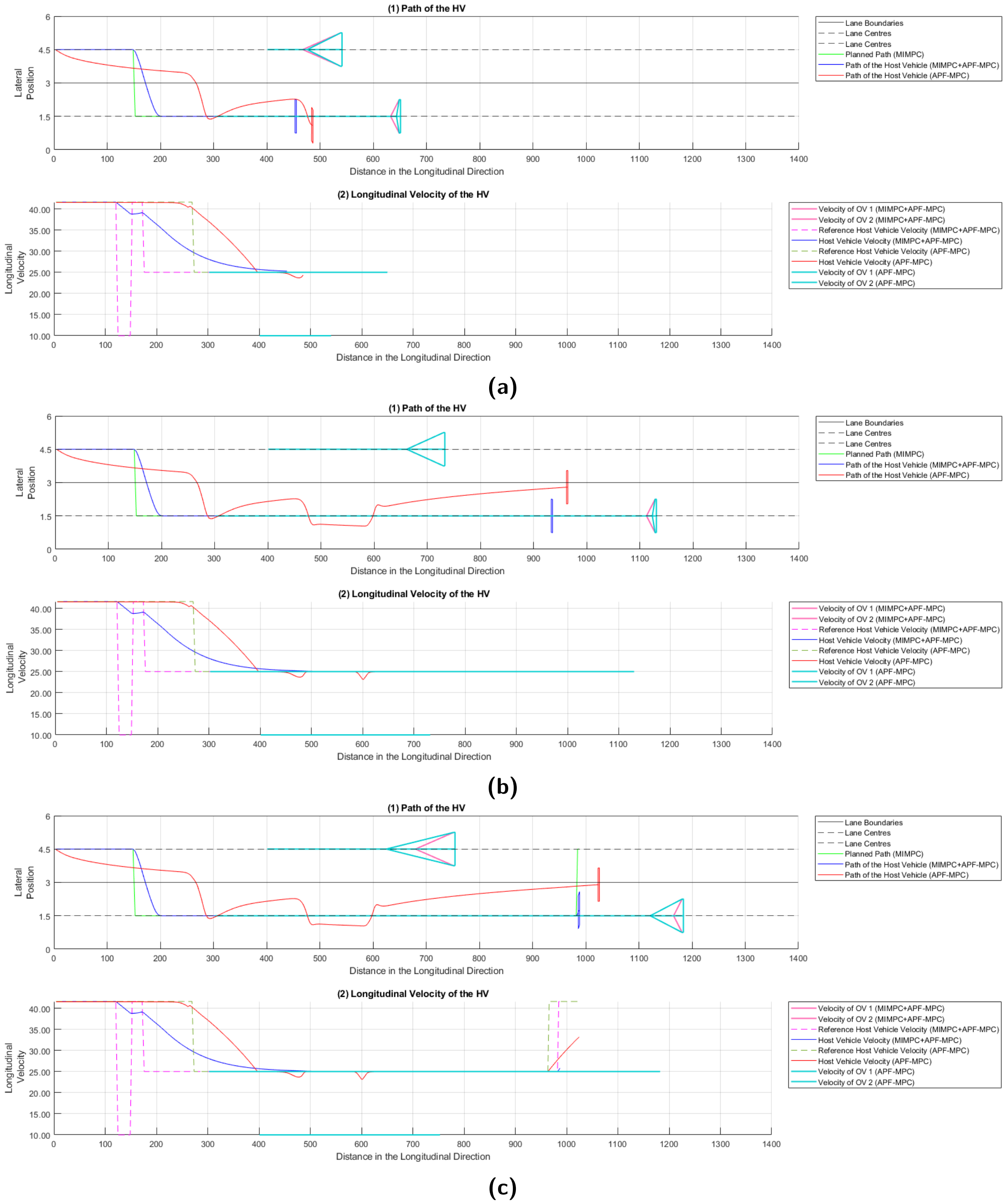

Figure 5-13: Manoeuvres in a simulation of Double Lane Change scenario-3

- Acceleration of the HV as lane change becomes possible.
- Lane change of the HV.
- and repeat three manoeuvres.

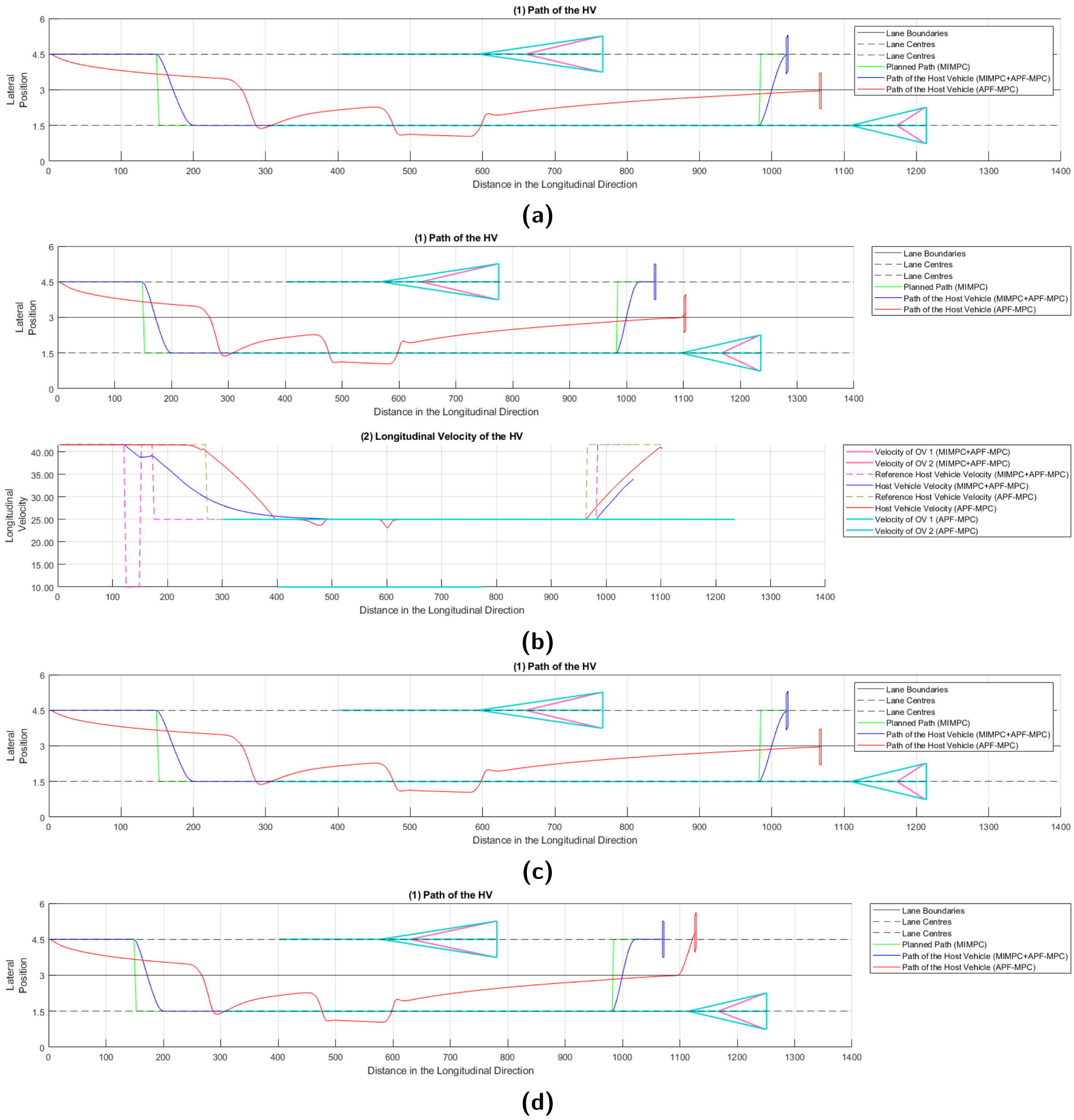

Figure 5-14: Manoeuvres in a simulation of Double Lane Change scenario-4

MIMPC + APF-MPC control strategy

Figure 5-11a (2) and 5-11b (2) show the longitudinal velocity at the start and end of the first change in reference velocity respectively while following the OV in front of the HV in the same lane. This is due to the fact that the distance between the OV and the HV becomes less than the safe distance and because the lane change is not possible (Line 6-Line 8, Algorithm 1). As soon as lane change is possible due to the movement of the OV in the adjacent lane, the velocity reference increases back to the base value as defined in (5-4) (Algorithm 3). This also leads to the beginning of the lane change which starts in Figure 5-11b (1) and ends in Figure 5-11d (1). However, when the HV crosses the centre of the road during the process

Figure	Explanation
5-11a	Start of deceleration by the HV in the MIMPC+APF-MPC control strategy due to change in reference velocity
5-11b	End of deceleration and the start of lane change and the start of acceleration by the HV in the MIMPC+APF-MPC control strategy
5-11c	End of acceleration and start of deceleration by the HV in the MIMPC+APF-MPC control strategy due to change in reference velocity
5-11d	End of lane change by the HV in the MIMPC+APF-MPC control strategy
5-12a	Start of lane change by the HV in the APF-MPC control strategy
5-12b	Start of deceleration by the HV in the MIMPC+APF-MPC control strategy due to change in reference velocity
5-12c	End of lane change by the HV in the APF-MPC control strategy
5-12d	End of deceleration by the HV in the APF-MPC control strategy
5-13a	End of deceleration by the HV in the MIMPC+APF-MPC control strategy
5-13b	Start of lane change and acceleration by the HV in the APF-MPC control strategy
5-13c	Start of lane change and acceleration by the HV in the MIMPC+APF-MPC control strategy
5-14a	End of lane change by the HV in the MIMPC+APF-MPC control strategy
5-14b	End of acceleration by the HV in the APF-MPC control strategy
5-14c	End of lane change by the HV in the APF-MPC control strategy
5-14d	End of acceleration by the HV in the MIMPC+APF-MPC control strategy

Table 5-5: Basic explanation of different sub-figures shown in Figures 5-11-5-14

of changing lanes, the distance between the OV in the newly entered lane and the HV will become less than the safe distance measure if the HV continues with the same velocity and therefore the velocity reference changes again as shown in Figure 5-11c (2) (Equation (4-53a)). This leads to the deceleration of the HV which ends in Figure 5-13a (2). The start and end of the next lane change are shown in Figures 5-13c (1) and 5-14a (1) respectively. The reference velocity also changes back to the base velocity as defined in (5-4) with the start of the second lane change leading to the acceleration of the HV (Algorithm 3). The start and end of this change in velocity are shown in Figures5-13c (2) and 5-14c (2).

APF-MPC control strategy

Figure 5-12a (1) and 5-12c (1) show the start and of the first lane change. The lane change starts due to the potential of the OV in front of the HV in the same lane ($\mathrm{OV}_{\mathrm{SL},f}$) (Equation

(4-47)). The lane change is followed by a change in reference velocity as soon as it crosses the centre of the road to keep outside wedge shaped block of the OV potential (Algorithm 3). This leads to the change in reference velocity and therefore deceleration of the HV whose start and end are shown in Figures 5-12b (2) and 5-12d (2).

The start of the second lane and velocity reference change are shown in Figures 5-13b (1) and (2) and ends in Figures 5-14c (1) and 5-14b (2) respectively. The velocity reference changes before the lane change begins because the velocity reference changes as soon as there is a possibility for lane change (Algorithm 3 but the lane change only happens when the HV moves close to the OV in front of it (Equation (4-47)).

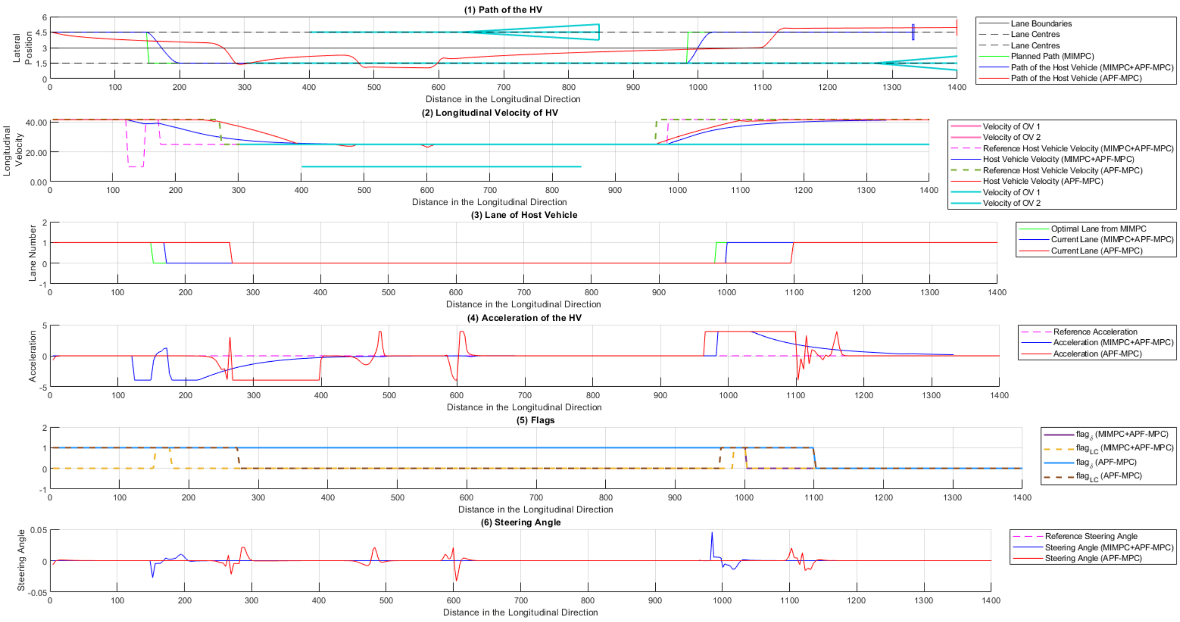

Figure 5-15: Final state of the HV and OV for the Double Lane Change scenario

Figure 5-15 shows the final path for both the controllers taken by the different states of the HV. It can be seen that the acceleration of the APF-MPC control strategy changes more rapidly because of the higher influence of the potentials and the tighter steering angles when compared to the MIMPC + APF-MPC control strategy. The RMS values of the vehicle longitudinal acceleration and jerk are given in Table 5-6.

Root Mean Square	MIMPC + APF-MPC	APF-MPC
rms_{accel}	1.4252	1.8364
rms_{jerk}	0.3622	0.8614

Table 5-6: RMS values of the acceleration and jerk for the control strategies for simulation of the Double Lane Change scenario

5-1-4 Deceleration of the OV

The deceleration of the OV scenario shows the response of both the algorithms in case of a sudden velocity change of the leading OV. The initial state of the HV and the OV at the start of the scenario is given by

$$\mathbf{x}_{\mathrm{HV}_{base}} = \begin{bmatrix} 41.6 & 0 & 4.5 & 0 & 0 & 0 \end{bmatrix}^T, \ \mathbf{x}_{\mathrm{OV}_{base}} = \begin{bmatrix} 15 & 450 & 1.5 & 0 & 0 & 0 \\ 20 & 450 & 4.5 & 0 & 0 & 0 \end{bmatrix}^T \tag{5-5}$$

and is shown in Figure 5-16.

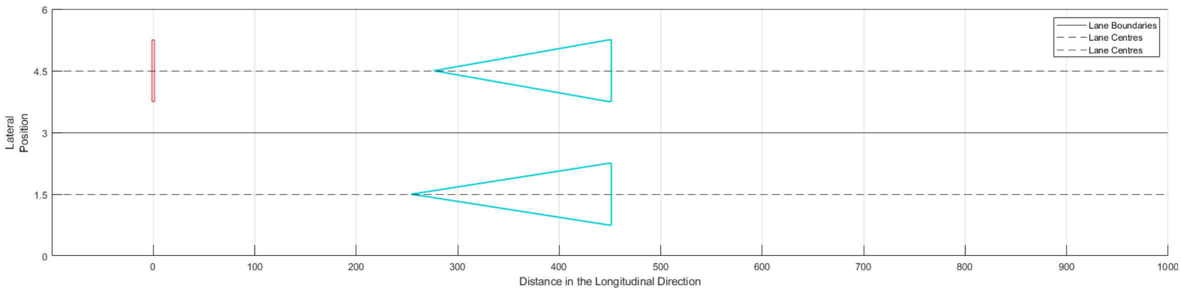

Figure 5-16: Initial state of the HV and OV for the Deceleration of the OV manoeuvre

Figure 5-17, 5-18 and Figure 5-19 show the key instance of the scenario. The scenario consists of two deceleration situations,

- Deceleration behind the OV in front in the same lane due to no possibility of the lane change.
- Deceleration behind the OV in front in the same lane due to no possibility of the lane change and to adapt to decelerating OV.

Table 5-7 gives the basic explanation of the different sub-figures showing the different key instances during the simulation of the Deceleration of OV scenario.

MIMPC + APF-MPC control strategy

Figure 5-17a (1) and 5-17a (2) shows the position and velocity of the HV at the beginning of deceleration of the HV to follow the OV in front. The deceleration is due to the change in reference velocity used to maintain a safe distance from the OV in front (Equation (4-53a)). The velocity of the HV reduces to that of the OV in front over time and the deceleration becomes zero as seen in Figure 5-18b (Algorithm 3). Figure 5-18d shows the response of the HV to the deceleration of the OV. As the OV on both lanes decelerate, the reference velocity of the HV also reduces leading to further deceleration of the HV. Figure 5-19b shows the position and velocity of the HV after the relative velocity between the OV and HV becomes zero.

Figure	Explanation
5-17a	Start of braking by the HV in the MIMPC+APF-MPC control strategy
5-17b	Start of braking by the HV in the APF-MPC control strategy
5-18a	End of braking by the HV in the APF-MPC control strategy
5-18b	End of braking by the HV in the MIMPC+APF-MPC control strategy
5-18c	Start of braking by the HV in the APF-MPC control strategy
5-18d	Start of braking by the HV in the MIMPC+APF-MPC control strategy
5-19a	End of braking by the HV in the APF-MPC control strategy
5-19b	End of braking by the HV in the MIMPC+APF-MPC control strategy

Table 5-7: Basic explanation of different sub-figures shown in Figure 5-17 and 5-19

.

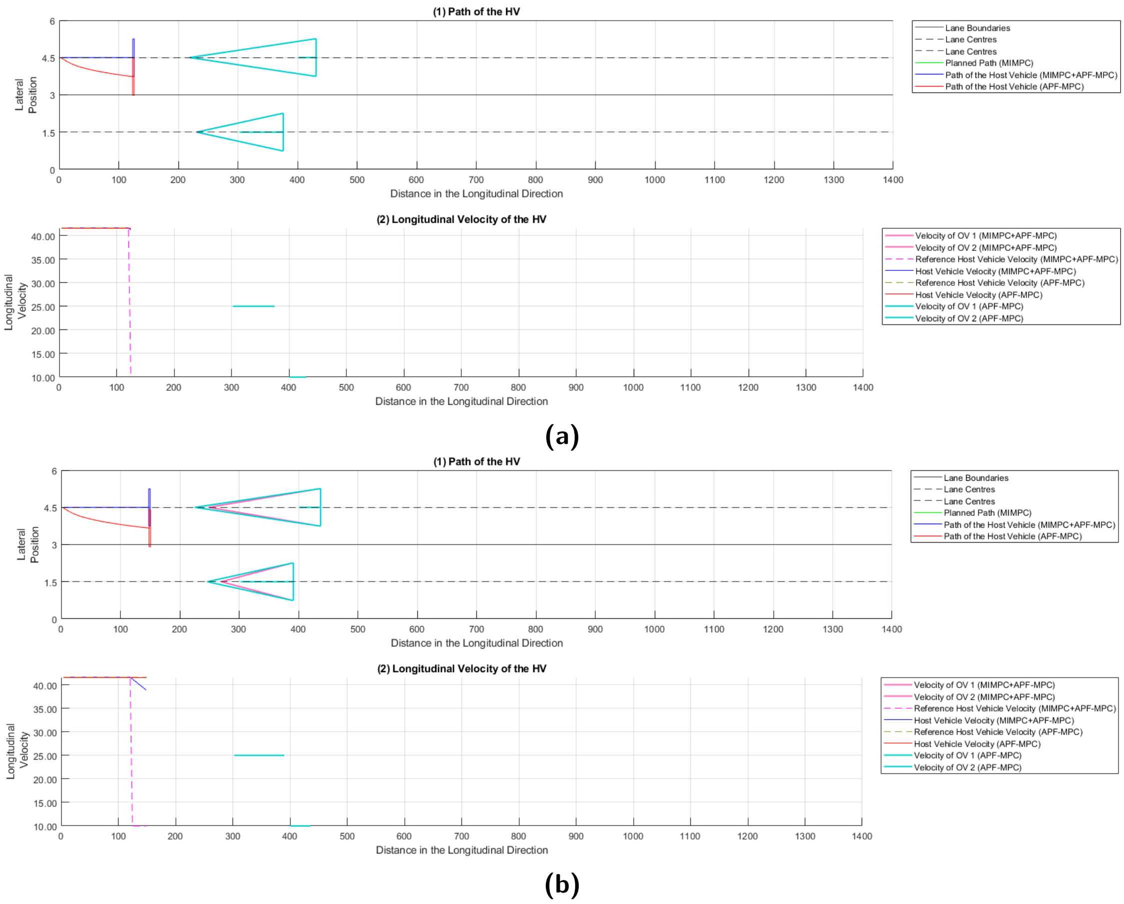

Figure 5-17: Manoeuvres in a simulation of Deceleration of OV scenario- 1

APF-MPC control strategy

The HV in the APF-MPC control strategy follows a very similar pattern of deceleration. Figure 5-17b (2) and 5-18a (2) shows the start and end of the deceleration of the HV in

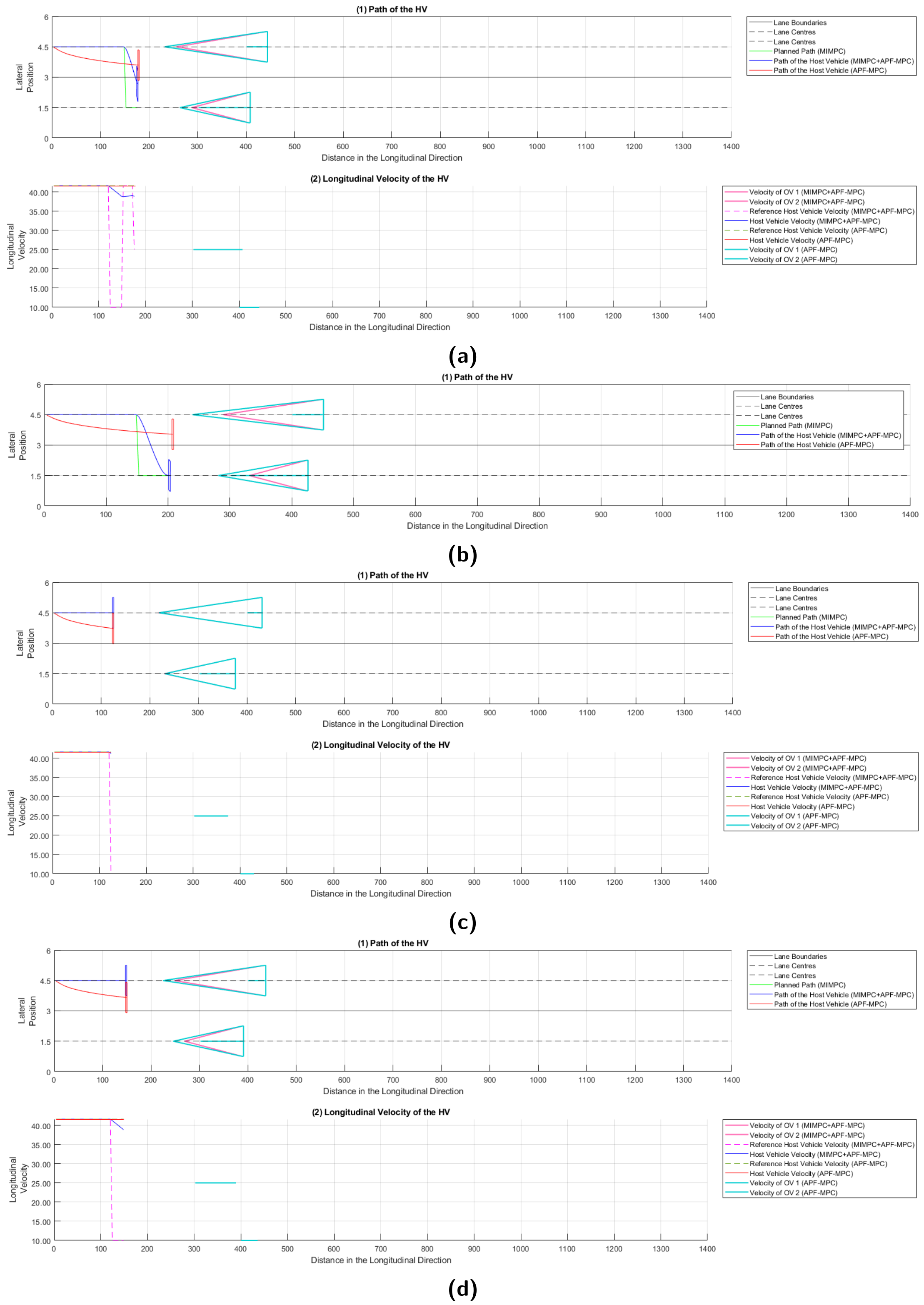

Figure 5-18: Manoeuvres in a simulation of Deceleration of OV scenario- 2

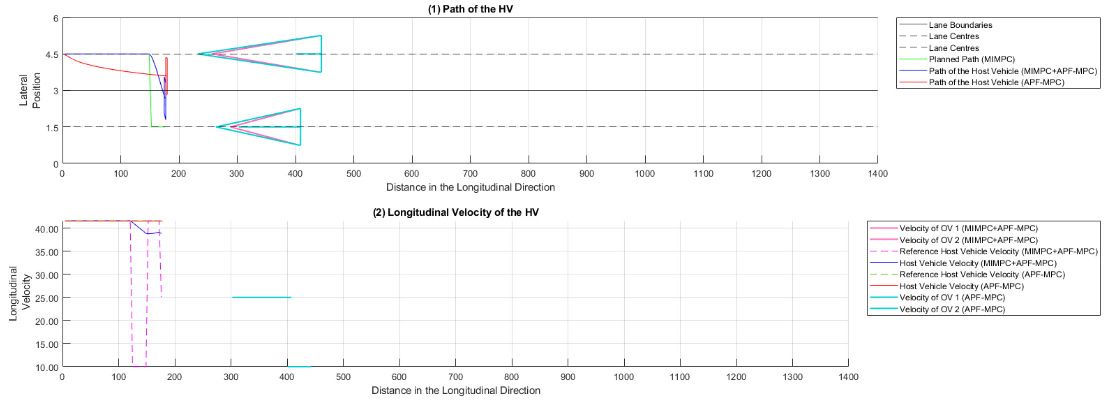

(a)

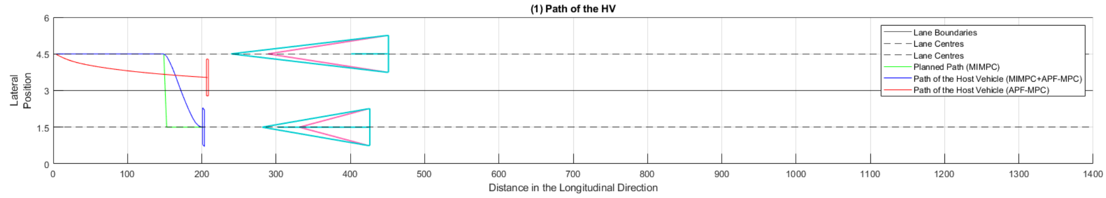

(b)

Figure 5-19: Manoeuvres in a simulation of Deceleration of OV scenario- 3

response to the change in reference velocity of the HV. Figure 5-18c (2) and 5-19a (2) shows the deceleration of the HV in response to the braking of the OV. However, the velocity of the HV follows the change in reference velocity without delay. This shows that the HV is more responsive in the APF-MPC control strategy.

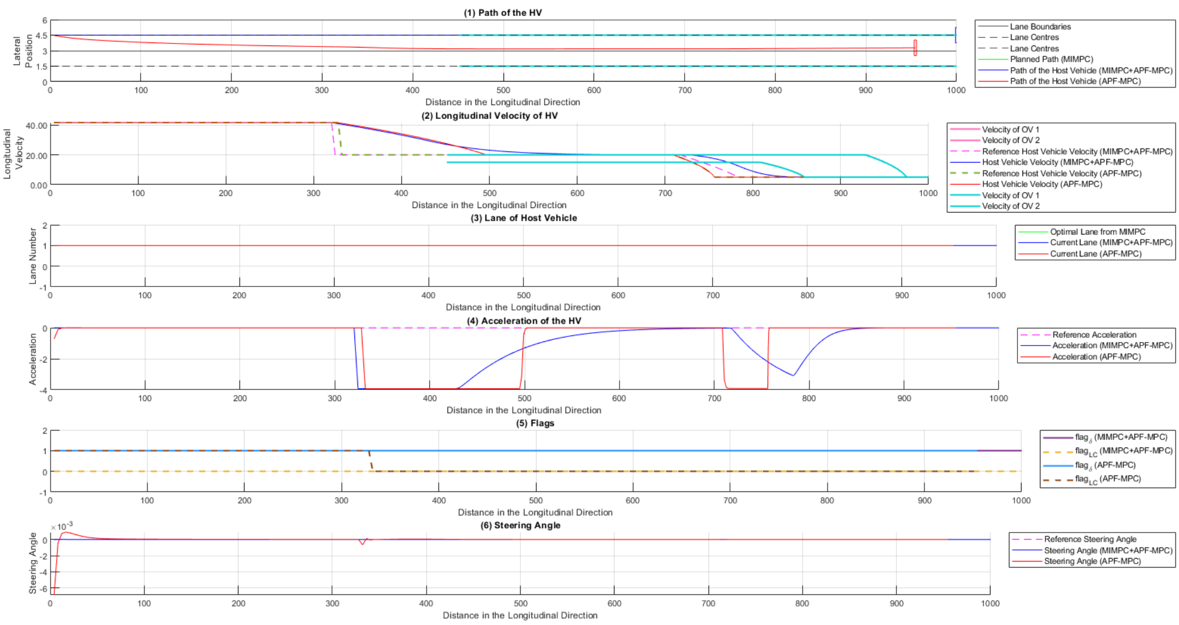

Figure 5-20: Final state of the HV and OV for the Deceleration of the OV manoeuvre

Figure 5-20 shows the final states and path of the system. It can be seen that the lane change flag for the HV was initially true due to the staggered position of the HV on both the lane but as it moved closer to the OV in front of it, the HV does not change lane due to the presence of the OV in the adjacent lane. Table 5-8 shows the RMS values of acceleration and jerk for both the control strategies.

Root Mean Square	**MIMPC + APF-MPC**	**APF-MPC**
$\mathrm{rms}_{\mathrm{accel}}$	1.1884	1.3614
$\mathrm{rms}_{\mathrm{jerk}}$	0.1548	0.2385

Table 5-8: RMS values of the acceleration and jerk for the control strategies for simulation of the Deceleration of OV scenario

Chapter 6

Conclusion and Future Work

The goal of this thesis was the design of a control algorithm which can integrate the path planning and motion control blocks of an AV. The APF method was chosen to achieve this goal as it can help integrate the path planning and motion control blocks of an AV by acting as a cost to be added to the objective function of an optimization-based control strategy for collision avoidance. An MPC based framework was chosen to formulate the path planning problem and was motivated due to the advantages of working with multi-input multi-output systems, the inclusion of system dynamics and constraints and re-planning nature of an MPC based control strategy. The design of the APF potential for obstacle and road was formulated such as to keep the vehicle away from the OV at a safe distance in case of sudden deceleration by the OV and to aid lane change and to keep the HV away from the road boundaries. As the obstacle potential was non-convex in nature, the obstacle potential underwent a convexification process to simplify the optimization problem. The obtained obstacle APF is further simplified using a Taylor series approximation to obtain a quadratic objective function of the APF-MPC optimal control problem. The model of the HV is linearized at each loop to obtain a prediction model of higher accuracy. The simulation on MATLAB shows that the HV avoids obstacles by keeping a safe distance even in complex scenarios.

However, this control strategy suffers from a few disadvantages: first, the HV does not stay in the centre of its lane but drifts to stay on the centre of the road due to the lack of an APF to guide the HV to its particular lane centre, second, the HV can take risky manoeuvres and third, the obstacle cannot follow an OV well. To overcome these problems, an MIMPC + APF-MPC control strategy was defined. This control strategy runs an MIMPC algorithm and an APF-MPC successively on each loop to calculate the optimal inputs to the actuators of the HV. The MIMPC algorithm uses a set of logical constraints to maintain a safe distance from the OV in front of it and uses a lane change flag to decide when to change lanes. The lane change flag is designed such that the HV does not perform risky manoeuvres. Each of these logical constraints are converted into a set of linear inequalities to transform the MIMPC problem into an MIQP problem with a quadratic objective function. The output of the MIMPC optimal control problem is the optimal lane to travel in based on simplified vehicle dynamics and above-defined linear inequalities. Having obtained the optimal lane to travel in, a set of road potentials are designed so that they can help guide the HV to the optimal lane. The obstacle APF is convexified and a quadratic approximation is obtained to be used in the objective function of the APF-MPC part of the control strategy. The objective function also contains the road potential chosen based on the value of the optimal lane. This simulation also avoids obstacles and also overcomes the disadvantages that the APF-MPC control strategy entailed. However,MIMPC + APF-MPC control strategy also has its own set of disadvantages: first, the time taken for the calculation of the MIMPC + APF-MPC control strategy is considerably higher than the other due to the computation complexity of an MIQP problem and second, the vehicles are much less dynamic in nature due to the dependence of the lane change flag on the OV in the same lane and the adjacent lanes and on the safe distance measure.

The simulations for both the APF-MPC and MIMPC + APF-MPC control strategies are carried out in multiple scenarios as discussed in Section 5-1. The simulations also consider multiple obstacles vehicles to check how well each of the algorithms works in complex scenarios. The control strategies were however not tested on real vehicles.

6-1 Future Work

The implementation of the MIMPC + APF-MPC control strategy for hardware-in-loop simulations is the first logical recommendation to understand its performance. The model of the HV and the OV can be improved for better prediction of their respective states over the prediction horizon. Though the use of a non-linear prediction model of the HV is not recommended due to a large increase in computation time, a better tire model like the Pacejka Magic tire formula [79] can be used to better handling capabilities of the prediction model to be closer to that of the actual HV. Another improvement could be the additional consideration of other external forces affecting the HV such as air drag or rolling resistance can improve the real-world application of the algorithm. The stability and robustness of the control strategy should be studied thoroughly for real-world application as sensor data obtained is never deterministic in nature. After ample testing in simulation, the control strategy has to be implemented on an actual vehicle for validation.

The second area of improvement is the extension of this thesis to work in a large number of different environmental conditions. This would extend the idea of this thesis limited to straight roads, a single friction coefficient and the shape of all OV being the same to different kinds of road profiles including but not limited to different road curvatures, banking angles, different friction coefficients and a multitude of road participants. This can lead to the formulation of a control strategy which can work well in multiple different environmental conditions and make it ready for real-world implementation.

A major issue while designing the control strategies was the tuning of the weights in the objective function. A trial and error method was used to find the current weights but they are far from optimal. A machine learning or neural network-based model can be used to tune the model online to obtain better performance from the controller [80].

It can be seen from the results that the rate of change of the steering angle of the HV is not smooth. The controller can therefore be redesigned to use a steering torque-based control strategy instead of the steering angle-based control strategy with the advantages of lesser control effort and smoother steering angle. The use of steering torque as a control input to the HV leads to more human-like driving characteristics where the controller gives more importance to smooth and continuous steering characteristics rather than staying at the lane centre at the end of a lane change manoeuvre. As most vehicles run on fly-by-wire systems, a steering torque control input removes the necessity for the conversion of the steering wheel angle to steering torque which needs to be applied to the wheels.

The idea of this thesis was to generate a collision-free path using an integrated path planning and vehicle control block for the HV. However, the idea can be extended to work with all the vehicles on the road within a given distance from the HV so as to design a multi-vehicle autonomous driving coordination problem that can generate the respective inputs for all the considered vehicles for safe and efficient driving [15]. The advantage of this idea is to make sure that all the vehicles can satisfy their respective goals while taking into account the goals of the others to generate a path which works the best for all the given vehicles.

Appendix A

Quadratic Taylor-series approximation

The Taylor-series approximation generates an p^{th}-order polynomial as its approximation for a given p-times differentiable function around a given point. As the function under consideration is a convex function, a quadratic approximation with $p = 2$ is used. The general form of a multi-variable quadratic Taylor-series approximation for a function h dependent on variable $\boldsymbol{x}$ around given point $\boldsymbol{x}_0$ is given by

$$T_h = h\left(\boldsymbol{x}_0\right) + \nabla_h\left(\boldsymbol{x}_0\right)\left(\boldsymbol{x} - \boldsymbol{x}_0\right) + \frac{1}{2}\left(\boldsymbol{x} - \boldsymbol{x}_0\right)^T H_h\left(\boldsymbol{x}_0\right)\left(\boldsymbol{x} - \boldsymbol{x}_0\right) \tag{A-1}$$

where $\nabla_h\left(\boldsymbol{x}_0\right)$ and $H_h\left(\boldsymbol{x}_0\right)$ are the partial derivative and the hessian of $h\left(\boldsymbol{x}\right)$ at the given point $\boldsymbol{x}_0$. The partial derivative and the hessian of $h\left(\boldsymbol{x}\right)$ where $\boldsymbol{x} = \left[\begin{smallmatrix} x & y \end{smallmatrix}\right]$ at the given point $\boldsymbol{x}_0 = \left[\begin{smallmatrix} x_0 & y_0 \end{smallmatrix}\right]$ for a quadratic Taylor-series approximation can then be written as

$$\begin{aligned} \nabla_h\left(\boldsymbol{x}_0\right) &= \begin{bmatrix} h_x\left(x_0, y_0\right) & h_y\left(x_0, y_0\right) \end{bmatrix} \\ H_h\left(\boldsymbol{x}_0\right) &= \begin{bmatrix} h_{xx}\left(x_0, y_0\right) & h_{xy}\left(x_0, y_0\right) \\ h_{yx}\left(x_0, y_0\right) & h_{yy}\left(x_0, y_0\right) \end{bmatrix} \end{aligned} \tag{A-2}$$

where h_x and h_y are first order partial derivatives and h_{xx}, h_{xy}, h_{yx} and h_{yy} are the second-order partial derivatives with respect to $\boldsymbol{x}_0$. By substituting (A-2) in (A-1), we get

$$\begin{aligned}
T_h =& h\left(x_0, y_0\right) + \begin{bmatrix} h_x\left(x_0, y_0\right) & h_y\left(x_0, y_0\right) \end{bmatrix} \begin{bmatrix} x - x_0 \\ y - y_0 \end{bmatrix} + \\
& \frac{1}{2} \begin{bmatrix} x - x_0 \\ y - y_0 \end{bmatrix}^T \begin{bmatrix} h_{xx}\left(x_0, y_0\right) & h_{xy}\left(x_0, y_0\right) \\ h_{yx}\left(x_0, y_0\right) & h_{yy}\left(x_0, y_0\right) \end{bmatrix} \begin{bmatrix} x - x_0 \\ y - y_0 \end{bmatrix} \\
=& h\left(x_0, y_0\right) + h_x\left(x_0, y_0\right)\left(x - x_0\right) + h_x\left(x_0, y_0\right)\left(y - y_0\right) + \frac{1}{2} h_{xx}\left(x_0, y_0\right)\left(x - x_0\right)^2 + \\
& h_{xy}\left(x_0, y_0\right)\left(x - x_0\right)\left(x_0, y_0\right) + \frac{1}{2} h_{yy}\left(x_0, y_0\right)\left(y - y_0\right)^2 \\
=& h_0 + h_1 \begin{bmatrix} x \\ y \end{bmatrix} + \frac{1}{2} \begin{bmatrix} x \\ y \end{bmatrix}^T h_2 \begin{bmatrix} x \\ y \end{bmatrix}
\end{aligned} \tag{A-3}$$

where h_0, h_1 and h_2 are defined as

$$\begin{aligned}
h_0 =& h\left(x_0, y_0\right) - h_x\left(x_0, y_0\right) x_0 - h_y\left(x_0, y_0\right) y_0 + \frac{1}{2} h_{xx}\left(x_0, y_0\right) x_0^2 + h_{xy}\left(x_0, y_0\right) x_0 y_0 + \\
& \frac{1}{2} h_{yy}\left(x_0, y_0\right) y_0^2 \\
h_1 =& \begin{bmatrix} h_x\left(x_0, y_0\right) - h_{xx}\left(x_0, y_0\right) x_0 - h_{xy}\left(x_0, y_0\right) y_0 \\ h_y\left(x_0, y_0\right) - h_{yy}\left(x_0, y_0\right) y_0 - h_{xy}\left(x_0, y_0\right) x_0 \end{bmatrix} \\
h_2 =& \begin{bmatrix} h_{xx}\left(x_0, y_0\right) & h_{xy}\left(x_0, y_0\right) \\ h_{yx}\left(x_0, y_0\right) & h_{yy}\left(x_0, y_0\right) \end{bmatrix}
\end{aligned} \tag{A-4}$$

This can therefore be extended to work with the road and obstacle potential. The Taylor-series approximation of a general potential U for the future position $\mathcal{X}_{\mathrm{HV}_{q+k|q}} = \left[X_{\mathrm{HV}_{q+k|q}} \; Y_{\mathrm{HV}_{q+k|q}} \right]^T$ around the current position $\mathcal{X}_{\mathrm{HV}_{q+k-1|q}} = \left[X_{\mathrm{HV}_{q+k-1|q}} \; Y_{\mathrm{HV}_{q+k-1|q}} \right]^T$ is calculated by replacing the general function h with potential U, $\boldsymbol{x}$ with $\mathcal{X}_{\mathrm{HV}_{q+k|q}}$ and $\boldsymbol{x}_0$ with $\mathcal{X}_{\mathrm{HV}_{q+k-1|q}}$ in (A-3) and (A-4). Let us define functions equivalent to $h\left(x_0, y_0\right)$, $h_x\left(x_0, y_0\right)$, $h_y\left(x_0, y_0\right)$, $h_{xx}\left(x_0, y_0\right)$, $h_{xy}\left(x_0, y_0\right)$, $h_{yx}\left(x_0, y_0\right)$ and $h_{yy}\left(x_0, y_0\right)$ when defining the quadratic Taylor-series approximation for a general potential U for the future position $\mathcal{X}_{\mathrm{HV}_{q+k|q}} = \left[X_{\mathrm{HV}_{q+k|q}} \; Y_{\mathrm{HV}_{q+k|q}} \right]^T$ around the current position $\mathcal{X}_{\mathrm{HV}_{q+k-1|q}} = \left[X_{\mathrm{HV}_{q+k-1|q}} \; Y_{\mathrm{HV}_{q+k-1|q}} \right]^T$ as

$$
\begin{aligned}
h\left(x_0, y_0\right) &\Rightarrow U\left(X_{\mathrm{HV}_{q+k-1|q}}, Y_{\mathrm{HV}_{q+k-1|q}}\right) \\
h_x\left(x_0, y_0\right) &\Rightarrow U_{X_{\mathrm{HV}_{q+k|q}}}\left(X_{\mathrm{HV}_{q+k-1|q}}, Y_{\mathrm{HV}_{q+k-1|q}}\right) \\
h_y\left(x_0, y_0\right) &\Rightarrow U_{Y_{\mathrm{HV}_{q+k|q}}}\left(X_{\mathrm{HV}_{q+k-1|q}}, Y_{\mathrm{HV}_{q+k-1|q}}\right) \\
h_{xx}\left(x_0, y_0\right) &\Rightarrow U_{X_{\mathrm{HV}_{q+k|q}} X_{\mathrm{HV}_{q+k|q}}}\left(X_{\mathrm{HV}_{q+k-1|q}}, Y_{\mathrm{HV}_{q+k-1|q}}\right) \\
h_{xy}\left(x_0, y_0\right) &\Rightarrow U_{X_{\mathrm{HV}_{q+k|q}} Y_{\mathrm{HV}_{q+k|q}}}\left(X_{\mathrm{HV}_{q+k-1|q}}, Y_{\mathrm{HV}_{q+k-1|q}}\right) \\
h_{yx}\left(x_0, y_0\right) &\Rightarrow U_{Y_{\mathrm{HV}_{q+k|q}} X_{\mathrm{HV}_{q+k|q}}}\left(X_{\mathrm{HV}_{q+k-1|q}}, Y_{\mathrm{HV}_{q+k-1|q}}\right) \\
h_{yy}\left(x_0, y_0\right) &\Rightarrow U_{Y_{\mathrm{HV}_{q+k|q}} Y_{\mathrm{HV}_{q+k|q}}}\left(X_{\mathrm{HV}_{q+k-1|q}}, Y_{\mathrm{HV}_{q+k-1|q}}\right)
\end{aligned}
\tag{A-5}
$$

Table A-1 further simplifies the expressions in (A-5) for easier representation. The final

Actual Expression	**Simplified Representation**
$U\left(X_{\mathrm{HV}_{q+k-1\|q}}, Y_{\mathrm{HV}_{q+k-1\|q}}\right)$	U_{01}
$U_{X_{\mathrm{HV}_{q+k\|q}}}\left(X_{\mathrm{HV}_{q+k-1\|q}}, Y_{\mathrm{HV}_{q+k-1\|q}}\right)$	U_X
$U_{Y_{\mathrm{HV}_{q+k\|q}}}\left(X_{\mathrm{HV}_{q+k-1\|q}}, Y_{\mathrm{HV}_{q+k-1\|q}}\right)$	U_Y
$U_{X_{\mathrm{HV}_{q+k\|q}} X_{\mathrm{HV}_{q+k\|q}}}\left(X_{\mathrm{HV}_{q+k-1\|q}}, Y_{\mathrm{HV}_{q+k-1\|q}}\right)$	U_{XX}
$U_{X_{\mathrm{HV}_{q+k\|q}} Y_{\mathrm{HV}_{q+k\|q}}}\left(X_{\mathrm{HV}_{q+k-1\|q}}, Y_{\mathrm{HV}_{q+k-1\|q}}\right)$	U_{XY}
$U_{Y_{\mathrm{HV}_{q+k\|q}} X_{\mathrm{HV}_{q+k\|q}}}\left(X_{\mathrm{HV}_{q+k-1\|q}}, Y_{\mathrm{HV}_{q+k-1\|q}}\right)$	U_{YX}
$U_{Y_{\mathrm{HV}_{q+k\|q}} Y_{\mathrm{HV}_{q+k\|q}}}\left(X_{\mathrm{HV}_{q+k-1\|q}}, Y_{\mathrm{HV}_{q+k-1\|q}}\right)$	U_{YY}

Table A-1: Simplified representation of expressions in (A-5)

approximated potential is given by

$$
U_{q+k|q} == U_0 + U_1 \begin{bmatrix} X_{\mathrm{HV}_{q+k|q}} \\ Y_{\mathrm{HV}_{q+k|q}} \end{bmatrix} + \frac{1}{2} \begin{bmatrix} X_{\mathrm{HV}_{q+k|q}} \\ Y_{\mathrm{HV}_{q+k|q}} \end{bmatrix}^T U_2 \begin{bmatrix} X_{\mathrm{HV}_{q+k|q}} \\ Y_{\mathrm{HV}_{q+k|q}} \end{bmatrix}
\tag{A-6}
$$

where values of U_0, U_1 and U_2 are given by

$$
\begin{aligned}
&U_0 = U_{01} - U_X X_{\mathrm{HV}_{q+k-1|q}} - U_Y Y_{\mathrm{HV}_{q+k-1|q}} + \frac{1}{2} U_{XX} X^2_{\mathrm{HV}_{q+k-1|q}} + U_{XY} X_{\mathrm{HV}_{q+k-1|q}} Y_{\mathrm{HV}_{q+k-1|q}} + \\
&\quad \frac{1}{2} U_{YY} Y^2_{\mathrm{HV}_{q+k-1|q}} \\
&U_1 = \begin{bmatrix} U_X - U_{XX} X_{\mathrm{HV}_{q+k-1|q}} - U_{XY} Y_{\mathrm{HV}_{q+k-1|q}} \\ U_Y - U_{YY} Y_{\mathrm{HV}_{q+k-1|q}} - U_{XY} X_{\mathrm{HV}_{q+k-1|q}} \end{bmatrix} \\
&U_2 = \begin{bmatrix} U_{XX} & U_{XY} \\ U_{YX} & U_{YY} \end{bmatrix}
\end{aligned}
\tag{A-7}
$$

Equation (A-6) therefore defines the quadratic approximation of a given potential U at prediction step k in loop q. Let us define a function $quad\left(U\left(\mathcal{X}_{\mathrm{HV}_{q+k-1|q}}\right)\right)$ which is a simplified representation of Equation (A-6) such that

$$U_{q+k|q} = quad\left(U\left(\mathcal{X}_{\mathrm{HV}_{q+k-1|q}}\right)\right) \tag{A-8}$$

Appendix B

Algorithms

Algorithm 5 gives the algorithm for the *CalculateHVRegion* and is used to check the region around a given OV that the HV lies in. Let A_i, B_{i_1} and C_{i_1} be vectors representing the coefficients of the lines L_{i_1} where $i_1 \in \{1, 2, \ldots 10\}$ around the j^{th} OV which divide the area around the given OV into ten regions. Let $\mathcal{X}_{v_{i_2}}$ where $i_1 \in \{1, 2, \ldots 5\}$ represent the coordinates of the vertices of the j^{th} OV. The current position of the HV is given by $\mathcal{X}_{\text{HV}} = [\, X_{\text{HV}} \; Y_{\text{HV}} \,]^T$ and the heading angle, θ_{HV}.

The algorithm receives the data about the lines dividing the region around the j^{th} OV into ten regions given along with the vertices of the vehicle and the position and heading angle data of HV as input. The algorithm runs a nested if-else tree for the different values of theta within each region is calculated. The algorithm uses the logical expressions shown in Figure 3-5 for different values of θ_{HV}.

Algorithm 6 gives the algorithm to calculate the value of the Euclidean distance for the region that the HV lies in. Let us define LS_{i_2} as a line segment representing the edge of the extended obstacle as seen in Figure 3-5. Let us also define $\mathcal{X}_{1,LS} = [\, X_{1,LS} \; Y_{1,LS} \,]$ and $\mathcal{X}_{2,LS} = [\, X_{2,LS} \; Y_{2,LS} \,]$ as the vertices of any given line segment LS. It is to be remembered that $\mathcal{X}_{1,LS}$ and $\mathcal{X}_{1,LS}$ are a subset of $\mathcal{X}_{v_{i_2}}$. The algorithm is then given by

The algorithm receives the vertices of the line segment corresponding to the respective region, the position of the CoG of the HV along with the constants of the obstacle APF as given in Table 3-2 as its input. The value of t is calculated as defined in (3-11) based on the relative position of the CoG of the HV and the selected line segment LS. Based on the value of t, calculate the corresponding euclidian distance function, $K_{\text{obs}_{\text{conv}}}$ based on (3-12) . The value of $K_{\text{obs}_{\text{conv}}}$ thus obtained is used to form the convex approximation of the obstacle APF.

Algorithm 5: Algorithm for *CalculateHVRegion*

Data: $\mathcal{X}_{\mathrm{HV}}$, A_{i_1}, B_{i_1}, C_{i_1}, $\mathcal{X}_{v_{i_2}}$

Result: region

begin
- **if** $\theta_{HV} < 0$ **then**
  - **if** $(A_1 X_{HV} + B_1 Y_{HV} + C_1 < 0) \wedge (A_2 X_{HV} + B_2 Y_{HV} + C_2 \leq 0) \wedge (A_3 X_{HV} + B_5 Y_{HV} + C_5 > 0)$ **then**
    - region= R_1
  - $\vdots$
  - **else if** $(A_1 X_{HV} + B_1 Y_{HV} + C_1 < 0) \wedge (A_5 X_{HV} + B_5 Y_{HV} + C_5 \leq 0)$ **then**
    - region= R_{10}
- **else if** $\theta_{HV} = 0$ **then**
  - **if** $(X_{HV} - X_{v_1} > 0) \wedge (Y_{HV} - Y_{v_1} \leq 0) \wedge (Y_{HV} - Y_{v_5} > 0)$ **then**
    - region= R_1
  - $\vdots$
  - **else if** $(X_{HV} - X_{v_1} > 0) \wedge (Y_{HV} - Y_{v_1} \leq 0)$ **then**
    - region= R_{10}
- **else if** $\theta_{HV} > 0$ **then**
  - **if** $(A_1 X_{HV} + B_1 Y_{HV} + C_1 > 0) \wedge (A_2 X_{HV} + B_2 Y_{HV} + C_2 \leq 0) \wedge (A_3 X_{HV} + B_5 X_{HV} + C_5 > 0)$ **then**
    - region= R_1
  - $\vdots$
  - **else if** $(A_1 X_{HV} + B_1 Y_{HV} + C_1 > 0) \wedge (A_5 Y_{HV} + B_5 Y_{HV} + C_5 \leq 0)$ **then**
    - region= R_{10}

Algorithm 6: Algorithm for *CalculateDist*

Data: *region*, $\mathcal{X}_{\mathrm{HV}}$, $\mathcal{X}_{1,LS_{i_2}}$, $\mathcal{X}_{2,LS_{i_2}}$

Result: $K_{\mathrm{obs}_{\mathrm{conv}}}$

begin
- $t = \frac{\left(X_{\mathrm{HV}} - X_{1,LS}\right)\left(X_{2,LS} - X_{1,LS}\right) + \left(Y_{\mathrm{HV}} - Y_{1,LS}\right)\left(Y_{2,LS} - Y_{1,LS}\right)}{\left(X_{2,LS} - X_{1,LS}\right)^2 + \left(Y_{2,LS} - Y_{1,LS}\right)^2}$
- **if** $t < 0$ **then**
  - $d_{p-ls}\left(\mathcal{X}_{\mathrm{HV}}, LS_5\right) = \sqrt{(X_{\mathrm{HV}} - X_{1,LS})^2 + (Y_{\mathrm{HV}} - Y_{1,LS})^2}$
- **else if** $0 \leq t \leq 1$ **then**
  - $d_{p-ls}\left(\mathcal{X}_{\mathrm{HV}}, LS_5\right) = \sqrt{\left(X_{\mathrm{HV}} - \left(X_{1,LS} + t\left(X_{2,LS} - X_{1,LS}\right)\right)\right)^2 + \left(Y_{\mathrm{HV}} - \left(Y_{1,LS} + t\left(Y_{2,LS} - Y_{1,LS}\right)\right)\right)^2}$
- **else**
  - $t > 1$
- $d_{p-ls}\left(\mathcal{X}_{\mathrm{HV}}, LS_5\right) = \sqrt{(X_{\mathrm{HV}} - X_{2,LS})^2 + (Y_{\mathrm{HV}} - Y_{2,LS})^2}$

Appendix C

Matrices of the Bicycle Model

Given the current state of the system $\mathbf{x}(q) = \mathbf{x}_{q|q}$ and the current input to the system $\mathbf{u}(q) = \mathbf{u}_{q|q}$, the matrices of the linearized HV model are given by.

$$\dot{\mathbf{x}}_{\text{HV}} = A_{\text{HV}}\mathbf{x}_{\text{HV}} + B\mathbf{u}_{\text{HV}} \text{ where}$$

$$A_{\text{HV}} = \begin{bmatrix} A_{1,1} & 0 & 0 & A_{1,4} & A_{1,5} & 0 \\ \cos\theta_{\text{HV}} & 0 & 0 & -\sin\theta_{\text{HV}} & 0 & A_{2,6} \\ \sin\theta_{\text{HV}} & 0 & 0 & \cos\theta_{\text{HV}} & 0 & A_{3,6} \\ A_{4,1} & 0 & 0 & A_{4,4} & A_{4,5} & 0 \\ A_{5,1} & 0 & 0 & A_{5,4} & A_{5,5} & 0 \\ 0 & 0 & 0 & 0 & 0 & 1 \end{bmatrix}_{(\mathbf{x}_0,\mathbf{u}_0)}, B_{\text{HV}} = \begin{bmatrix} 1 & B_{1,2} \\ 0 & 0 \\ 0 & 0 \\ 0 & B_{4,2} \\ 0 & B_{5,2} \\ 0 & 0 \end{bmatrix}_{(\mathbf{x}_0,\mathbf{u}_0)}, C_{\text{HV}} = C_c \tag{C-1}$$

where

$$A_{1,1} = \frac{2C_f \sin\delta_{\text{HV}} \left(v_y + \ell_f \dot{\theta}_{\text{HV}}\right)}{m v_{x,\text{HV}}^2}$$

$$A_{1,4} = \dot{\theta}_{\text{HV}} - \frac{2C_f \sin\delta_{\text{HV}}}{m v_{x,\text{HV}}}$$

$$A_{1,5} = v_{y,\text{HV}} - \frac{2C_f \ell_g \sin\delta_{\text{HV}}}{m v_{x,\text{HV}}}$$

$$A_{2,6} = -v_{x,\text{HV}} \sin\theta_{\text{HV}} - v_{y,\text{HV}} \cos\theta_{\text{HV}}$$

$$A_{3,6} = v_{x,\text{HV}} \cos\theta_{\text{HV}} - v_{y,\text{HV}} \sin\theta_{\text{HV}}$$

$$A_{4,1} = \frac{2C_r \left(v_{y,\text{HV}} - \ell_r \dot{\theta}_{\text{HV}}\right)}{m v_{x,\text{HV}}^2} - \frac{2C_f \cos\delta_{\text{HV}} \left(v_{y,\text{HV}} + \ell_f \dot{\theta}_{\text{HV}}\right)}{m v_{x,\text{HV}}^2}$$

$$A_{4,4} = \frac{2\left(C_f \cos\delta_{\mathrm{HV}} - C_r\right)}{m v_{x,\mathrm{HV}}}$$

$$A_{4,5} = -v_{x,\mathrm{HV}} + \frac{2C_r\ell_r}{m v_{x,\mathrm{HV}}} + \frac{2C_f\ell_f\cos\delta_{\mathrm{HV}}}{m v_{x,\mathrm{HV}}}$$

$$A_{5,1} = -\frac{C_r\ell_r\left(v_{y,\mathrm{HV}} - \ell_r\dot{\theta}_{\mathrm{HV}}\right)}{I_z v_{x,\mathrm{HV}}^2} - \frac{C_f\ell_f\cos\delta_{\mathrm{HV}}\left(v_{y,\mathrm{HV}} + \ell_f\dot{\theta}_{\mathrm{HV}}\right)}{I_z v_{x,\mathrm{HV}}^2}$$

$$A_{5,4} = \frac{C_r\ell_r + C_f\ell_f\cos\delta_{\mathrm{HV}}}{I_z v_{x,\mathrm{HV}}}$$

$$A_{5,5} = \frac{-C_r\ell_r^2 - C_f\ell_f^2\cos\delta)\mathrm{HV}}{I_z v_{x,\mathrm{HV}}}$$

$$B_{1,2} = \frac{2C_f\left(v_{x,\mathrm{HV}}\sin\delta_{\mathrm{HV}} + \left(v_{x,\mathrm{HV}}\delta_{\mathrm{HV}} - v_{y,\mathrm{HV}} - \ell_f\dot{\theta}_{\mathrm{HV}}\right)\cos\delta_{\mathrm{HV}}\right)}{m v_{x,\mathrm{HV}}}$$

$$B_{4,2} = \frac{2C_f\left(v_{x,\mathrm{HV}}\delta_{\mathrm{HV}} - v_{y,\mathrm{HV}} - \ell_f\dot{\theta}_{\mathrm{HV}}\right)\sin\delta_{\mathrm{HV}} - v_{x,\mathrm{HV}}\cos\delta_{\mathrm{HV}}}{m v_{x,\mathrm{HV}}}$$

$$B_{5,2} = \frac{C_f\ell_f\left(v_{x,\mathrm{HV}}\delta_{\mathrm{HV}} - v_{y,\mathrm{HV}} - \ell_f\dot{\theta}_{\mathrm{HV}}\right)\sin\delta_{\mathrm{HV}} - v_{x,\mathrm{HV}}\cos\delta_{\mathrm{HV}}}{I_z v_{x,\mathrm{HV}}}$$

Bibliography

[1] M. T. Wolf and J. W. Burdick, "Artificial potential functions for highway driving with collision avoidance," *Proceedings - IEEE International Conference on Robotics and Automation*, pp. 3731–3736, 2008.

[2] B. Cottam, "Transportation planning for connected autonomous vehicles: How it all fits together," *Transportation Research Record: The Journal of the Transportation Research Board*, vol. 2672, March 2018.

[3] D. J. Yeong, G. Velasco-Hernandez, J. Barry, and J. Walsh, "Sensor and sensor fusion technology in autonomous vehicles: A review," *Sensors*, vol. 21, no. 6, pp. 1–37, 2021.

[4] T. Winkle, "Safety Benefits of Automated Vehicles: Extended Findings from Accident Research for Development, Validation and Testing," pp. 335–364, 2016.

[5] G. Velasco-Hernandez, D. J. Yeong, J. Barry, and J. Walsh, "Autonomous driving architectures, perception and data fusion: A review," pp. 315–321, 2020.

[6] J. Van Brummelen, M. O'Brien, D. Gruyer, and H. Najjaran, "Autonomous vehicle perception: The technology of today and tomorrow," *Transportation Research Part C: Emerging Technologies*, vol. 89, no. February, pp. 384–406, 2018.

[7] Z. Wang, Y. Wu, and Q. Niu, *Multi-Sensor Fusion in Automated Driving: A Survey*, vol. 8. Institute of Electrical and Electronics Engineers Inc., 2020.

[8] E. Arnold, O. Y. Al-Jarrah, M. Dianati, S. Fallah, D. Oxtoby, and A. Mouzakitis, "A Survey on 3D Object Detection Methods for Autonomous Driving Applications," *IEEE Transactions on Intelligent Transportation Systems*, vol. 20, no. 10, pp. 3782–3795, 2019.

[9] A. Singh Rathore, "State-of-the-Art Self Driving Cars: Comprehensive Review," *International Journal of Conceptions on Computing and Information Technology*, vol. 4, no. 1, pp. 2345–9808, 2016.

[10] L. Claussmann, M. Revilloud, D. Gruyer, and S. Glaser, “A review of motion planning for highway autonomous driving,” *IEEE Transactions on Intelligent Transportation Systems*, vol. 21, no. 5, pp. 1826–1848, 2020.

[11] M. Schwenzer, M. Ay, T. Bergs, and D. Abel, “Review on model predictive control: an engineering perspective,” *The International Journal of Advanced Manufacturing Technology*, vol. 117, pp. 1327–1349, November 2021.

[12] “Average car length guide (car lengths in meters and inches),” Jan 2022.

[13] D. Fernandez, “How wide is the average car? [inc. 20 examples],” *Vehicle HQ*, March 2020.

[14] H. Yang, J. Zhang, Z. Chen, F. Zhao, and H. Liu, “Curb weight probability distribution and the recommended gross weight of passenger car in mechanical parking garage design,” *Journal of Asian Architecture and Building Engineering*, pp. 1–13, 2022.

[15] F. Fabiani and S. Grammatico, “Multi-vehicle automated driving as a generalized mixed-integer potential game,” *IEEE Transactions on Intelligent Transportation Systems*, vol. 21, no. 3, pp. 1064–1073, 2020.

[16] E. Yurtsever, J. Lambert, A. Carballo, and K. Takeda, “A Survey of Autonomous Driving: Common Practices and Emerging Technologies,” *IEEE Access*, vol. 8, pp. 58443–58469, 2020.

[17] S. Thrun, M. Montemerlo, H. Dahlkamp, D. Stavens, A. Aron, J. Diebel, P. Fong, J. Gale, M. Halpenny, G. Hoffmann, K. Lau, C. Oakley, M. Palatucci, V. Pratt, P. Stang, S. Strohband, C. Dupont, L.-E. Jendrossek, C. Koelen, C. Markey, C. Rummel, J. van Niekerk, E. Jensen, P. Alessandrini, G. Bradski, B. Davies, S. Ettinger, A. Kaehler, A. Nefian, and P. Mahoney, “Stanley: The robot that won the darpa grand challenge,” pp. 1–43, 2006.

[18] “Grand Challenge 2004 Final Report,” tech. rep., Defense Advanced Research Projects Agency, 2004.

[19] On-Road Automated Driving (ORAD) committee, “Taxonomy and definitions for terms related to driving automation systems for on-road motor vehicles,” Ground Vehicle Standard J3016_202104, SAE International, April 2021.

[20] European Commission. (EC), “Sustainable and Smart Mobility Strategy—Putting European Transport on Track for the Future,” 2020.

[21] J. Manyika, M. Chui, J. Bughin, R. Dobbs, P. Bisson, and A. Marrs, “Disruptive technologies: advances that will transform life, business, and the global economy,” tech. rep., McKinsey Global Institute, 2013.

[22] T. Lozano-Pérez, J. L. Jones, P. A. O’Donnell, and E. Mazer, *Handey: A Robot Task Planner*. Cambridge, MA, USA: MIT Press, 1992.

[23] M. Rokonuzzaman, N. Mohajer, S. Nahavandi, and S. Mohamed, “Review and performance evaluation of path tracking controllers of autonomous vehicles,” *IET Intelligent Transport Systems*, vol. 15, 05 2021.

[24] P. E. Hart, N. J. Nilsson, and B. Raphael, "A formal basis for the heuristic determination of minimum cost paths," *IEEE Transactions on Systems Science and Cybernetics*, vol. 4, no. 2, pp. 100–107, 1968.

[25] E. W. Dijkstra, "A note on two problems in connexion with graphs," *Numerische mathematik*, vol. 1, no. 1, pp. 269–271, 1959.

[26] S. LaValle, "Rapidly-exploring random trees : a new tool for path planning," *The annual research report*, 1998.

[27] O. Khatib, "Real-time obstacle avoidance for manipulators and mobile robots," in *Proceedings. 1985 IEEE International Conference on Robotics and Automation*, vol. 2, pp. 500–505, 1985.

[28] D. González, J. Pérez, V. Milanés, and F. Nashashibi *IEEE Transactions on Intelligent Transportation Systems*.

[29] Y. Kuwata, J. Teo, G. Fiore, S. Karaman, E. Frazzoli, and J. P. How, "Real-time motion planning with applications to autonomous urban driving," *IEEE Transactions on Control Systems Technology*, vol. 17, no. 5, pp. 1105–1118, 2009.

[30] X. Qian, I. Navarro, A. de La Fortelle, and F. Moutarde, "Motion planning for urban autonomous driving using bézier curves and mpc," in *2016 IEEE 19th International Conference on Intelligent Transportation Systems (ITSC)*, pp. 826–833, 2016.

[31] C. Liu, S. Lee, S. Varnhagen, and H. E. Tseng, "Path planning for autonomous vehicles using model predictive control," in *2017 IEEE Intelligent Vehicles Symposium (IV)*, pp. 174–179, 2017.

[32] J. Li, M. Ran, H. Wang, and L. Xie, "MPC-based Unified Trajectory Planning and Tracking Control Approach for Automated Guided Vehicles," *IEEE International Conference on Control and Automation, ICCA*, vol. 2019-July, pp. 374–380, 2019.

[33] H. Guo, C. Shen, H. Zhang, H. Chen, and R. Jia, "Simultaneous Trajectory Planning and Tracking Using an MPC Method for Cyber-Physical Systems: A Case Study of Obstacle Avoidance for an Intelligent Vehicle," *IEEE Transactions on Industrial Informatics*, vol. 14, no. 9, pp. 4273–4283, 2018.

[34] C. Shen, Y. Shi, and B. Buckham, "Integrated path planning and tracking control of an AUV: A unified receding horizon optimization approach," *IEEE/ASME Transactions on Mechatronics*, vol. 22, no. 3, pp. 1163–1173, 2017.

[35] C. Ko, S. Han, M. Choi, and K. S. Kim, "Integrated path planning and tracking control of autonomous vehicle for collision avoidance based on model predictive control and potential field," *International Conference on Control, Automation and Systems*, pp. 956–961, 2020.

[36] J. Dentler, *Real-time Model Predictive Control of Cooperative Aerial Manipulation*. PhD thesis, University of Luxembourg, 10 2018.

[37] S. Scheggi and S. Misra, "An experimental comparison of path planning techniques applied to micro-sized magnetic agents," in *2016 International Conference on Manipulation, Automation and Robotics at Small Scales (MARSS)*, pp. 1–6, 2016.

[38] Y. Du, Y. Wang, and C.-Y. Chan, "Autonomous lane-change controller," in *2015 IEEE Intelligent Vehicles Symposium (IV)*, pp. 386–393, 2015.

[39] A. Bemporad and M. Morari, "Control of systems integrating logic, dynamics, and constraints," *Automatica*, vol. 35, p. 407–427, March 1999.

[40] B. Siciliano and O. Khatib, *Springer Handbook of Robotics*. Berlin, Heidelberg: Springer-Verlag, 2007.

[41] S. Campbell, N. O'Mahony, A. Carvalho, L. Krpalkova, D. Riordan, and J. Walsh, "Path Planning Techniques for Mobile Robots A Review," *2020 6th International Conference on Mechatronics and Robotics Engineering, ICMRE 2020*, pp. 12–16, 2020.

[42] N. Berger, "Lane Change Path Planning: with State-Dependent Safety Constraints," master's thesis, TU Delft, February 2018.

[43] J. Souman, K. Adjenughwure, E. van Dam, M. van Weperen, and A. Tejada, "Quantification of safe driving," Tech. Rep. TNO 2021 R12632 0.1, TNO, December 2021.

[44] S. Zhang, W. Deng, Q. Zhao, H. Sun, and B. Litkouhi, "Dynamic trajectory planning for vehicle autonomous driving," pp. 4161–4166, 10 2013.

[45] B. van Kampen, "Case study: Rear end or chain accidents," tech. rep., 2003.

[46] W. G. Najm, B. Sen, J. D. Smith, B. Campbell, *et al.*, "Analysis of light vehicle crashes and pre-crash scenarios based on the 2000 general estimates system," tech. rep., United States. National Highway Traffic Safety Administration, 2003.

[47] K. N. de Winkel, T. Irmak, R. Happee, and B. Shyrokau, "Standards for passenger comfort in automated vehicles: Acceleration and jerk," *Applied Ergonomics*, vol. 106, p. 103881, 2023.

[48] H. Jula, E. B. Kosmatopoulos, and P. A. Ioannou, "Collision avoidance analysis for lane changing and merging," *IEEE Transactions on vehicular technology*, vol. 49, no. 6, pp. 2295–2308, 2000.

[49] Y. Koren and J. Borenstein, "Potential field methods and their inherent limitations for mobile robot navigation," in *Proceedings. 1991 IEEE International Conference on Robotics and Automation*, pp. 1398–1404 vol.2, 1991.

[50] P. Khosla and R. Volpe, "Superquadric artificial potentials for obstacle avoidance and approach," in *Proceedings. 1988 IEEE International Conference on Robotics and Automation*, pp. 1778–1784 vol.3, 1988.

[51] X. Yang, W. Yang, H. Zhang, H. Chang, C.-Y. Chen, and S. Zhang, "A new method for robot path planning based artificial potential field," in *2016 IEEE 11th Conference on Industrial Electronics and Applications (ICIEA)*, pp. 1294–1299, 2016.

[52] R. Volpe and P. Khosla, "Manipulator Control with Superquadric Artificial Potential Functions: Theory and Experiments," *IEEE Transactions on Systems, Man and Cybernetics*, vol. 20, no. 6, pp. 1423–1436, 1990.

[53] D. Eberly, "Distance between point and line, ray, or line segment," March 1999.

[54] J. Perina, "Shortest distance between a point and a line segment," May 2009.

[55] F. S. Al-Duais and M. Y. Hmood, "Bayesian and non-bayesian estimation of the lomax model based on upper record values under weighted linex loss function," *Periodicals of Engineering and Natural Sciences (PEN)*, vol. 8, no. 3, pp. 1786–1794, 2020.

[56] J. B. Rawlings, D. Q. Mayne, and M. Diehl, *Model predictive control: theory, computation, and design*, vol. 2. Nob Hill Publishing Madison, WI, 2017.

[57] Y.-G. XI, D. Li, and S. Lin, "Model predictive control — status and challenges," *Acta Automatica Sinica*, vol. 39, p. 222–236, March 2013.

[58] J. Richalet, A. Rault, J. Testud, and J. Papon, "Model predictive heuristic control: Applications to industrial processes," *Automatica*, vol. 14, no. 5, pp. 413–428, 1978.

[59] A. Bemporad, W. Heemels, and B. De Schutter, "On hybrid systems and closed-loop mpc systems," *IEEE Transactions on Automatic Control*, vol. 47, no. 5, pp. 863–869, 2002.

[60] M. Verhaegen and V. Verdult, *Filtering and System Identification: A Least Squares Approach*. Cambridge University Press, 2007.

[61] C. Chen and L. Shaw, "On receding horizon feedback control," *Automatica*, vol. 18, no. 3, pp. 349–352, 1982.

[62] D. Q. Mayne, J. B. Rawlings, C. V. Rao, and P. O. Scokaert, "Constrained model predictive control: Stability and optimality," *Automatica*, vol. 36, pp. 789–814, June 2000.

[63] J. Hebib and S. Dam, "Vehicle dynamic models for virtual testing of autonomous trucks," master's thesis, Linköping University, February 2019.

[64] V. Patil, "Generic and complete vehicle dynamic models for open-source platforms," master's thesis, TU Delft, August 2017.

[65] R. Rajamani, *Vehicle Dynamics and Control*. January 2006.

[66] W. Jansen, "Lateral Path-Following Control of Automated Vehicle Platoons," master's thesis, TU Delft, July 2016.

[67] M. Isaksson Palmqvist, "Model Predictive Control for Autonomous Driving of a Truck," master's thesis, Kungliga Tekniska Hgskolan (KTH), 2016.

[68] F. Borrelli, P. Falcone, T. Keviczky, J. Asgari, and D. H. , "Mpc-based approach to active steering for autonomous vehicle systems," *International Journal of Vehicle Autonomous Systems*, vol. 3, no. 2-4, pp. 265–291, 2005.

[69] K. J. Åström and B. Wittenmark, *Computer-Controlled Systems: Theory and Design (2nd Ed.)*. USA: Prentice-Hall, Inc., 1990.

[70] A. Wysocki and M. Ławryńczuk, "On choice of the sampling period and the horizons in generalized predictive control," in *Recent Advances in Automation, Robotics and Measuring Techniques* (R. Szewczyk, C. Zieliński, and M. Kaliczyńska, eds.), (Cham), pp. 329–339, Springer International Publishing, 2014.

[71] I. Bilik, O. Longman, S. Villeval, and J. Tabrikian, "The rise of radar for autonomous vehicles: Signal processing solutions and future research directions," *IEEE Signal Processing Magazine*, vol. 36, pp. 20–31, September 2019.

[72] M. Lee, S. Kim, D. Jung, H. Lee, J. Choi, H. Han, and J. H. Yang, "Simulator-based study of the response time and defensive behavior of drivers in unexpected dangers at an intersection," in *Adjunct Proceedings of the 14th International Conference on Automotive User Interfaces and Interactive Vehicular Applications*, AutomotiveUI '22, (New York, NY, USA), p. 10–14, Association for Computing Machinery, 2022.

[73] P. Droździel, S. Tarkowski, I. Rybicka, and R. Wrona, "Drivers' reaction time research in the conditions in the real traffic," *Open Engineering*, vol. 10, pp. 35–47, January 2020.

[74] E. Snapper, "Model-based Path Planning and Control for Autonomous Vehicles using Artificial Potential Fields," master's thesis, TU Delft, January 2018.

[75] J. Ji, A. Khajepour, W. W. Melek, and Y. Huang, "Path planning and tracking for vehicle collision avoidance based on model predictive control with multiconstraints," *IEEE Transactions on Vehicular Technology*, vol. 66, no. 2, pp. 952–964, 2017.

[76] R. N. Jazar, *Steering Dynamics*, pp. 379–454. Boston, MA: Springer US, 2008.

[77] J. Löfberg, "Yalmip : A toolbox for modeling and optimization in matlab," in *In Proceedings of the CACSD Conference*, (Taipei, Taiwan), 2004.

[78] Gurobi Optimization, LLC, "Gurobi Optimizer Reference Manual," 2022.

[79] H. B. Pacejka, "Chapter 4 - semi-empirical tyre models," in *Tyre and Vehicle Dynamics (Second Edition)* (H. B. Pacejka, ed.), pp. 156–215, Oxford: Butterworth-Heinemann, second edition ed., 2006.

[80] B. Zarrouki, V. Klös, N. Heppner, S. Schwan, R. Ritschel, and R. Voßwinkel, "Weights-varying mpc for autonomous vehicle guidance: a deep reinforcement learning approach," in *2021 European Control Conference (ECC)*, pp. 119–125, 2021.

Glossary

List of Acronyms

DARPA	Defense Advanced Research Projects Agency
AV	Autonomous Vehicles
APF	Artificial Potential Fields
MPC	Model Predictive Control
SAE	Society of Automotive Engineers
CV	Conventional Vehicles
LiDAR	Light Detection And Ranging
RADAR	RAdio Detection And Ranging
RRT	Rapidly-exploring Random Trees
HV	Host Vehicle
OV	Obstacle Vehicle
MIMPC	Mixed-Integer Model Predictive Control
MLD	Mixed-Logical Dynamical
ROI	Region Of Interest
USA	United States of America
CoG	Center of Gravity
LINEX	LINear EXponential
VCS	Vehicle Control System
CV	Constant Velocity
ZOH	Zero Order Hold
MIQP	Mixed Integer Quadratic Programming
MATLAB	MATrix LABoratory
YALMIP	Yet Another LMI Parser

SDP Semi-Definite Programming

LMI Linear Matrix Inequalities

RMS Root Mean Square